

**A HYBRID ANALOG-DIGITAL CODING SCHEME FOR DIGITAL  
SOURCES**

by

Lu Li

A dissertation submitted to the Faculty of the University of Delaware in partial fulfillment of the requirements for the degree of Doctor of Philosophy in Electrical and Computer Engineering

Summer 2018

© 2018 Lu Li  
All Rights Reserved

**A HYBRID ANALOG-DIGITAL CODING SCHEME FOR DIGITAL  
SOURCES**

by

Lu Li

Approved: \_\_\_\_\_  
Kenneth E. Barner, Ph.D.  
Chair of the Department of Electrical and Computer Engineering

Approved: \_\_\_\_\_  
Babatunde A. Ogunnaike, Ph.D.  
Dean of the College of Engineering

Approved: \_\_\_\_\_  
Ann L. Ardis, Ph.D.  
Senior Vice Provost for Graduate and Professional Education

I certify that I have read this dissertation and that in my opinion it meets the academic and professional standard required by the University as a dissertation for the degree of Doctor of Philosophy.

Signed: \_\_\_\_\_  
Javier Garcia-Frias, Ph.D.  
Professor in charge of dissertation

I certify that I have read this dissertation and that in my opinion it meets the academic and professional standard required by the University as a dissertation for the degree of Doctor of Philosophy.

Signed: \_\_\_\_\_  
Gonzalo R. Arce, Ph.D.  
Member of dissertation committee

I certify that I have read this dissertation and that in my opinion it meets the academic and professional standard required by the University as a dissertation for the degree of Doctor of Philosophy.

Signed: \_\_\_\_\_  
Xiang-Gen Xia, Ph.D.  
Member of dissertation committee

I certify that I have read this dissertation and that in my opinion it meets the academic and professional standard required by the University as a dissertation for the degree of Doctor of Philosophy.

Signed: \_\_\_\_\_  
Pedro Crespo, Ph.D.  
Member of dissertation committee

## ACKNOWLEDGEMENTS

During this long and rewarding Ph.D. experience, many people have helped and encouraged me through difficult times. I would like to express the most sincere gratitude to them.

First of all, I would like to thank my academic advisor, Dr. Javier Garcia-Frias. For the past seven years, he continued to support and guide me in research and life. He introduced me into the area of channel coding, and led me through many challenges. He has great insights into many difficult problems and inspired me with invaluable suggestions. I greatly appreciate his patience and flexibility during this long period. Without him, this dissertation would never have been a reality. I would also like to thank all my dissertation committee, Dr. Gonzalo R. Arce, Dr. Xiang-Gen Xia, and Dr. Pedro Crespo, who gave me many suggestions and inspired me with new perspectives into the research.

I would also like to thank the members of the Information Processing and Communications Lab, who made great contributions to my life at the University of Delaware. I am especially thankful to Bo Lu, who has been my great companion in the research discussion and personal life. His help on my career life was important. I am also grateful to other past and present group members, including Mohamed Hassanin, Inaki Iglesias, Mariano Eduardo Burich, Kejing Liu, and Inaki Esnaola. They all provided me with great help at different stages of my Ph.D. life. I greatly appreciate their kindness and understanding.

In addition, I would like to thank all of my friends, who have supported me consistently and have made life at the University of Delaware interesting and memorable. I have to mention a few of them here. Chen Liu was my roommate for a long time and was a great companion in my personal life. We have had discussions on many

academic, industry and life problems, which contributed a lot to my growth. Yongwei Ma, whose humor and help during my difficult times was a great treasure to me, also had a long friendship with me during his time here. Bohan Zhang, Guangyi Liu and Yuan Xue were also kind to me and offered any help when I needed it. I am also grateful to other friends I have not mentioned here, who I have had the pleasure to meet with in my life.

Importantly, I would like to thank my family for their unconditionally love. They have taught me a lot on tolerance, patience, persistence and hard working, which was the source of the strength for my Ph.D. study. I am proud of their support and love. Finally, I would like to thank my girlfriend Tongtong Shan, who gave me consistent support, and provided me with strength to overcome difficulties during this period.

## TABLE OF CONTENTS

<b>LIST OF TABLES</b> . . . . .	<b>x</b>
<b>LIST OF FIGURES</b> . . . . .	<b>xii</b>
<b>ABSTRACT</b> . . . . .	<b>xvi</b>
 <b>Chapter</b>	
<b>1 INTRODUCTION</b> . . . . .	<b>1</b>
1.1 Motivation . . . . .	2
1.2 Joint Source-Channel Coding . . . . .	3
1.2.1 Separation Principle . . . . .	3
1.2.2 Joint Source-Channel Coding Techniques . . . . .	4
1.2.3 Distributed Joint Source Channel Coding for Correlated Sources . . . . .	5
1.3 Compressive Sensing . . . . .	6
1.4 Dissertation Organization . . . . .	8
<b>2 HYBRID ANALOG-DIGITAL ENCODER</b> . . . . .	<b>11</b>
2.1 Introduction . . . . .	11
2.2 Rate Compatible Modulation . . . . .	11
2.3 Low Density Generator Matrix (LDGM) Codes . . . . .	15
2.4 The Structure of the Hybrid Scheme . . . . .	18
2.5 Conclusion . . . . .	20
<b>3 HYBRID ANALOG DIGITAL DECODER: BELIEF PROPAGATION</b> . . . . .	<b>21</b>
3.1 Introduction . . . . .	21
3.2 Decoder Structure . . . . .	21
3.3 Message Passing for the Hybrid Scheme . . . . .	23
3.3.1 Initialization . . . . .	23

3.3.2	Computation at the RP symbol nodes . . . . .	25
3.3.3	Computation at the coded bit nodes . . . . .	27
3.3.4	Computation at the source bit nodes . . . . .	29
3.4	Decoding Schedule . . . . .	30
3.5	Conclusion . . . . .	30
<b>4</b>	<b>APPLICATION TO POINT-TO-POINT AWGN CHANNELS . .</b>	<b>31</b>
4.1	Introduction . . . . .	31
4.2	Design Objective . . . . .	32
4.3	Uniform Memoryless Sources . . . . .	33
4.4	Non-uniform Memoryless Sources . . . . .	37
4.4.1	Background . . . . .	37
4.4.2	Simulation Results . . . . .	39
4.5	Conclusion . . . . .	47
<b>5</b>	<b>SIMPLIFIED DECODING ALGORITHM . . . . .</b>	<b>49</b>
5.1	Introduction . . . . .	49
5.2	Proposed Simplified Decoding Algorithm . . . . .	50
5.2.1	Computation at the RP Symbol Nodes . . . . .	50
5.2.2	Computation at the LDGM Coded Bit Nodes . . . . .	53
5.2.3	Computation at the Source Bit Nodes . . . . .	53
5.2.4	Decision . . . . .	54
5.3	Computational Complexity Analysis . . . . .	54
5.3.1	Complexity of the Original Method . . . . .	55
5.3.1.1	Convolution . . . . .	55
5.3.1.2	Deconvolution . . . . .	57
5.3.1.3	Computation of Outgoing Messages . . . . .	58
5.3.2	Complexity of the Simplified Method . . . . .	58
5.3.3	Complexity Comparison . . . . .	59
5.4	Simulation Results . . . . .	60
5.4.1	Optimization of the Hybrid Scheme with Simplified Decoding	60

5.4.2	Performance Comparison with the Original Decoding Method	64
5.4.2.1	Uniform Sources	65
5.4.2.2	Non-uniform Sources	67
5.4.2.3	Observations	70
5.5	Conclusion	72
<b>6</b>	<b>MULTIPLE ACCESS CHANNEL</b>	<b>74</b>
6.1	Introduction	74
6.2	Multiple Access Channel	75
6.3	Proposed Joint Source Channel Coding Structure	77
6.3.1	Proposed Hybrid Encoder	77
6.3.2	Synthetic Joint Decoder	78
6.4	Algorithm for Synthetic Decoding	81
6.4.1	Computation at the Synthetic RP node	82
6.4.2	Computation at the LDGM Coded Bit Node	85
6.4.3	Computation at the Synthetic Source Bit Node	85
6.4.3.1	Messages to synthetic RP nodes ( $\mathbf{P}^{b \rightarrow a}$ )	87
6.4.3.2	Individual messages to coded bit nodes ( $L^{b \rightarrow c^1}, L^{b \rightarrow c^2}$ )	88
6.4.3.3	Decision	88
6.4.4	Simplified Method for MAC	89
6.5	Simulation Results	90
6.5.1	System Optimization	90
6.5.2	High Transmission Rate System	93
6.5.3	System with Simplified Decoding Method	96
6.6	Conclusion	98
<b>7</b>	<b>CONCLUSION AND FUTURE WORK</b>	<b>100</b>
7.1	Summary of Contributions	100
7.1.1	Point to Point AWGN Channels	100
7.1.2	Simplified Decoding Method	101

7.1.3	Transmission of Correlated Sources over Multiple Access Channels . . . . .	102
7.2	Future Work . . . . .	102
7.2.1	Density Evolution . . . . .	102
7.2.2	Matrix Design . . . . .	103
7.2.3	Rate Adaptation . . . . .	103
7.2.4	Multi-User Communication . . . . .	103
7.2.5	General Coding Designs . . . . .	103
	<b>BIBLIOGRAPHY . . . . .</b>	<b>104</b>
	<b>Appendix</b>	
	<b>DECONVOLUTION TECHNIQUE FOR MAC . . . . .</b>	<b>114</b>

## LIST OF TABLES

3.1	Notation used in the message passing for the hybrid scheme . . . . .	24
4.1	Theoretical limit and gap to the limit for $BER < 10^{-4}$ . A throughput of 10 source bits per channel use is considered. Three nonuniform binary memoryless sources with $p_1 = 0.1, p_1 = 0.01, p_1 = 0.005$ are considered. . . . .	47
5.1	Complexity Analysis of the Convolution . . . . .	56
5.2	Computational Complexity of the Original Method . . . . .	58
5.3	Complexity of the Simplified Method . . . . .	59
5.4	Complexity Comparison . . . . .	60
5.5	Gap to the theoretical limit for hybrid schemes using the original and the simplified decoding methods when $p_1 = 0.5$ . The theoretical limit is in terms of $E_s/N_0$ . The gap is measured at $BER < 10^{-4}$ . All results are in dB. . . . .	67
5.6	Gap to the theoretical limit for hybrid schemes using the original and simplified decoding methods when $p_1 = 0.1$ . The theoretical limit is in terms of $E_s/N_0$ . The gap is measured at $BER < 10^{-4}$ . All the results are in dB. . . . .	69
5.7	Gap to the theoretical limit for hybrid schemes using the original and simplified decoding methods when $p_1 = 0.01$ . The theoretical limit is in terms of $E_s/N_0$ . The gap is measured at $BER < 10^{-4}$ . All results are in dB. . . . .	69
5.8	Gap to the theoretical limit for hybrid schemes using the original and simplified decoding methods when $p_1 = 0.005$ . The theoretical limit is in terms of $E_s/N_0$ . The gap is measured at $BER < 10^{-4}$ . All results are in dB. . . . .	72

6.1	Definitions for the synthetic decoding algorithm . . . . .	82
6.2	Theoretical limits for different values of $p$ ( $R_c = 1/3$ ) . . . . .	91
6.3	Gap to the theoretical limit assuming separation for hybrid schemes using the original and the simplified decoding methods over MAC when $p_1 = 0.01$ . The theoretical limit is in terms of $E_{so}/N_0$ . The gap is measured at $BER < 10^{-4}$ . All results are in dB. . . . .	97
6.4	Gap to the theoretical limit assuming separation for hybrid schemes using the original and the simplified decoding methods over MAC when $p_1 = 0.005$ . The theoretical limit is in terms of $E_{so}/N_0$ . The gap is measured at $BER < 10^{-4}$ . All results are in dB. . . . .	97

## LIST OF FIGURES

2.1	Bipartite graph representation of an RCM system. . . . .	13
2.2	Illustration of constellation for an RCM scheme with weight set $\{\pm 1, \pm 2, \pm 4, \pm 4\}$ . . . . .	15
2.3	Bipartite graph representation of an LDGM code . . . . .	17
2.4	Encoder diagram of the proposed hybrid system consisting of the parallel concatenation of an RCM sub-block and an LDGM code. . . . .	19
3.1	Bipartite graph representation of the proposed hybrid system consisting of the parallel concatenation of an RCM sub-block and an LDGM sub-block. . . . .	22
3.2	Computation at an RP symbol node. . . . .	25
3.3	Computation at a coded bit node. . . . .	28
3.4	(a) Computation of the message exchanged from a source bit node to an RP symbol node, (b) Computation of the message exchanged from a source bit node to a digital coded bit node. . . . .	29
4.1	System performance for the pure RCM system and three hybrid schemes when the weight set of the RCM sub-block is $\{\pm 1, \pm 2, \pm 4, \pm 4\}$ . The length of the information bits is 37,000 and the number of channel uses is 5000 for a rate of 7.4 information bits per channel use. . . . .	34
4.2	System performance for the pure RCM system and three hybrid schemes when the weight set of the RCM sub-block is $\{\pm 2, \pm 3, \pm 4, \pm 8\}$ . The length of the information bits is 37,000 and the number of channel uses is 5000 for a rate of 7.4 information bits per channel use. . . . .	36

4.3	System performance of a pure RCM system and four hybrid systems when $p = 0.1$ . In all the hybrid systems $d_{vc} = 1$ and the weight set is the same as in the pure RCM system, as defined in the text. Different number of coded bits, $I$ , are considered as indicated in the figure. . . . .	40
4.4	System performance of a pure RCM system and seven hybrid systems when $p = 0.01$ . In all the hybrid systems $d_{vc} = 8$ and the weight set is the same as in the pure RCM system, as defined in the text. Different number of coded bits, $I$ , are considered as indicated in the figure. . . . .	41
4.5	System performance for five hybrid schemes when $p_1 = 0.01$ . In all the hybrid systems $I = 2500$ . Different values of $d_{vc}$ are considered as indicated in the figure. . . . .	42
4.6	System performance for the pure RCM system and two pairs of hybrid schemes when $p_1 = 0.01$ . The first pair has 1,000 coded bits within 10,000 generated symbols and the values of $d_{vc}$ are 6, 8 and 10 respectively. The second pair has 1250 coded bits within 10000 generated symbols and the values of $d_{vc}$ are also 6, 8 and 10. . . . .	43
4.7	System performance for the pure RCM system and two pairs of hybrid schemes when $p_1 = 0.005$ . In all the hybrid systems $d_{vc} = 14$ and the weight set is the same as in the pure RCM system, as defined in the text. Different number of coded bits, $I$ , are considered as indicated in the figure. . . . .	44
4.8	System performance for five hybrid schemes when $p_1 = 0.01$ . In all the hybrid schemes $I = 2,500$ . Different value of $d_{vc}$ are considered as indicated in the figure. . . . .	45
4.9	System performance for the pure RCM system and two groups of hybrid schemes when $p_1 = 0.005$ . The first group has 1,000 coded bits within 10,000 generated symbols and the values of $d_{vc}$ are 10, 12 and 14 respectively. The second group has 1,250 coded bits within 10,000 generated symbols and the values of $d_{vc}$ are also 10, 12 and 14. . . . .	46
5.1	Simplified computation at RP symbol nodes . . . . .	51
5.2	System performance for the simplified decoding method in the case of uniform sources when $T = 1$ . The labels represent parameters $(I, d_{vc})$ . The dashed line curve corresponds to the system performance using the original decoding method. . . . .	61

5.3	System performance for the simplified decoding method in the case of uniform sources when $T = 2$ . The labels represent parameters $(I, d_{vc})$ . The dashed line curve corresponds to the system performance using the original decoding method. . . . .	63
5.4	System performance for the simplified decoding method in the case of non-uniform sources with $p_0 = 0.1$ when $T = 2$ . The labels represent parameters $(I, d_{vc})$ . The dashed line curve corresponds to the system performance using the original decoding method. . . . .	64
5.5	Performance comparison of the simplified decoding method and the original decoding method for i.i.d. uniform sources. The labels represent parameters $\{(K, M, I)\}$ , throughput $T$ , and $d_{vc}$ . The blue dashed line indicates the performance of the original method, while the black solid line indicates the performance of the simplified method with the same design. . . . .	66
5.6	Performance comparison of the simplified decoding method and the original decoding method for i.i.d. non-uniform sources with $p_1 = 0.1$ . The labels represent parameters $\{(K, M, I)\}$ , throughput $T$ , and $d_{vc}$ . The blue dashed line indicates the performance of the original method, while the black solid line indicates the performance of the simplified method with the same design. . . . .	68
5.7	Performance comparison of the simplified decoding method and the original decoding method for i.i.d. non-uniform sources with $p_1 = 0.01$ . The labels represent parameters $\{(K, M, I)\}$ , throughput $T$ , and $d_{vc}$ . The blue dashed line indicates the performance of the original method, while the black solid line indicates the performance of the simplified method with the same design. . . . .	70
5.8	Performance comparison of the simplified decoding method and the original decoding method for i.i.d. non-uniform sources with $p_1 = 0.005$ . The labels represent parameters $\{(K, M, I)\}$ , throughput $T$ , and $d_{vc}$ . The blue dashed line indicates the performance of the original method, while the black solid line indicates the performance of the simplified method with the same design. . . . .	71
6.1	System diagram for a multiple access channel. . . . .	76
6.2	Encoder structure of the proposed hybrid coding scheme for the MAC. . . . .	77
6.3	Standard joint decoder for MAC applied to the hybrid scheme. . . . .	79

6.4	Structure of the proposed synthetic decoder for the MAC. . . . .	80
6.5	Structure of a synthetic RP node for the MAC. . . . .	83
6.6	Structure of a synthetic source bit node. . . . .	86
6.7	Simulation results for three groups of hybrid schemes when $p = 0.01$ . For each group, $(M, I)$ is fixed and $d_{vc}$ varies from 18 to 30. . . . .	92
6.8	Simulation results for three groups of hybrid schemes when $p = 0.005$ . For each group, $(M, I)$ is fixed and $d_{vc}$ varies from 18 to 30. . . . .	93
6.9	Performance of the proposed system with different information rates when $p = 0.01$ and $M = I$ . . . . .	94
6.10	Performance of the proposed system with different information rates when $p = 0.005$ and $M = I$ . . . . .	95
6.11	Performance comparison between the original decoding method and the simplified decoding method when $p = 0.01$ and $M = I$ . . . . .	96
6.12	Performance comparison between the original method and the simplified method when $p = 0.005$ and $M = I$ . . . . .	98

## ABSTRACT

Traditional analog and digital coding systems present their own advantages and constraints. Digital systems show excellent BER performance, but optimizing them over a wide range of signal to noise ratios (SNR) requires switching between different systems (e.g., adaptive coding). Analog systems allow high throughput communications over a wide dynamic range, but their bit error rate (BER) performance is not as good as in digital schemes. The aim of this work is to explore how to overcome these drawbacks by properly integrating both analog and digital systems into a hybrid one.

The proposed hybrid coding scheme is realized by parallel concatenation of Rate Compatible Modulation (RCM) and a Low Density Generator Matrix (LDGM) code. RCM generates its output symbols by standard linear combinations of input bits. In addition, an LDGM code produces a few output bits. Because of dense constellation and fine-grain energy accumulation, RCM is able to achieve smooth rate adaptation, but it experiences performance degradation due to the presence of error floors. The introduction of the LDGM code allows to reduce most of the residual errors, substantially improving the system performance.

This work considers the application of the hybrid scheme to point-to-point AWGN channels and to multiple access channels (MAC). For AWGN channels, our study focuses on optimizing the design for uniform and non-uniform memoryless sources. Decoding is implemented by building an appropriate graph and performing belief propagation. The influence of several design parameters on the system performance and the existing trade-offs are discussed. The proposed hybrid coding scheme achieves better performance than traditional joint source channel coding techniques in terms of gaps to the theoretical limit. We also introduce a simplified decoding technique for the proposed hybrid scheme. The idea is to treat the coded symbols as real values, and to use

a Gaussian approximation, so that very simple analog message passing can be applied. This substantially reduces the decoding complexity, while the system performance does not experience significant degradation.

For the MAC, a synthetic decoder structure and decoding algorithm has been developed and studied to tackle the ambiguity problem resulting from the existence of multi-level symbols proceeding from the RCM sub-block. The synthetic decoder also reduces the computational complexity by jointly considering messages propagated in the graph. As we will see, the hybrid scheme can achieve high transmission rates with good BER performance in MAC environments, even when the simplified decoding technique is applied.

## Chapter 1

### INTRODUCTION

This dissertation focuses on developing a hybrid analog-digital coding scheme for digital sources in different scenarios. The first problem we are trying to address is how to properly combining the analog and digital coding systems so that they do not degrade the performance of each other. The first part of the dissertation focuses on this problem, where we choose the analog and the digital components, and propose encoding and decoding structures. The second problem is to design good hybrid coding schemes over point-to-point AWGN channels for memoryless uniform and non-uniform sources. The decoding complexity of the proposed scheme is relatively high. Although the implementation is feasible by introducing proper decoding techniques, it is desirable to have a more efficient decoding algorithm. We address this problem in the third part. In the last part, we focus on the problem of transmission of correlated sources over MAC with the proposed hybrid coding scheme. This problem plays a critical part in many important applications, such as video compression and sensor networks. For this problem, there are two important questions. The first question is how to apply the proposed hybrid coding scheme in the MAC scenario. This results in two sub-problems. The first is how to design the joint decoder structure so that the decoding complexity is practical and the performance good. The second sub-problem is how to exploit the correlation between sources at the decoder site. The second important question is what factors contribute to the good design of a hybrid coding scheme over MAC. We try to address these problems by proposing a novel decoding structure for the MAC, and analyzing the effects of various design factors on the system performance.

## 1.1 Motivation

Digital coding and analog coding schemes have their respective advantages. Digital codes such as turbo codes and low-density parity check (LDPC) codes can achieve near capacity performance. They generally perform better than analog coding schemes in terms of rate distortion and capacity performance, which makes them good candidates in practical communication systems. However, digital codes lack robustness to changes in channel quality, i.e., they have a narrow dynamic range. Therefore, a group of coding systems has to be designed to adapt to different channel conditions. Even with the mechanism of switching between different systems, rate adaptation is staircase-like instead of a smooth one, resulting in the waste of spectrum resources. On the other hand, analog coding is robust to changing channel conditions. It has wide dynamic range, smooth rate adaptation, and high throughput capability. Moreover, for many analog coding schemes, there is low encoding and decoding complexity, and zero delay due to short block lengths. However, performance of linear analog coding systems is not as good as that of digital ones.

A new coding scheme that can overcome the disadvantages of analog and digital coding can be a promising design for future communication systems. As we will see in this dissertation, by properly combining analog and digital coding schemes, it is possible to maintain their respective advantages, while overcoming the drawbacks. This results in a hybrid coding scheme, where both analog and digital coding schemes work jointly. In this dissertation, we focus on binary sources.

The realization of this hybrid coding scheme requires a number of concepts and techniques. As the scheme is considered in various scenarios, such as in the presence of source redundancy or correlated sources, the idea of joint source channel coding is applied to jointly consider the compression and error protection for the source. Moreover, in the context of binary source inputs, it is challenging to find a proper “analog” coding scheme, as the input of most analog coding schemes are real-valued symbols. Compressive sensing, which has been studied in the literature in recent years, can be considered as an analog coding technique in broad sense, and a subset of the

studies on compressive sensing has considered binary data as the input to the system. Moreover, compressive sensing can be used for source compression and noise protection, making it good as a joint source channel coding scheme. These properties make it a good candidate for the analog component of the hybrid coding scheme, while a digital code with low encoding and decoding complexity will be chosen for the digital part.

## 1.2 Joint Source-Channel Coding

### 1.2.1 Separation Principle

In his fundamental work "A Mathematical Theory of Communication" [1], Shannon proved that reliable communications can be achieved as long as the transmission rate is below the channel capacity. This can be achieved by a separation approach, which divides the encoding process into two steps: first, compress the source up to its theoretical limit, which is given by the entropy  $H$ , by applying a source encoder. Then, protect the sequence by applying a capacity achieving channel code. This procedure maintains optimality, and also simplifies the construction of the system, as the source encoder can be optimized without any knowledge of the channel statistics, while the channel encoder can be optimized irrespectively of the source. Changes in either the source or the channel only lead to the modification of one part in the system, leaving the other unchanged.

However, the separation approach has several limitations in practical applications, and the optimality fails in general time-varying channels [2, 3], and multi-user channels. The separation approach requires long sequences, leading to high complexity and large delays, which is a problem for real-time communications. For multi-user channels, we no longer have an optimal system with this approach. In addition, the separation method may lead to catastrophic error propagation, as the channel code is not able to correct the errors when the channel quality falls below a certain threshold, which leads to the breaking down of the whole system. This lack of the robustness to changes in the channel quality may make it impractical to implement a system based on separation in scenarios where the channel quality changes.

### 1.2.2 Joint Source-Channel Coding Techniques

To address the aforementioned problems, source coding and channel coding can be considered and optimized jointly under certain constraints, which is referred to as joint source-channel coding (JSCC). The objective of JSCC is to integrate the source and channel coding modules into one processing module in order to reduce the complexity and achieve better results. Moreover, this may make transmission more robust to the effects of channel fading, noise and interference. JSCC can greatly improve the performance of the system in terms of distortion when there are complexity concerns, as shown in [4]. [5, 6, 7, 8, 9] study joint source-channel coding with complexity constraints for AWGN channels. In [5], an algorithm is developed to obtain the necessary conditions to achieve a local optimum solution by jointly considering the encoder and the modulation. [8] observes that with the same length constraint, the jointly optimized codes are better than separately designed and optimized codes.

As mentioned before, the separation theorem does not hold for fluctuating channels. Jointly considering many modules in the design would be more feasible and practical. [3] and [10] consider the case of time-varying channels. In [3], a joint optimization of a variable channel coder with a source coder is studied to minimize the distortion, while [10] extends the study by substituting the capacity achieving channel codes by channel codes with non-zero distortion to adapt to practical applications. [12] proposes an optimal rate allocation policy with a modified Gilbert noise channel, which models the combination of channel encoder, channel, and channel decoder, to minimize end-to-end distortion. [13, 14] use automatic repeat request (ARQ) for adaptive JSCC over independent and nonindependent channels. Implementation of JSCC over fading channels is studied in [15, 16, 17]. Using minimum mean-squared error as the optimality criterion, [15] presents a non-linear receiver to jointly optimize the vector quantizer and the modulation signal set using an iterative algorithm, while [16] uses linear coding and shows the power allocation strategy with and without channel state information (CSI) available at the transmitter. To simplify these algorithms, a header field with variable length coded data is inserted with minimum distance decoding [17].

There are many other works dealing with JSCC [19, 18, 20, 21, 22, 23, 24]. Unequal error protection (UEP) [25] has been designed to better protect more sensitive information bits which are prone to errors or to protect more important contents with stronger channel codes. This technique has been studied widely for the transmission of multimedia material [26, 27, 28]. Index assignment is the labeling of source symbols by binary integer numbers [29]. It is important in determining the overall distortion of a communication system in the presence of channel noise [30, 31, 32].

### 1.2.3 Distributed Joint Source Channel Coding for Correlated Sources

JSCC has also been used in the compression and error protection of correlated sources. In the case of multiple access channels (MAC), it is necessary to design the codewords for the different sources to take advantage of the correlation existing between sources [33]. [34] considers joint source-channel coding for two correlated binary information sequences with turbo codes. [35], [36], [37], and [38] propose practical coding schemes to deal with the problem with Turbo codes and concatenated LDGM codes, where the correlation is exploited by exchanging extrinsic information between two decoders constituting the joint decoder. If the correlation model is not known at the decoder, it can be estimated iteratively at the decoder site. [39, 40] extend the work by taking full advantage of the correlation in the decoding process. [41] designs turbo codes and serially concatenated LDGM codes for correlated sources. The cases where the correlation is known and unknown at the decoder site are both studied, and the resulting performance is very close to the theoretical limit. [42] and [43] introduce the use of a more straightforward design, parallel concatenated LDGM codes, which allows the correlation between sources to be preserved in the codewords by using the same encoder structure for both senders. For the MAC, there is ambiguity at the codeword level, i.e., the decoder needs to assign recovered codewords to the right senders. To solve this problem, the outer coded bits are interleaved and a fraction of the inner coded bits are also interleaved with serial LDGM codes in [41]. With parallel LDGM codes, it is not necessary to interleave high rate coded bits when the degree is high, as

the ambiguity only exists at the codeword level. With the help of an identification bit at each sender, the ambiguity can be resolved. As shown in [42] and [43], the resulting performance is better than the theoretical limit assuming the separation approach. Other codes have also been studied in this scenario. LDPC codes are used for data collection in wireless sensor networks (WSNs) [44], and a single Raptor code is used for both video compression and packet loss protection for scalable video transmission over wireless networks [45]. However, few existing joint source-channel coding schemes are capable of high transmission rate with good performance.

### 1.3 Compressive Sensing

Compressive sensing (CS) was introduced in 2004 by Donoho, Candes, Romberg and Tao [46, 47, 48]. The idea is that a sparse signal can be recovered from a limited set of linear measurements, even when the dimension of the measurement is smaller than the dimension of the signal [47, 49]. The reason is that the whole information of the sparse signal can be represented with only a few significant components. Natural images, speech signals and medical images are all good examples of signals having sparse representation. The system model can be represented as

$$\underline{Y} = G\underline{X}, \quad (1.1)$$

where  $G \in \mathbb{R}^{m \times n}$  is sampling matrix or measurement matrix,  $\underline{Y} \in \mathbb{R}^m$  is the compressed measurements, and  $\underline{X}$  is the original signal we want to recover. There are generally three cases in terms of signal recovery:  $m = n$ , where a unique solution exists;  $m > n$ , i.e., the dimension of the compressed measurements is greater than that of the original signal, where a single best approximate solution can also be found; and  $m < n$ , which is the usual case. In this last case there are infinite solutions, and the sparsity of the source is exploited to recover  $\underline{X}$ . There are many recovery algorithms including convex relaxation [50, 51], matching pursuit [52, 53, 54], iterative threshold methods [55], subspace pursuit [56], and Bayesian frameworks [57, 58].

CS can be used as a joint source-channel coding scheme [59, 60, 61, 62, 63, 64, 65, 66, 67]. [68] develops a framework based on distributed compressed sensing (DCS),

which utilizes the joint sparsity to exploit intra-signal and inter-signal correlations. In [69], a distributed joint-source channel communication system, in which processing and communication are combined into one operation, is proposed to save scarce resources in wireless sensor networks such as power and bandwidth. [70] reveals many aspects of CS in joint source-channel coding. Sparse Distributed Compression is proposed for a family of correlated sources, which provides a trade-off between compression rate and decoding complexity. Similarly, sparse Channel Coding is proposed by combining CS with random channel coding, which provides a trade-off between the capacity loss and the decoding complexity. [71] considers the usage of CS for joint source-channel coding for sources exhibiting temporal and spatial dependencies. Similar to [69], [72] also considers the energy aspect of CS based wireless sensor applications. It evaluates the trade-off between the transmission energy and the recovery quality. Notice that these studies only consider highly-sparse real-valued signals and the complexity of the decoding algorithm is high. However, some of this research shows an important characteristic in CS: robustness, which is somehow the drawback of traditional digital coding techniques. In addition, CS provides a promising approach for high throughput systems, which are widely used in wireless communication networks [73, 74, 75].

Although these algorithms can be extended to digital signals, their high computational complexity and failure to effectively exploit the digital nature of binary sources require research of new methods. Several techniques have been studied including [76], where the principle of turbo encoding decoding is applied by the adoption of a permutation based sensing matrix and an iterative recovery algorithm with maximum likelihood (ML) local detector, [77], where the CS process is modeled with a bi-partite graph and a novel sampling matrix with unique sum property has been designed, and [78], where analog fountain codes (AFCs) [79] are used for the compression and reconstruction of sparse binary signals. In order to reduce the decoding complexity of CS, [80, 81, 82] proposes different ways of applying constraints. In [81] and [82], a closed form formulation has been derived for the decoding of binary input sources. Belief propagation is used for the decoding process of CS over noisy channels. Therefore,

the advantages of CS make it an excellent candidate for the analog component of the proposed hybrid scheme, but its drawbacks, shown in previous studies, have to be dealt with in the new scheme.

#### 1.4 Dissertation Organization

This dissertation starts by providing an overview of the proposed hybrid coding scheme. The hybrid coding scheme is realized by parallel concatenation of Rate Compatible Modulation (RCM) and a Low Density Generator Matrix (LDGM) code. RCM is essentially a CS scheme that generates most of the output symbols by standard linear combinations of input bits, and an LDGM code that generates a few digital bits. RCM is able to achieve high throughput and smooth rate adaptation, but it experiences performance degradation due to the presence of error floors. Because of this, its performance is far from the Shannon theoretical limits, especially at high SNR values. The introduction of the LDGM code is able to reduce most of the residual errors in the RCM scheme, substantially improving the system performance.

In Chapter 2, we discuss the structure of the hybrid coding scheme and its components: the RCM scheme as the analog component and the LDGM code as the digital component. The advantages and drawbacks of the RCM scheme will be studied, as well as those of LDGM codes. Then, we introduce the encoder structure of the hybrid coding scheme to explain how to combine the two components so that they encode the source jointly without interfering with each other.

After defining the type of hybrid schemes that will be studied in this work, we present the decoding architecture and algorithms for the proposed scheme in Chapter 3. Due to the operations involved in the encoding process, the generated symbols are related to the original information block through generator matrices. Therefore, a bipartite graph can be formed from this relationship. Belief propagation is a powerful technique to perform decoding in graphs, and we apply it to the decoding of the hybrid system. We will discuss how to integrate the message passing for the analog and the digital components within the hybrid scheme.

In Chapter 4, we will investigate the application of the hybrid scheme to point-to-point AWGN channels. For AWGN channels, our study focuses on optimizing the design for uniform and non-uniform memoryless sources. For uniform sources, we approach the design by tackling the problems existing in RCM systems. RCM is able to achieve smooth rate adaptation in a broad dynamic range, but it suffers from performance degradation, especially at high SNRs, resulting from high error floors. By properly introducing LDGM codes, the error floor can be significantly reduced. For non-uniform sources, we will design hybrid schemes for different degrees of source sparsity. The redundancy existing in the source can be exploited to further improve the throughput in communication systems. The influence of several design parameters on the system performance and their trade-offs will be discussed. We will see that the proposed hybrid coding scheme has better performance than traditional joint source channel coding schemes in terms of gaps to the theoretical limit.

In Chapter 5, we will discuss a simplified decoding algorithm for the proposed hybrid schemes in the context of AWGN channels. Because of the usage of random projections in the encoding process, obtaining the probability mass function (pmf) of the weighted combination of the inputs at the constraint node (RP symbol node) in the iterative decoding process is expensive. In order to reduce the computational complexity, we propose a simplified method to approximate the distribution of the linear combination as Gaussian, so that only the mean and the variance of the approximated distribution are to be computed. We can also approximate the distribution of each input bit as Gaussian in the iterative decoder, so that analog message passing can be applied [115]. We provide the complexity analysis for the original decoding method and the proposed simplified method. The complexity is measured in number of additions and multiplications. As will be shown, the simplified decoding algorithm substantially reduces the decoding complexity by one order of magnitude. Simulation results show that the BER performance of the system using the simplified method is similar to the original one, experiencing small degradation in some cases. This makes it possible to implement faster systems when necessary.

In Chapter 6, we will study the application of the hybrid scheme for the transmission of correlated sources over multiple access channels. In this case, it is well known that separation between source and channel coding is not optimal, although the theoretical limit is not known. The basic idea for the transmission of correlated sources over a multiple access channel is to keep the existing correlation in the codewords produced at the encoders, which allows the exploitation of the correlation at the decoder. The superposition of the multi-level RP symbols proceeding from the senders introduces ambiguity in the standard decoding process. To solve the problem, we propose a novel synthetic decoder structure and a decoding algorithm for the new structure to consider messages jointly for the RCM sub-block, so that the ambiguity introduced by the multi-level RP symbols can be effectively eliminated. In order to evaluate the proposed approach, we compare the system performance with the theoretical limit assuming that the separation approach is used. Simulation results will show that the performance of the system is close to that bound when high transmission rate is considered, and that the hybrid scheme is robust to the sparsity of the source, as in the case of point to point AWGN channels. The results also show that the proposed scheme is capable of implementing a communication system that transmits at a much higher information rate than standard digital coding techniques. The simplified method is also extended for the MAC. Finally, Chapter 7 summarizes the contributions of this dissertation and provides suggestions for future work.

## Chapter 2

### HYBRID ANALOG-DIGITAL ENCODER

#### 2.1 Introduction

In this chapter, we study the encoder structure of the hybrid analog-digital coding scheme. It consists of an RCM system, the analog component and essentially CS with binary inputs, and an LDGM code, the digital component. The structure and work flow of an RCM system is explained, as well as the structure of an LDGM code. After that, we study the parallel concatenation of an RCM system and an LDGM code to build the proposed hybrid coding scheme.

The remainder of the chapter is organized as follows. In Section 2.2 we review the structure of the RCM scheme, mainly of the matrix design, encoding and modulation process. Section 2.3 discusses the encoding structure of the LDGM code. In Section 2.4, we provide the encoder structure of the hybrid coding scheme. Finally, the conclusion is given in Section 2.5.

#### 2.2 Rate Compatible Modulation

Adaptive modulation and coding (AMC) [84], [85], is a popular rate adaptation technique that has been deployed widely in practice. It requires accurate and instant channel estimation, but, even if the sender knows the channel conditions perfectly, only stair-case rate adjustments can be achieved. Hybrid automatic repeat request (HARQ) [86] can obtain a smoother rate adjustment through an acknowledgment mechanism that controls the retransmission activity of the sender. However, the dynamical rate range of HARQ is limited. RCM [87] tackles the adaptation problem by generating random projections (RP) from weighted sums of information bits, similar to compressed

sensing with binary input symbols. The generated symbols are used to form a constellation directly, without the need of any labeling. RCM is robust to changes in the channel quality, provides a smooth rate adaptation, and is robust to variations in the sparsity of the source.

The basic idea of RCM is to generate multi-level real-valued symbols by weighted linear combinations of input bits. This process is realized by using a random mapping matrix with real-valued entries. This bit-to-symbol mapping is essentially a CS scheme with binary input. On the other hand, since the generated RP symbols are directly mapped into constellation points, RCM can be considered as a coded modulation scheme. Moreover, in addition to the function of error protection, RCM also performs compression of the data. Therefore, it is an enhanced version of coded modulation. In conventional modulation, the free distance, i.e. the minimum Euclidean distance between adjacent constellation points, is controlled by the rate of the modulation. The rate of modulation is determined by the number of bits a constellation symbol contains (for instance, 16-QAM or 64-QAM). However, there is a second way to adjust the free distance instead of switching between different modulations for channel adaptation. As mentioned in [89], the free distance is proportional to  $E_b$ , the average energy per information bit. Therefore, different free distances can be obtained by varying the number of transmitted symbols to accumulate the average energy per information bit. More specifically, larger distances can be obtained by accumulating symbols at the receiver. However, with conventional modulation, the accumulation of the energy is not even, which leads to uneven BER. With RCM, even energy allocation is achieved [87]. The reason is that each constellation point is formed by a random mapping from bits instead of a fixed mapping, allowing each bit to be sampled by multiple symbols.

Figure 2.1 represents the encoding graph. Each one of the RP symbols is formed by a weighted linear combination of input bits. Each link has an associated weight and the source bits connected to each RP symbol are randomly chosen. Specifically, if the input block is denoted as  $\underline{b} = [b_1, b_2, \dots, b_K]^T$ , the vector of RP symbols  $\underline{a}$  is generated as  $\underline{a} = G_r \cdot \underline{b}$ , where  $G_r$  is a generator matrix with entries belonging to the weight set

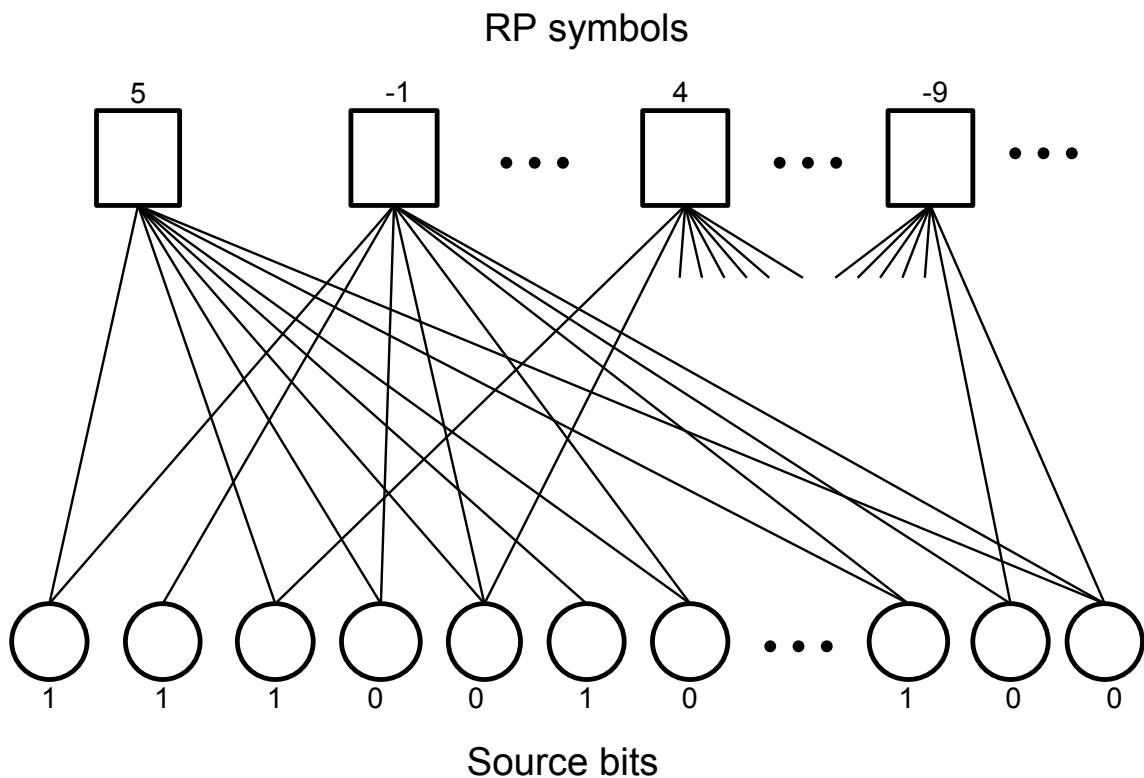


**Figure 2.1:** Bipartite graph representation of an RCM system.

$\{\pm g_1, \pm g_2, \dots, \pm g_F\}$ . The choice of weight set determines the characteristics of the constellation, and the number of sampled bits per RP symbol. Therefore, this choice is crucial to the performance of an RCM scheme.

There are certain constraints in constructing the generator matrix (see [87, 88] for details). Basically, the generator matrix,  $G_r$ , is constructed from a unit matrix  $G_0$ . Without loss of generality, let us assume the weight set is  $\{\pm g_1, \pm g_2, \pm g_3, \pm g_4\}$ . We construct matrix  $G_0$ , with dimension  $K/2 \times K$ , where  $K$  is the number of input bits,

as

$$G_0 = \begin{bmatrix} \pi(A_{g_3}) & \pi(A_{g_4}) & \pi(A_{g_1}) & \pi(A_{g_2}) \\ \pi(A_{g_1}) & \pi(A_{g_2}) & \pi(A_{g_3}) & \pi(A_{g_4}) \\ \pi(A_{g_4}) & \pi(A_{g_3}) & \pi(A_{g_2}) & \pi(A_{g_1}) \\ \pi(A_{g_2}) & \pi(A_{g_1}) & \pi(A_{g_4}) & \pi(A_{g_3}) \end{bmatrix},$$

where  $\pi(\cdot)$  is the operation of random column permutations of a matrix, which is different for each sub-matrix, and  $A_{g_i}$  is the elementary matrix with specific structure

$$A_{g_i} = \begin{bmatrix} +g_i & -g_i & & & & \\ & & +g_i & -g_i & & \\ & & & & \ddots & \\ & & & & & +g_i & -g_i \end{bmatrix}.$$

By using different permutation choices and arrangements of  $A_{g_i}$  positions in  $G_0$ , different matrices  $G_0$  can be constructed, each leading to different system performance. Notice that, in general, the proposed scheme is used at high rates, so the number of RP symbols will be much less than the number of input bits. In this case, we construct matrix  $G_r$  by using the desired number of rows in matrix  $G_0$ . To generate one RP symbol, one row from  $G_r$  is used. If more rows are needed, we would stack two or more matrices  $G_0$ , and then choose the appropriate number of rows. Since every weight from the weight set appears exactly once in each row, every RP symbol node has a degree of  $2F$ , i.e.,  $2F$  links connected to every RP node in Figure 2.1, and every weight has exactly one associated link.

Finally, RP symbols are grouped two by two and transmitted directly through the channel. Notice that the resulting constellation is QAM, but the number of symbols in the constellation will depend on the cardinality of the RP symbols. For instance, if the RP symbols range from integer  $-x$  to integer  $x$  and the values are consecutive, the number of constellation points would be  $(2x+1) \times (2x+1)$ . Based on the distribution of the constellation points, the expected energy of a constellation point can be obtained and the normalization factor can be computed. For instance, Figure 2.2 shows the constellation for the modulation of a RCM scheme with weight set  $\{\pm 1, \pm 2, \pm 4, \pm 4\}$ .

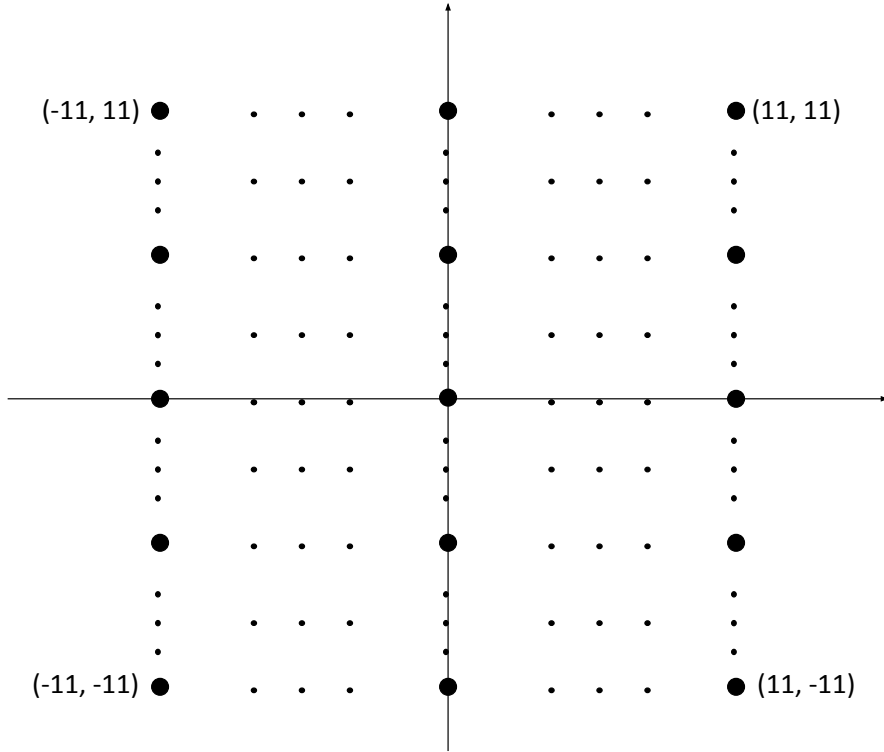


**Figure 2.2:** Illustration of constellation for an RCM scheme with weight set  $\{\pm 1, \pm 2, \pm 4, \pm 4\}$ .

The value range of an RP symbol can be computed:  $a_m \in [-11, 11]$ . Notice that not every weight set can generate an interval with consecutive values. Thus, two consecutive RP symbols with value  $x_1$  and  $x_2$  are mapped into  $(x_1, x_2)$  directly in the constellation. Since each dimension has 23 candidate values, a  $23 \times 23$  QAM constellation can be formed. Notice that due to the transmission power constraint, the constellation is normalized based on its distribution.

### 2.3 Low Density Generator Matrix (LDGM) Codes

Random-like codes with iterative decoding are able to approach capacity. Turbo codes [90] and low-density parity check (LDPC) codes [91, 92, 93, 94] have been widely studied and applied in a variety of systems. Turbo codes have been the primary coding

scheme in the third and fourth generation (3G and 4G), while LDPC will replace them in 5G. However, complexity constraints in some practical applications present challenges. Turbo codes have low encoding complexity, but the decoding complexity is high. On the other hand, LDPC codes have low decoding complexity and high encoding complexity. Therefore, a random-like code with low encoding and decoding complexity would be a good candidate in many applications.

Low density generator matrix (LDGM) codes, first recognized by MacKay [94], are a special family of LDPC codes which, due to the sparse nature of their generator matrix, have low encoding complexity. On the other hand, LDGM codes also utilize the sparse matrix for decoding as in LDPC, so they also have low decoding complexity. Different from the standard LDPC codes, regular LDGM codes have excellent performance, and the improvement that can be obtained using irregular LDGM codes rather than regular ones is very small<sup>1</sup>. However, LDGM codes suffer from error floors that are independent of the block length. LDGM codes with small degrees have high error floors but good convergence thresholds, which the contrary happens when the degrees are high [98]. Because of the existence of error floors, LDGM codes were first considered bad codes [94] or error-reduction codes [96]. However, with some adaptation, LDGM codes can be very good for standard communication channels: serial [98], [97], [99] or parallel [100] concatenation of two regular LDGM codes can reduce the error floors significantly to achieve performance comparable to state-of-the-art codes. The idea of the parallel scheme is to use a powerful low rate code together with a high rate code. The low rate code is capable of correcting most of the errors, while the high rate code is designed to eliminate as many of the residual errors as possible.

For a systematic LDGM code of rate  $R_c = K/N$ , the generator matrix with binary entries can be expressed as  $G_l = [I; P]$ , where  $I$  is a  $K \times K$  identity matrix and  $P$  is a  $K \times (N - K)$  sparse matrix. If the systematic bits are denoted as  $\underline{b} = [b_1, b_2, \dots, b_K]$ , the coded bits are generated as  $\underline{c} = \underline{b}P$ , with  $\underline{c} = [c_1, \dots, c_M]$ . These bits, together

---

<sup>1</sup> Irregular codes are those in which the number of ones changes for different rows/columns in the generator matrix.

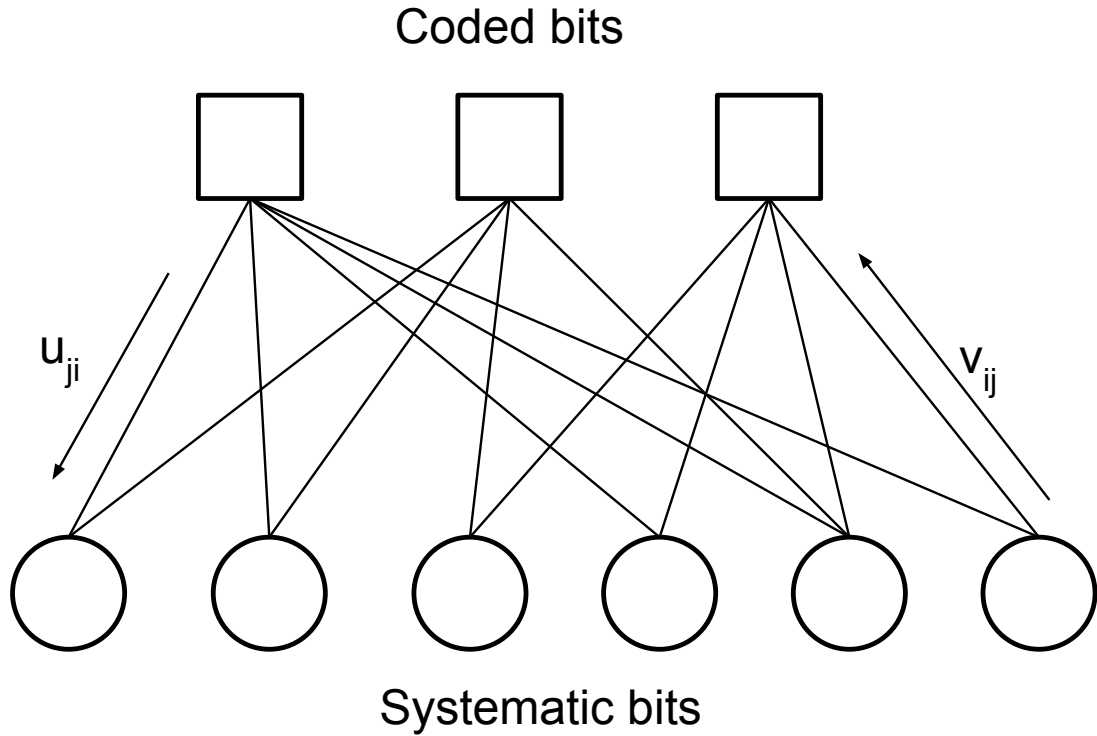


**Figure 2.3:** Bipartite graph representation of an LDGM code

with the information bits are transmitted through the channel. Figure 2.3 shows the structure of an LDGM code. Circle nodes represent systematic bits,  $\underline{b}$ , while rectangular nodes represent coded bits,  $\underline{c}$ . Links between the nodes are constructed from the generator matrix  $G_l$ . Therefore, the degree of a coded bit node, i.e., the number of links a coded bit node has, is the number of 1's in each column of  $G_l$ , while the degree of a systematic node is the number of 1's in each row. At the decoder, instead of using the parity check matrix to decode as in the case of LDPC codes, LDGM codes use the generator matrix for the decoding process. A regular LDGM code can be defined by the parameter set  $(N, K, d_u, d_c)$ , which denote the codeword length, the systematic bits block length, and the row weight and column weight of matrix  $G_l$ .

## 2.4 The Structure of the Hybrid Scheme

Performance degradation in RCM is expected, as random projections using XOR combinations of input bits (as in Low Density Generator Matrix, LDGM, codes) present error floors, while linear random projections of real numbers (e.g., compressed sensing) also get stuck in terms of performance at high SNRs [112]. This explains the need to utilize a digital channel code, in this case an LDGM code, as the digital coding sub-block of the hybrid scheme, aiming at reducing the error floor. Interestingly, LDGM codes are also able to achieve smooth rate adaptation [95], and thus, since both sub-blocks are able to achieve smooth error adaptation, the hybrid scheme will also have this property.

The fact that the proposed hybrid coding scheme utilizes LDGM codes as the digital sub-block to reduce the error floor proceeding from the RCM sub-block requires some comments. It is well known that LDGM codes are characterized by the existence of significant error floors, which can be reduced greatly by serial or parallel concatenation of two regular LDGM codes. The idea of the parallel scheme in LDGM codes is to use a powerful low rate code and a high rate code. The low rate code is capable of correcting most of the errors, while the high rate code is designed to eliminate as many of the residual errors as possible. In the proposed parallel concatenated hybrid system, the digital-to-analog RCM sub-block substitutes the low rate LDGM code. The RCM sub-block generates RP symbols and uses a QAM modulation so that RP symbols are directly mapped to the corresponding constellation point. On the other hand, a high rate LDGM code generates a small number of bits and uses an independent 4-QAM modulation in which the average energy of the channel symbols is the same as that in RCM sub-block. At the receiver, the RCM and LDGM sub-blocks perform decoding jointly using belief propagation/message passing [113, 114]. As we will see later, the RCM sub-block is able to correct most of the errors, while the LDGM sub-block corrects most of the remaining ones, so that the error floors of pure RCM schemes are eliminated in practice and much better performance can be achieved.

The encoder structure of the proposed hybrid system is shown in Figure 2.4.

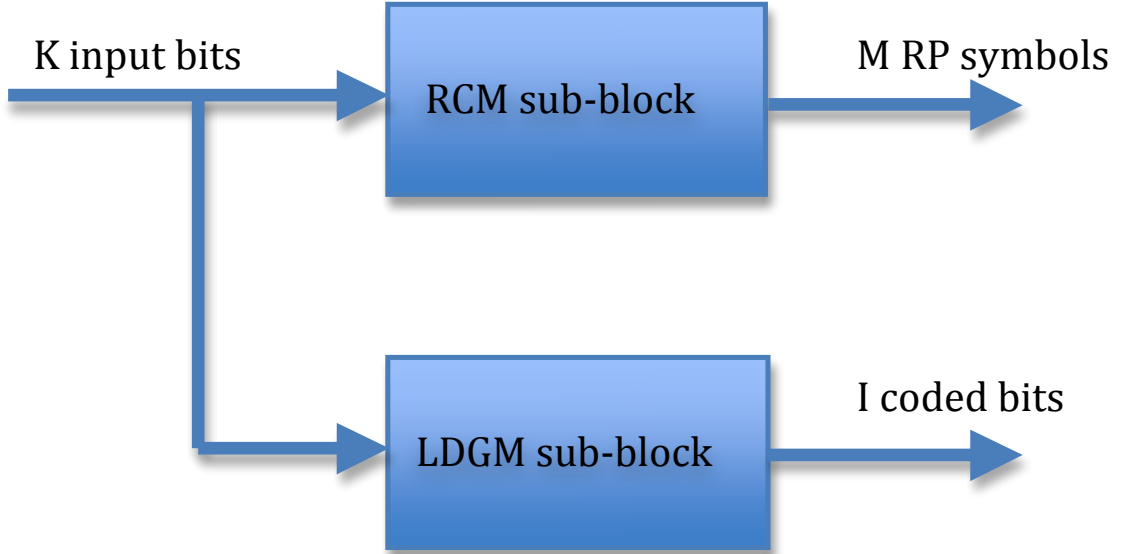


**Figure 2.4:** Encoder diagram of the proposed hybrid system consisting of the parallel concatenation of an RCM sub-block and an LDGM code.

It consists of a parallel encoder structure of an RCM scheme, which from  $K$  input bits produces  $M$  RP symbols, and a high-rate regular LDGM code that produces  $I$  non-systematic coded bits from the  $K$  input bits. We denote the input source bits as  $\underline{b} = [b_1, b_2, \dots, b_K]^T$ . The sparse generator matrices for the RCM sub-block and LDGM sub-block are denoted as  $G_r$  and  $G_l = [I; P_l]$ , respectively. The coded symbols are generated as  $\underline{C}_s = [G_r \underline{b}; \underline{b}^T P_l] = [\underline{a}, \underline{c}] = [a_1, \dots, a_M, c_1, \dots, c_I]$ , which are transmitted through a noisy channel. Notice that the matrix operations involved in generating  $\underline{a}$  and  $\underline{c}$  are different:  $G_r \underline{b}$  is a normal linear combination while  $\underline{b}^T P_l$  is modular operation.  $\underline{a}$  and  $\underline{c}$  use different modulations: every two consecutive RP symbols in  $\underline{a}$  are grouped and mapped to one constellation point directly, while bits in  $\underline{c}$  use a 4-QAM constellations. At the receiver, the corrupted sequence at the decoder is denoted as  $\underline{r} = [\underline{a}', \underline{c}']$ , where  $a'_m = a_m + e_m$  and  $c'_l = c_l + e_l$ , with  $e_m$  and  $e_l$  being the noise introduced by the channel.

As explained before, RP symbols and coded bits are grouped two by two and

transmitted using a QAM constellation, so that the throughput,  $T$ , is

$$T = \frac{2 \cdot K}{M + I}, \quad (2.1)$$

and the information rate,  $R$ , is calculated as

$$R = TH. \quad (2.2)$$

where  $H$  is the entropy of the binary source.

## 2.5 Conclusion

In this chapter, we have reviewed the analog and digital components of the proposed hybrid coding scheme. The RCM, which can be seen as a compressive sensing scheme with digital input, as well as coded modulation with compression function, is robust to the channel conditions and has a smooth rate adaptation by providing an even distribution of energy to the information bits. However, it suffers from error floors. LDGM codes are very good codes when used in concatenated schemes, and they have low encoding and decoding complexity. Based on the idea of parallel concatenation, we have proposed the encoder structure for the hybrid scheme. The encoding process has been explained, as well as the modulation method.

## Chapter 3

### HYBRID ANALOG DIGITAL DECODER: BELIEF PROPAGATION

#### 3.1 Introduction

The decoding for the hybrid scheme can be seen as a method to find the most probable solution for the equation  $\underline{a} = G_r \underline{b}$  and  $\underline{c} = \underline{b}^T P_l$ , where  $\underline{a}$  is the vector of RP symbols generated at the RCM encoder,  $\underline{c}$  is the vector of coded bits generated at the LDGM encoder and  $\underline{b}$  is the source vector that we want to calculate. Denote the received vectors as  $\underline{r} = [\underline{a}', \underline{c}']$ , the optimum decoder aims at finding the bit vector with the maximum a posteriori (MAP) probability:

$$\hat{\underline{b}} = \arg \max_{\underline{b} \in \{0,1\}^K} P(\underline{b}|\underline{r}). \quad (3.1)$$

As a brute force approach to obtain  $\hat{\underline{b}}$  is not practical, we will build a factor graph for the hybrid system and utilize belief propagation/message passing [114] to perform decoding.

The remainder of the chapter is organized as follows. Section 3.2 explains the decoder structure of the hybrid scheme, i.e., the way to build the bipartite graph for belief propagation. Section 3.3 provides a detailed description of the message update rule for each group of nodes. Section 3.4 briefly discusses the order to activate the nodes in the graph. Finally, Section 3.5 concludes the chapter.

#### 3.2 Decoder Structure

Because RP symbols and coded bits are associated with source bits through their respective generator matrix, a factor graph/bipartite graph can be formed [113], [114], as shown in Figure 3.1. The graph consists of three groups of nodes: RP symbol

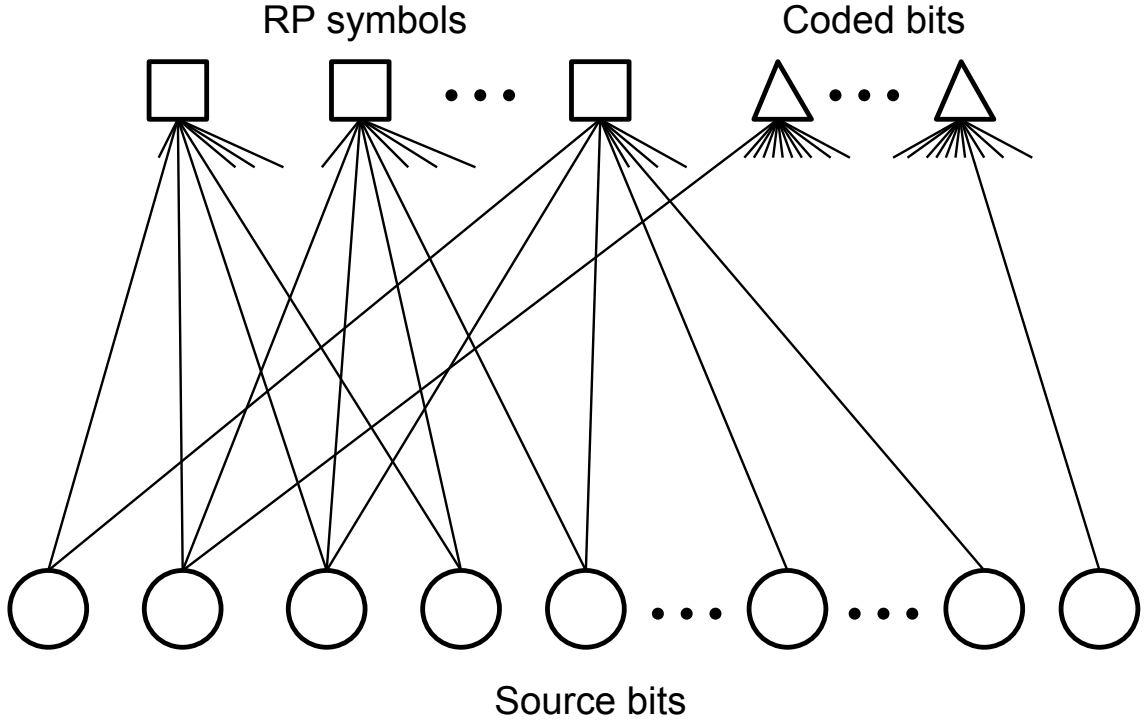


**Figure 3.1:** Bipartite graph representation of the proposed hybrid system consisting of the parallel concatenation of an RCM sub-block and an LDGM sub-block.

nodes, coded bit nodes and source bit nodes. Each node connects to some other nodes, i.e., neighboring nodes, in a different group. Notice that links are only between source bit nodes and RP symbol nodes, and between source bit nodes and coded bit nodes. These links are constructed from two generator matrices: the links between RP symbol nodes and source bit nodes are from  $G_r$ , and the links connecting coded bit nodes and source bit nodes are from  $G_l$ . The difference is that in the RCM sub-block the links are weighted, but there is no weight associated with links in the LDGM sub-block. As explained in Section 2.2, because of the special structure in  $G_r$ , every RP symbol node has the same degree, which is equal to the size of the weight set.

### 3.3 Message Passing for the Hybrid Scheme

The decoding algorithm is obtained by applying belief propagation/message passing to the graph [114], [96]. One problem we need to address is how to integrate the message passing of both sub-blocks: in RCM pmf messages are usually exchanged, while log likelihood ratio (LLR) messages are normally used in LDGM codes. As the source bits are binary, the pmf can be represented by LLR values. Thus, the messages can be easily exchanged between the RCM sub-block and the LDGM sub-block by just using LLR values. The LLR values are only converted to a pmf representation when updating the links of the RP node, as the operation of linear combination of input bits for multi-leveled RP symbols require the use of the corresponding pmfs for the computation of messages.

The details of the decoding algorithm are provided below, defining all the messages as Log-Likelihood Ratios (LLRs). In the description, we will use  $b$  to denote a source bit node,  $a$  to denote an RP symbol node, and  $c$  to denote a coded bit node. An overview of the notation used in the sequel is shown in Table 3.1. Notice that the same algorithm can be applied for pure RCM schemes by just discarding the steps in the coded bit nodes.

#### 3.3.1 Initialization

Message passing starts with the initial information on the source bit nodes. Assume source bits are transmitted, and let the channel observation be  $r_b$ . The initial information consists of two parts: channel information and the prior knowledge of the input bits. Thus, the Log-Likelihood Ratio (LLR) value of the initial information can be computed as

$$u_0 = \log \frac{Pr(r_b|b=0)}{Pr(r_b|b=1)} + \log \frac{p_0}{p_1} = -\frac{2\sqrt{E_s}r_b}{\sigma^2} + \log \frac{p_0}{p_1}, \quad (3.2)$$

where as defined before  $p_0 = 1 - p_1$  is the probability that an input bit is equal to 0,  $E_s$  is the average energy used to transmit one symbol through the channel, and  $\sigma^2$  is the noise variance. Message  $u_0$  has to be taken into account in all iterations of the message

**Table 3.1:** Notation used in the message passing for the hybrid scheme

Notation	Definition
$b$	Source bit node
$a$	RP symbol node
$c$	Coded bit node
$r_b$	Channel observation of the source bit node
$r_s$	Channel observation of the RP symbol node
$r_c$	Channel observation of the coded bit node
$d_a$	Degree of an RP symbol node
$d_c$	Degree of a coded bit node
$d_{va}$	Degree of a source bit node only considering connections with RP symbol nodes
$d_{vc}$	Degree of a source bit node only considering connections with coded bit nodes
$v_i$	LLR message from a source bit node to its $i$ th neighboring node (an RP symbol node or an coded bit node)
$u_j$	LLR message from an RP symbol node or coded bit node to its $j$ th neighboring source bit node
$b_j$	The $j$ th neighboring source bit node of an RP symbol node or a coded bit node
$w_j$	The $j$ th weight of an RP symbol node

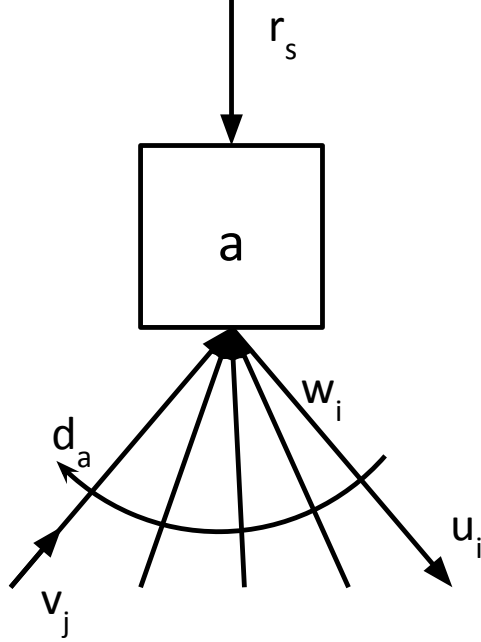


**Figure 3.2:** Computation at an RP symbol node.

passing algorithm. If the source bits are not sent through the channel,  $u_0$  would only be computed from the prior knowledge of the source bits.

### 3.3.2 Computation at the RP symbol nodes

As shown in Figure 3.2, an RP symbol node has channel observation  $r_s$ , and  $v_j$ 's as incoming messages. Channel observation  $r_s$  does not change throughout the iterations and is taken as the initial information for the RP symbol node. This initial information will be transformed to a pmf vector that contains the priori probability of each possible value for the RP symbol. Messages  $v_j$ 's come from neighboring source bit nodes and do change in each iteration as they are updated in the iterative process.

Assume we calculate the outgoing messages for the  $j$ th RP symbol node. There are  $d_a$  incoming LLR messages, with  $v_j = \log \frac{P(b_j=0)}{P(b_j=1)}$  corresponding to the one proceeding from the  $j$ th neighboring source bit node  $b_j$ . Because RP symbols are multi-leveled,

the computations are implemented using pmfs. Therefore,  $v_j$  will be converted to a pmf based on its value and the associated weight of the link. Specifically,

$$Pr(b_j^w = 0) = \frac{e^{v_j}}{1 + e^{v_j}} \quad (3.3)$$

$$Pr(b_j^w = w_j) = \frac{1}{1 + e^{v_j}}, \quad (3.4)$$

where  $b_j^w = w_j b_j$ , i.e., the weighted bit. As mentioned previously, the pmf messages are converted back to LLR messages when passed back to the neighboring source bit nodes. Notice that

$$r_s = \Gamma a + n = \Gamma \sum_{j=1}^{d_a} w_j \cdot b_j + n, \quad (3.5)$$

where  $r_s$  is the received value corresponding to the RP symbol node,  $\Gamma$  is the normalization factor,  $n \sim N(0, N_0/2)$ , and  $w_j$  is the weight associated with the link between RP node  $a$  and  $j$ th neighboring source bit node  $b_j$ . From (3.5), the probability of each possible value of  $a$  can be computed and the pmf of  $a$  can be obtained as  $\mathbf{P}_a$ , which is calculated only once throughout the iterations. If  $a \in [-l, l]$ , then  $\mathbf{P}_a$  is defined as

$$\mathbf{P}_a = [P_a(-l), \dots, P_a(l)], \quad (3.6)$$

where  $P_a(k)$  is the density at value  $k$ , computed from the distribution  $N(r_s, \sigma^2)$ , and  $\mathbf{P}_a$  is normalized so that the sum of the densities is equal to one. As discussed before,  $\mathbf{P}_a$  is taken as the initial information of the RP symbol node. By denoting the linear combination of all  $b_j$ 's except  $b_j$  as

$$x_i = \sum_{\substack{j=1, \\ j \neq i}}^{d_a} w_j \cdot b_j, \quad (3.7)$$

we can express

$$a = x_i + w_i \cdot b_i. \quad (3.8)$$

Therefore, the probability of  $b_i$  being 0 and 1 can be calculated as

$$P(b_i = 0) = P(a = x_i) = \sum_k P(x_i = k) \cdot P(r_s | a = k), \quad (3.9)$$

$$P(b_i = 1) = P(a = x_i + w_i) = \sum_k P(x_i = k) \cdot P(r_s | a = k + w_i), \quad (3.10)$$

where the sum in  $k$  is over all possible values of  $x$ . Notice that the pmf of  $x_i$ ,  $P(x_i = k)$ , is calculated in a straightforward manner by convolving the pmf of the terms in (3.7),  $w_j b_j$ , while  $P(a = k | r_s)$  and  $P(a = k + w_i | r_s)$  can be obtained from  $\mathbf{P}_a$ .

The operation of convolving the pmf of  $w_j \cdot b_j$  to obtain the pmf of  $x_i$ ,  $i = 1, \dots, d_a$  is computationally expensive. The number of convolution operations for each RP symbol node is  $d_a$  in each iteration, which makes this step the bottleneck of the decoding algorithm in terms of computational complexity. A solution is to compute the convolution only once and implement a deconvolution process  $d_a$  times, which takes much less complexity [88]. The first step is to compute the pmf of the overall linear combination  $\sum_{j=1}^{d_a} w_j b_j$ , denoted as  $\mathbf{P}_x$ , by convolving the pmfs of all  $w_j b_j$ 's. In the encoding process, the value of the RP symbol is equivalent to the result of the linear combination. However,  $\mathbf{P}_a$  and  $\mathbf{P}_x$  are different, as  $\mathbf{P}_a$  is obtained from the channel information, while  $\mathbf{P}_x$  is obtained by combining the information from other parts of the network. By deconvolving the pmfs of  $w_i b_i$ 's from  $\mathbf{P}_x$ , the pmf of  $x_i$  can be obtained. The deconvolution can be implemented recursively or iteratively. The detailed explanation can be found in [88].

Finally, the pmfs are converted back to an LLR message so that it can be easily exchanged in the graph. The LLR message exchanged from the RP node to its  $i$ th neighboring source bit node,  $b_i$ , is calculated as

$$u_i = \log \frac{P(b_i = 0)}{P(b_i = 1)}. \quad (3.11)$$

### 3.3.3 Computation at the coded bit nodes

A coded bit node is shown in Figure 3.3. Similar to an RP symbol node, it has channel observation  $r_s$ , and  $d_c$  incoming LLR messages,  $v_i$ , from its neighboring

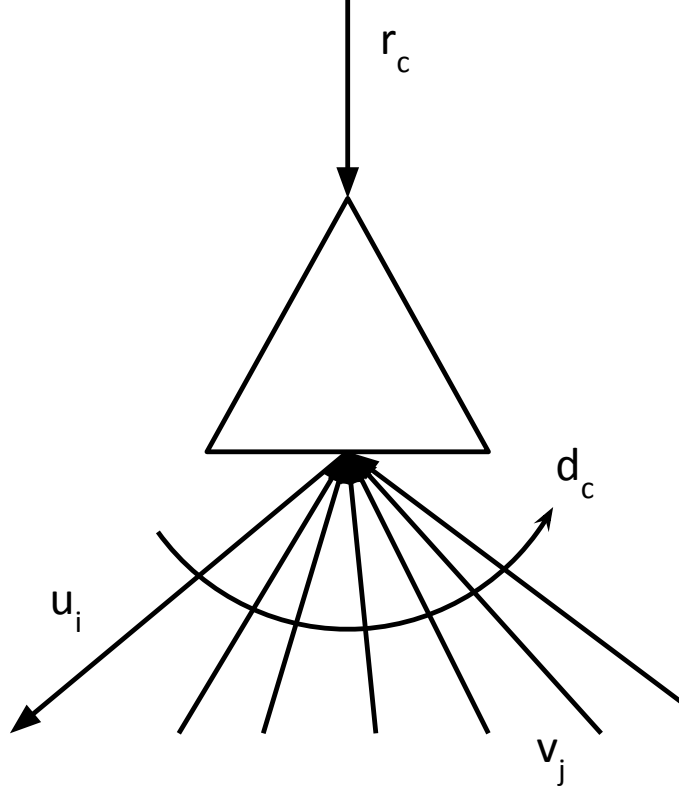


**Figure 3.3:** Computation at a coded bit node.

source bit nodes. We denote the channel message of the coded bit node  $c$  as  $v_0$ . Same as for  $u_0$ ,  $v_0$  should be taken into consideration in the computation of the messages proceeding from the coded bit nodes in each iteration. Its value is calculated as

$$v_0 = \log \frac{P(r_s | c = 0)}{P(r_s | c = 1)}. \quad (3.12)$$

As in standard LDGM codes, the LLR message transmitted from the coded bit node  $c_j$  to its  $i$ th neighboring source bit node  $b_i$  can be obtained as [98]

$$u_i = 2 \operatorname{atanh} \left( \prod_{\substack{j=0 \\ j \neq i}}^{d_c} \tanh \left( \frac{v_j}{2} \right) \right). \quad (3.13)$$

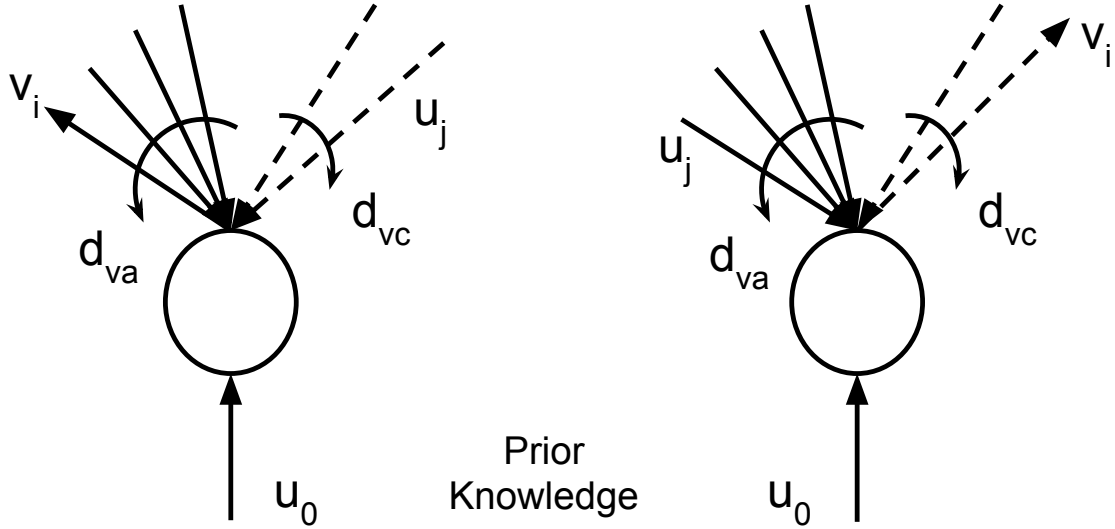


**Figure 3.4:** (a) Computation of the message exchanged from a source bit node to an RP symbol node, (b) Computation of the message exchanged from a source bit node to a digital coded bit node.

### 3.3.4 Computation at the source bit nodes

A source bit node is shown in Figure 3.4. Incoming information consists of three parts: the channel information, denoted as  $v_0$ , messages from the RP symbol nodes and messages from the coded bit nodes. For each source bit node, the message to the  $i$ th neighboring node (either RP symbol node or coded bit node) is computed as

$$v_i = \sum_{\substack{j=0 \\ j \neq i}}^{d_{va}+d_{vc}} u_j. \quad (3.14)$$

After any iteration, the value of information bit node  $i$  can be determined by calculating

$$d_i = \sum_{j=0}^{d_{va}+d_{vc}} u_j. \quad (3.15)$$

If  $d_i$  is greater than 0, the decision for this bit will be 0. Otherwise, it will be 1.

### 3.4 Decoding Schedule

Belief propagation starts from the source bit nodes with the initial information. The nodes are activated serially by order of appearance in the schedule definition. The schedule can be defined as:

- Decoding Schedule: Repeat  $\underline{b}, \underline{a}, \underline{c}$ ,

where  $\underline{b}$  is the group of source bit nodes,  $\underline{a}$  is the group of RP symbol node, and  $\underline{c}$  is the group of coded bit nodes. Thus, three groups of nodes are activated sequentially by the order defined repetitively until the decoding process ends.

It is possible to define other activation schedules by activating the source bit nodes between the activation of RP symbol nodes and coded bit nodes. Since there is no significant performance change, we just utilize the schedule indicated above. Therefore, each group of nodes are activated exactly once in each iteration. The process continues until the termination condition is satisfied: either a fixed number of iterations are completed or all source bit nodes make the same decision five times in a row.

### 3.5 Conclusion

The decoding algorithm is the cornerstone for the implementation of the hybrid scheme. We have explained the construction of the bipartite graph from the generator matrices of the RCM and the LDGM code. We have also discussed the problem of integrating the message passing for the RCM and the LDGM sub-blocks. The exchanged messages are maintained as LLRs except when computing the outgoing messages for the RP node. By converting the LLR messages to the corresponding pmf, RP symbol nodes can complete their computations and convert the pmf back to LLR messages to be passed to the source bit nodes. We have also provided the detailed message update algorithms for the RP symbol nodes, the coded bit nodes and the source bit nodes, as well as the decision method. Finally, we have provided the schedule for activating the nodes in the graph.

## Chapter 4

### APPLICATION TO POINT-TO-POINT AWGN CHANNELS

#### 4.1 Introduction

In this chapter, we design hybrid schemes for the point-to-point AWGN channel for sources with different degrees of non-uniformity. More specifically, the application of the hybrid scheme for the transmission of uniform and non-uniform sources over noisy AWGN channels is studied. We explain the design objectives for the RCM sub-system and the LDGM sub-system within the hybrid scheme. We adopt a non-systematic approach for the design, i.e., the source bits are not transmitted through the channel. The reason is that generally non-systematic codes have better performance than systematic ones [105], [106], [107].

We first consider the case of uniform sources. As will be shown, the incorporation of the LDGM code substantially reduces the error floor existing in the RCM scheme, and the overall performance improves significantly. We will extend our study to the transmission of non-uniform sources. Simulation results show that the hybrid coding scheme has excellent BER performance with high throughput. For non-uniform sources, the designed hybrid coding scheme is robust to the degree of source non-uniformity, and able to maintain the gap to the theoretical limit, outperforming many traditional digital coding techniques.

The remainder of the chapter is organized as follows. Section 4.2 summarizes the design objectives for the RCM sub-block and the LDGM sub-block within the hybrid coding schemes. Section 4.3 focuses on the problem of the transmission of i.i.d. uniform sources over AWGN channels, presenting simulation results, while Section 4.4 considers the transmission of i.i.d. non-uniform sources over AWGN channels. Section 4.5 concludes the chapter.

## 4.2 Design Objective

The key design parameters for the hybrid scheme are the weight set for the RCM scheme, the ratio between the number of RP symbols and the number of coded bits, and the degree of the source bit node only considering the LDGM sub-block. As discussed in Chapter 2, different weight sets generate RP symbols with different value ranges, which results in different constellations. The weight set also determines the number of source bits participating in producing an RP symbol, i.e., the degree of the RP symbol node. Therefore, the choice of weight set is critical to the performance of the RCM system, affecting the performance of the whole system. The ratio between the number of symbols produced by analog and digital sub-blocks determines their relative influences in the hybrid scheme. Each sub-block has its own design objectives and there is a trade off that depends on the ratio. Our approach is to search for a good weight set for the RCM sub-block, and fix it for our further study on the impact of the two other design factors on the system performance. Monte Carlo simulations are used to evaluate the performance of the hybrid scheme.

If the total number of generated symbols, including RP symbols and coded bits, is fixed, the ratio between the number of symbols produced by the analog and digital sub-blocks can be explicitly expressed by the number of the coded bits, denoted as  $I$ . As the LDGM encoder is a high rate encoder, the number of the coded bits would be small. As the intuition behind the hybrid scheme is that the analog part takes care of most of the errors while the digital part correct the residual errors, the introduction of an LDGM code should not interfere or degrade the performance of the RCM sub-block. Otherwise, the RCM sub-block would not be able to reduce errors to a certain level that can be corrected by the LDGM sub-block. On the other hand, if the number of the coded bits is too small, i.e., the rate of LDGM code is too high, the LDGM would not be powerful enough to reduce the error floors. Therefore, the ratio is critical.

The other important design factor is the degree of the source bit node when only considering the LDGM sub-block, which is denoted as  $d_{vc}$ . This degree and the number of coded bits determine the performance of the LDGM sub-block. Assume that the

number of the coded bits,  $I$ , is fixed. If  $d_{vc}$  is too large, there would be cycles in the LDGM sub-block graph, which could degrade the performance significantly. On the other hand, if  $d_{vc}$  is too small, the code would not be powerful enough to correct residual errors. The parameter  $d_{vc}$  largely determines the convergence threshold and where the “waterfall” region does happen: larger  $d_{vc}$ ’s delay the convergence threshold and lead to lower error floors. Therefore, different design requirements may need different  $d_{vc}$ ’s.

### 4.3 Uniform Memoryless Sources

The work started by tackling the error floor problem in the pure RCM system when the input is i.i.d and uniformly distributed. We performed Monte Carlo simulations for pure RCM systems and several proposed hybrid schemes to evaluate their performance and the impact of the design factors. For comparison purposes, in all simulations we fixed the transmission rate to 7.4 information bits per channel use, and considered an input block length of 37,000 bits. Therefore, the total number of symbols at the output of the hybrid system is 10,000,  $I$  of which proceeding from the LDGM code and  $10,000 - I$  from the RCM system ( $I \ll 10,000$ , with  $I=0$  for the pure RCM system). Since QAM signaling is utilized, the channel is used 5,000 times. Notice that we simulated 5,000 blocks for each hybrid scheme and obtained the average BER.

For the implementation of the pure RCM system we utilized the weight set  $\{\pm 1, \pm 2, \pm 4, \pm 4\}$ , which in [88] was the best choice for i.i.d. uniformly distributed input bits. To implement the hybrid system, we first fixed the weight set, and modified the value of  $I$ . Another parameter that affects the performance of the hybrid system is  $d_{vc}$ , as mentioned previously.

Figure 4.1 shows the resulting BER for the pure RCM system defined before and for three hybrid schemes using the same weight set as the pure RCM system for the RCM sub-block and a regular non-systematic LDGM with parameters  $(I, d_{vc})$  equal to (100,3), (148, 2) and (200,1)<sup>1</sup>. As shown in the figure, the pure RCM system has a

---

<sup>1</sup> Notice that since the input block length is fixed to 37,000 and the LDGM code is regular, the code is perfectly defined by  $I$  and  $d_{vc}$ .

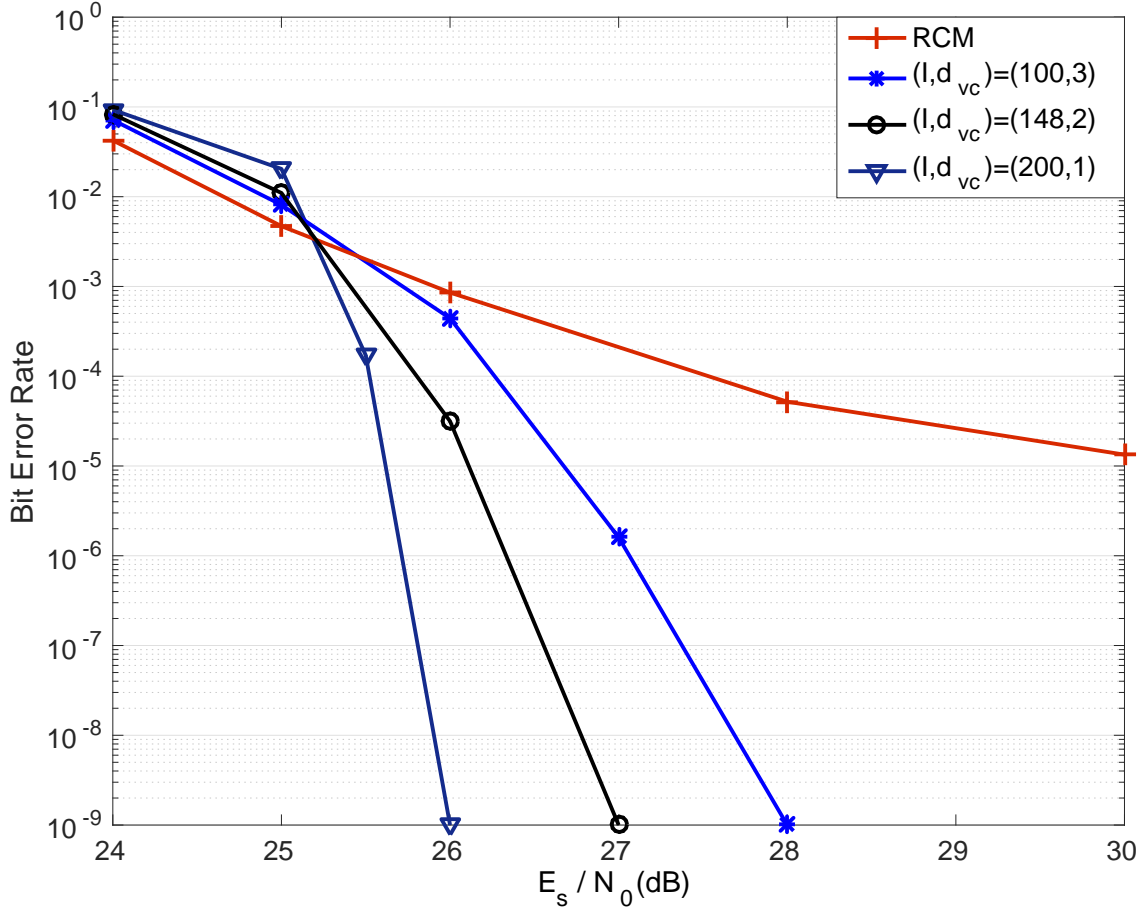


**Figure 4.1:** System performance for the pure RCM system and three hybrid schemes when the weight set of the RCM sub-block is  $\{\pm 1, \pm 2, \pm 4, \pm 4\}$ . The length of the information bits is 37,000 and the number of channel uses is 5000 for a rate of 7.4 information bits per channel use.

relatively high error floor of around  $10^{-4}$ - $10^{-5}$ , while the hybrid schemes are able to practically eliminate the error floor. Notice that the convergence threshold improves when  $I$  increases.

We performed numerous simulations of hybrid systems with different parameters  $(I, d_{vc})$ . For a fixed  $d_{vc}$ , we have investigated the system performance when the range of  $I$  varies between 50 and 400 bits. We have observed that when  $I$  decreases, the number of blocks that contain errors also decreases, as well the number of errors in the blocks in error. However, when  $I$  is too small the number of blocks in error begins to

increase again. As discussed before, if  $I$  is too large, the RCM sub-block will become weaker, as the number of RP symbols will decrease too much, and this will affect the behavior of the whole hybrid system. On the other hand, if  $I$  is too small, error floors can not be reduced and not much improvement is observed.

We have also studied the system performance when the value of  $I$  is kept constant and  $d_{vc}$  varies. Specifically, we have considered the values 0.8, 1, 2, 3, and 4 for  $d_{vc}$ . We have observed that when the degree decreases, the number of blocks that contain errors decreases, but the number will begin to increase for very small values of  $d_{vc}$ . The intuition behind this observation is that when the value of  $d_{vc}$  is high, the degree of the coded bit node will be very high (notice we have 37,000 input bits but only  $I$  coded bits). This will produce a graph with many cycles, in which the performance of message passing will suffer substantial degradation. On the other hand, if  $d_{vc}$  is smaller than 1, some information bit nodes will have no connection to the LDGM sub-block part, which will affect the performance of the whole hybrid scheme.

Notice that the hybrid designs that we have considered until now are based on using the best weight set found in [88] for the pure RCM scheme. However, a weight set that leads to the best possible performance in pure RCM will not necessarily be the optimal choice for the hybrid scheme. The reason is that in a pure RCM scheme the objective is to obtain the best possible performance, while, in the hybrid scheme, the objective of the RCM sub-block is to leave, for all blocks, a residual number of errors that can be corrected by the LDGM sub-block. This is an important difference. For instance, for a pure RCM scheme a weight set that led to one tenth of blocks with 200 residual errors would be a much better choice than a weight set with which all the blocks had 100 errors. However, if the high rate LDGM code were able to correct up to 150 residual errors, the hybrid scheme would not be able to help at all in the former case, while it would eliminate all the errors in the latter and obtain an overall much better performance. In other words, if the total number of errors is the same, the RCM scheme that has a more even distribution of errors among blocks is the better choice for the hybrid scheme.

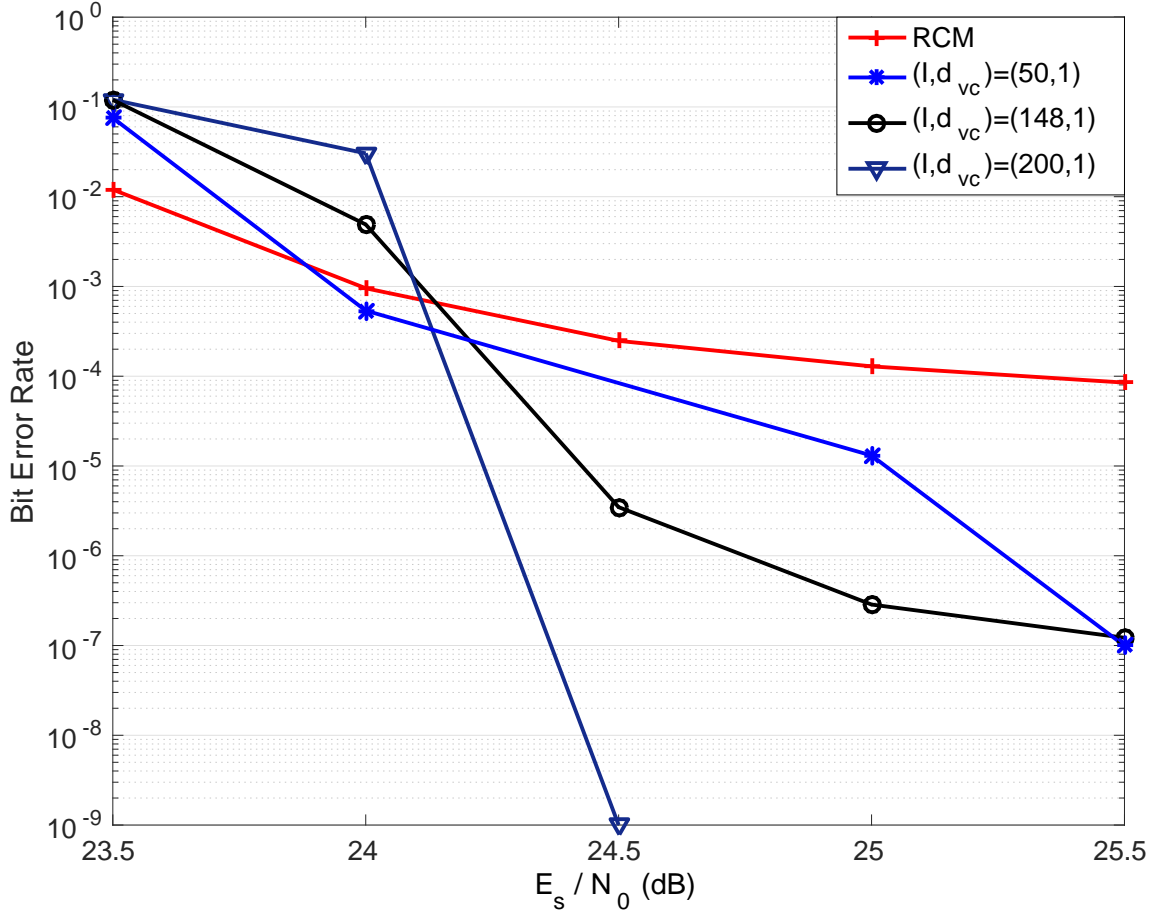


**Figure 4.2:** System performance for the pure RCM system and three hybrid schemes when the weight set of the RCM sub-block is  $\{\pm 2, \pm 3, \pm 4, \pm 8\}$ . The length of the information bits is 37,000 and the number of channel uses is 5000 for a rate of 7.4 information bits per channel use.

With this in mind, we searched for good weight sets for the hybrid scheme. Figure 4.2 shows the BER performance for a pure RCM and three hybrid systems that utilize  $\{\pm 2, \pm 3, \pm 4, \pm 8\}$  as the weight set in the RCM sub-block. Notice that the pure RCM system in Figure 4.2 gets to a BER level of  $10^{-3}$  at 24 dB, while Figure 4.1 gets to the same level at 26 dB. Although the RCM system in Figure 4.2 has a flatter and higher error floor at high SNR, the level of  $10^{-3}$  indicates that the average number of errors for each block is around 37, which is easy for the LDGM sub-block to correct. Therefore, the performance improvement when a hybrid scheme is used is

huge. Compared with the best case in Figure 4.1, where error free decoding is achieved at  $E_s/N_0 = 26$  dB, the hybrid scheme with parameters  $(I, d_{vc})=(200,1)$  achieves error free decoding at  $E_s/N_0 = 24.5$  dB, only 2.3 dB away from the Shannon limit. The reason is that, looking for instance at  $E_s/N_0 = 25.5$  dB, the RCM sub-block in Figure 4.1 presents errors in all blocks, with an average number of errors of 77 and a maximum number of 185. Therefore, there are many blocks that cannot be corrected by the high-rate LDGM sub-block. On the other hand, although the RCM sub-block in Figure 4.2 also presents errors in all blocks, the maximum number of errors is always less than 10 and thus the high-rate LDGM code will be able to correct all the residual errors, leading to error free performance.

## 4.4 Non-uniform Memoryless Sources

### 4.4.1 Background

In standard channel coding, the input to the channel encoder is assumed to be i.i.d. uniformly distributed, i.e., the input does not have any redundancy. However, in practical applications, sources like texts, images, and speech often present redundancy. In this case, a standard approach is to apply an ideal source encoder to compress the source and eliminate all the redundancy to produce i.i.d. uniform input for a capacity achieving channel encoder. This approach is referred to separation theorem. Thus, the theoretical limit can be expressed by

$$HR_c < \frac{1}{2} \log_2 \left( 1 + \frac{2E_s}{N_0} \right) \quad (4.1)$$

where  $H$  is the entropy of the source,  $R_c$  is the code rate, and  $E_s$  is the average energy per channel symbol. However, most source existing encoders are only suboptimal. Therefore, the input to the channel encoder still contains a certain degree of redundancy. Considering this and the reasons discussed in Section 1.2.1, it is important to study this joint source-channel coding problem to simplify the design and take advantage of the source redundancy to combat noise. Hagenauer first proposed in [101] a source-controlled channel decoding scheme. In [102, 103], a systematic approach was

adopted to optimize the encoder structure by modifying the extrinsic information to exploit the redundancy. However, the drawback of systematic codes is that the output coded sequences are not uniformly distributed for most redundant sources, which is far from the capacity achieving distribution [104]. The reason is that systematic codes force constraint on the channel input distribution by including source bits in the transmitted symbols. Without the constraint, the distribution of transmitted symbols can better match the channel. Based on this idea, the work in [102, 103] was extended in [105, 106], where non-systematic convolutional encoders are used as the constituent encoders to produce asymptotically uniform outputs: the channel mutual information is maximized, and substantial gains can be obtained over systematic turbo codes. In [107], non-systematic LDPC codes based on the concatenation of a pre-coder or post-coder with an LDPC or an LDGM encoder was proposed. The systematic bits are not sent over the channel, with only a-priori information provided for the systematic bit nodes at the decoder. The proposed encoder/decoder structures can be configured in many ways, providing design flexibility. [108] continues the study by using high rate non-systematic LDPC codes.

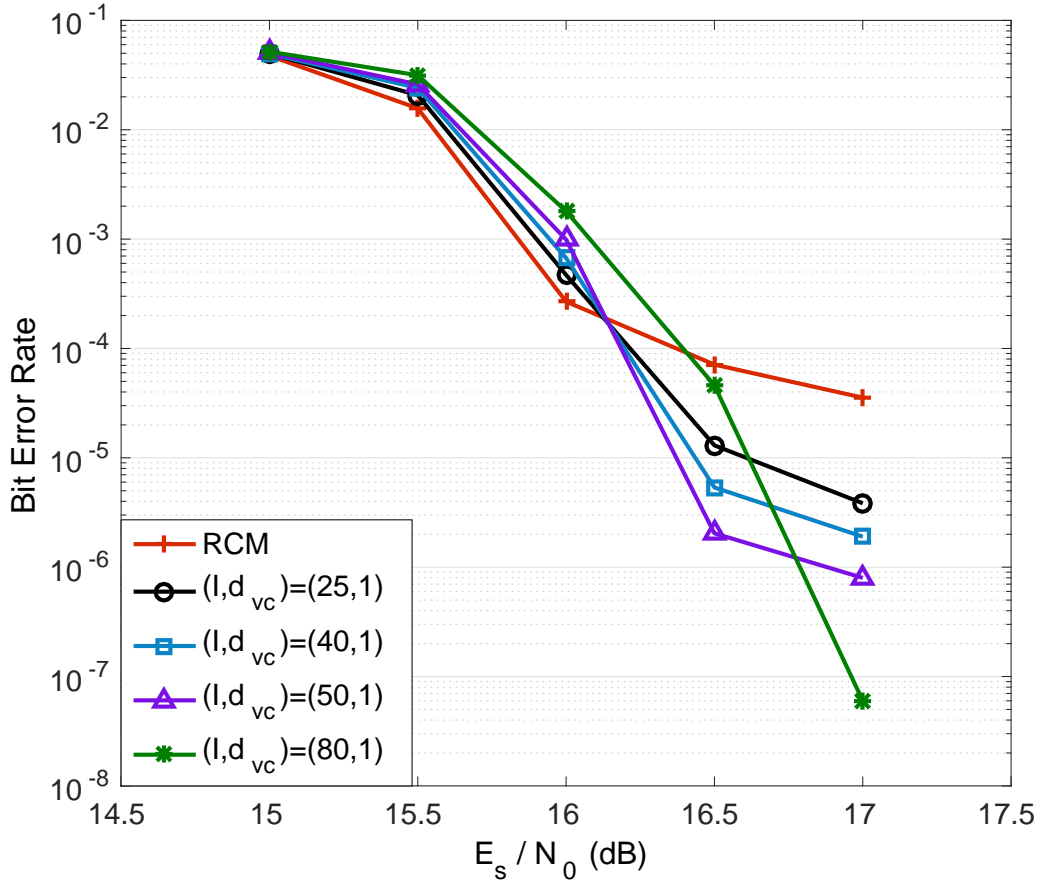
Other methods for this scenario have also been studied. In [109, 110], an unequal energy allocation (UEA) scheme with turbo codes was studied, where the non-uniformity of the source was taken into account to generate non-binary PAM symbols. This approach successfully lowered the sensitivity of the scheme to the degree of source non-uniformity, which was a problem in [105, 106]. Using unequal energy allocation, the gap to the theoretical limit increases less with the increase of source non-uniformity. Systematic and non-systematic LDPC codes with UEA were proposed in [111], resulting in better performance than previously LDPC based schemes for nonuniform sources. However, all previous schemes still present sensitivity to the degree of source non-uniformity, and performance degrades when the source becomes more asymmetric. Moreover, few of them consider the case in which high throughput is required, which is a common requirement in many practical communication systems.

#### 4.4.2 Simulation Results

As explained before, we adopt a non-systematic approach to design the hybrid coding scheme for non-uniform sources. For the simulations, we consider i.i.d. non-uniform sources with  $p_1 = 0.1, 0.01, 0.005$ , where  $p_1$  is the probability of a source bit being 1. In order to assess the system performance, we focus on the case in which the code rate is  $R_c = 5$ . Because QAM is used to transmit the generated symbols, the throughput of the system is 10. The length of the input binary stream is fixed to 50,000. Therefore, the total number of symbols at the output of the encoder will be 10,000,  $I$  of them proceeding from the LDGM sub-block and  $10,000 - I$  from the RCM sub-block ( $I = 0$  for the pure RCM system). Since QAM signaling is utilized, the channel will be used 5,000 times.

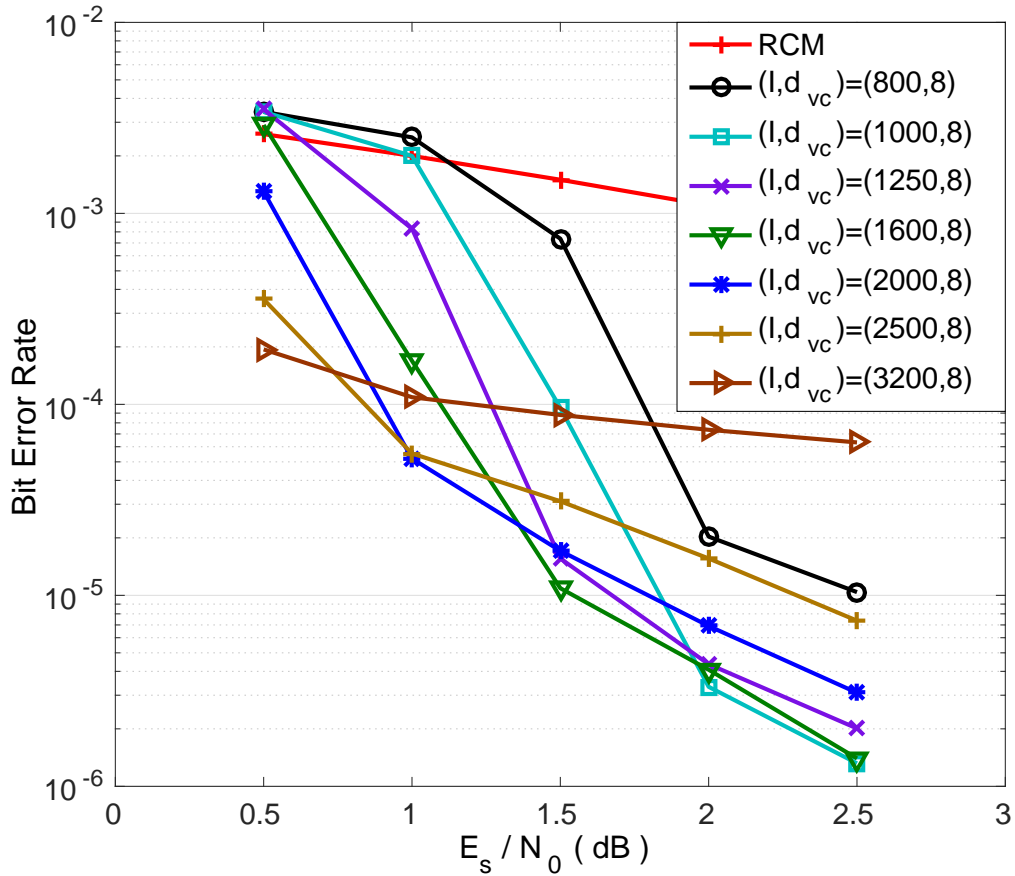
In our simulations, we use the weight set  $W = \{\pm 1, \pm 1, \pm 1, \pm 1, \pm 2, \pm 2, \pm 2, \pm 2\}$  for the implementation of the pure RCM system and of the RCM sub-block in the hybrid scheme. This weight set has been optimized via Monte-Carlo techniques for the hybrid system. After fixing the weight set, we still focus on optimizing the two important parameters that affect the performance of the hybrid scheme:  $I$ , the number of coded bits within the generated symbols, and  $d_{vc}$ , the degree of the input bit nodes when only the LDGM connections are considered. In general, the optimal parameter set  $(I, d_{vc})$  depends on the degree of the source non-uniformity.

Figure 4.3 shows the resulting performance for the source with  $p_1 = 0.1$ . The four hybrid schemes use the same weight set (defined before) for the RCM sub-block as the pure RCM system, and a regular non-systematic LDGM code with parameters  $(I, d_{vc})$  equal to  $(25, 1)$ ,  $(40, 1)$ ,  $(50, 1)$  and  $(80, 1)$ . For an objective of  $\text{BER} < 10^{-4}$  or  $\text{BER} < 10^{-5}$ , the best result is obtained with  $(I, d_{vc}) = (50, 1)$ . Notice that with the increase in the number of bits,  $I$ , within the generated symbols, the convergence threshold tends to degrade and the “waterfall” region tends to be steeper. The pure RCM system has a relatively high error floor of around  $10^{-4}$ - $10^{-5}$ , while the hybrid schemes are able to reduce and eventually practically eliminate the error floor.



**Figure 4.3:** System performance of a pure RCM system and four hybrid systems when  $p = 0.1$ . In all the hybrid systems  $d_{vc} = 1$  and the weight set is the same as in the pure RCM system, as defined in the text. Different number of coded bits,  $I$ , are considered as indicated in the figure.

For the source with  $p_1 = 0.01$ , Figure 4.4 shows the performance of hybrid systems with different number of coded bits,  $I$ , within the 10,000 generated symbols. For all seven hybrid schemes in the figure,  $d_{vc}$  has been fixed to 8, which is the optimal degree we have found through simulations. Again, the hybrid schemes use the same weight set (defined before) for the RCM sub-block as the pure RCM system. In this case, the gain obtained by using hybrid systems is more significant than in the case of  $p_1 = 0.1$ . When  $I$  increases from 0 to 1,000, the error floor experiences a substantial reduction with respect to the pure RCM system. However, when  $I$  continues to



**Figure 4.4:** System performance of a pure RCM system and seven hybrid systems when  $p = 0.01$ . In all the hybrid systems  $d_{vc} = 8$  and the weight set is the same as in the pure RCM system, as defined in the text. Different number of coded bits,  $I$ , are considered as indicated in the figure.

increase, the error floor becomes higher again. On the other hand, the convergence threshold experiences a consistent improvement with the increase in  $I$ . If  $BER < 10^{-4}$  is taken as a criterion, the best scheme would be the one having  $I = 2,500$  coded bits within the 10,000 generated symbols.

In order to study the impact of  $d_{vc}$ , the best scheme in Figure 4.4,  $(I, d_{vc}) = (2500, 8)$ , is chosen. Figure 4.5 shows the results when the number of coded bits is fixed and the degree is varied. An interesting observation is that here hybrid schemes also show the dangling performance with the increase of  $d_{vc}$  observed in Figure 4.4. The

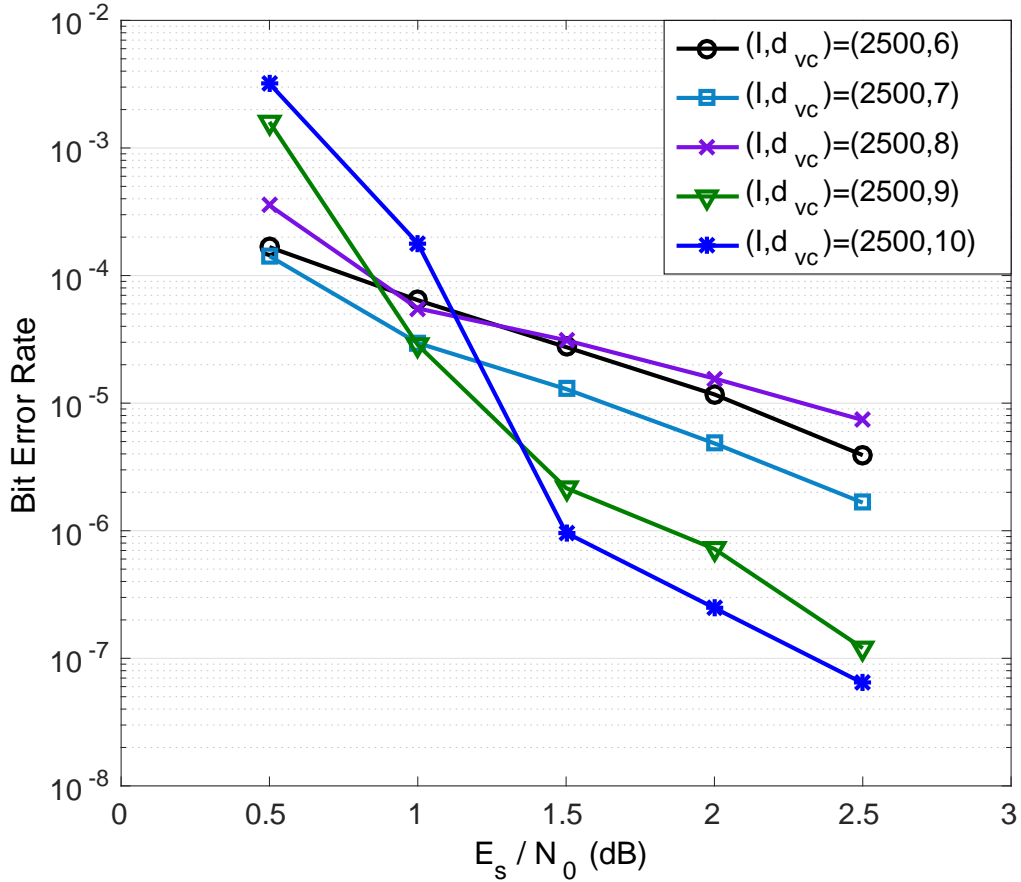


**Figure 4.5:** System performance for five hybrid schemes when  $p_1 = 0.01$ . In all the hybrid systems  $I = 2500$ . Different values of  $d_{vc}$  are considered as indicated in the figure.

error floor is reduced with the increase of  $d_{vc}$ , while the convergence threshold improves first and starts to degrade when  $d_{vc} = 7$ . In terms of  $BER < 10^{-4}$  or  $BER < 10^{-5}$ , the performance of the best scheme in Figure 4.4 is further improved.

We further simulate two groups of hybrid schemes, where each group has the same value of  $I$  but different values of  $d_{vc}$ , as shown in Figure 4.6. Schemes with both good convergence threshold and error floor performance are chosen from Figure 4.4: (1000, 8) and (1250, 8). The group with 1000 coded bits is represented by solid lines in Figure 4.6 and the other group with 1,250 coded bits is represented by dashed lines. Within each group,  $d_{vc}$  ranges from 6 to 10. A clear observation is that within each

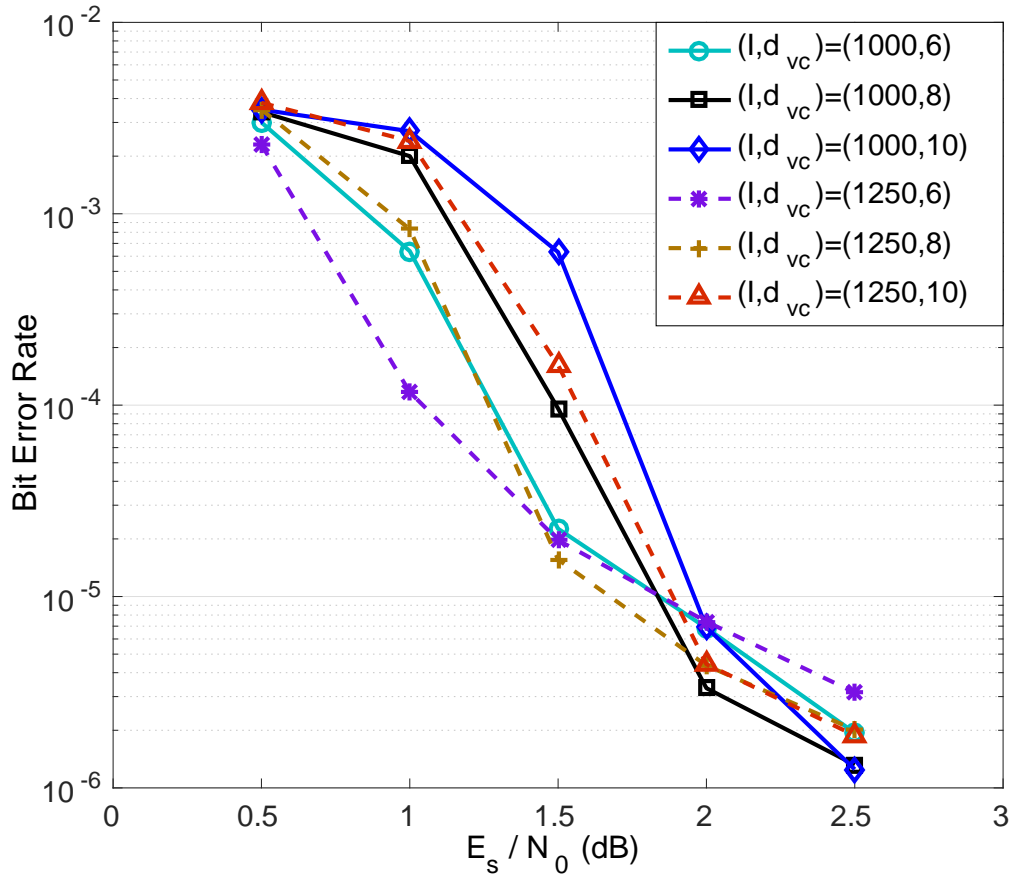


**Figure 4.6:** System performance for the pure RCM system and two pairs of hybrid schemes when  $p_1 = 0.01$ . The first pair has 1,000 coded bits within 10,000 generated symbols and the values of  $d_{vc}$  are 6, 8 and 10 respectively. The second pair has 1250 coded bits within 10000 generated symbols and the values of  $d_{vc}$  are also 6, 8 and 10.

group the convergence threshold degrades with the increase in  $d_{vc}$ , while the change in the error floor is not relevant.

For the source with  $p_1 = 0.005$ , Figure 4.7 shows the performance of hybrid systems with different number of coded bits,  $I$ , within the 10,000 generated symbols. For all seven hybrid schemes in the figure,  $d_{vc}$  has been fixed to 14, which is the optimal degree we have found through simulations. Compared to the case where  $p_1 = 0.01$ ,  $d_{vc}$  needs to be higher, as the coded bit nodes need more connections to distinguish bits when the sparsity increases. Again, the hybrid schemes use the same weight set

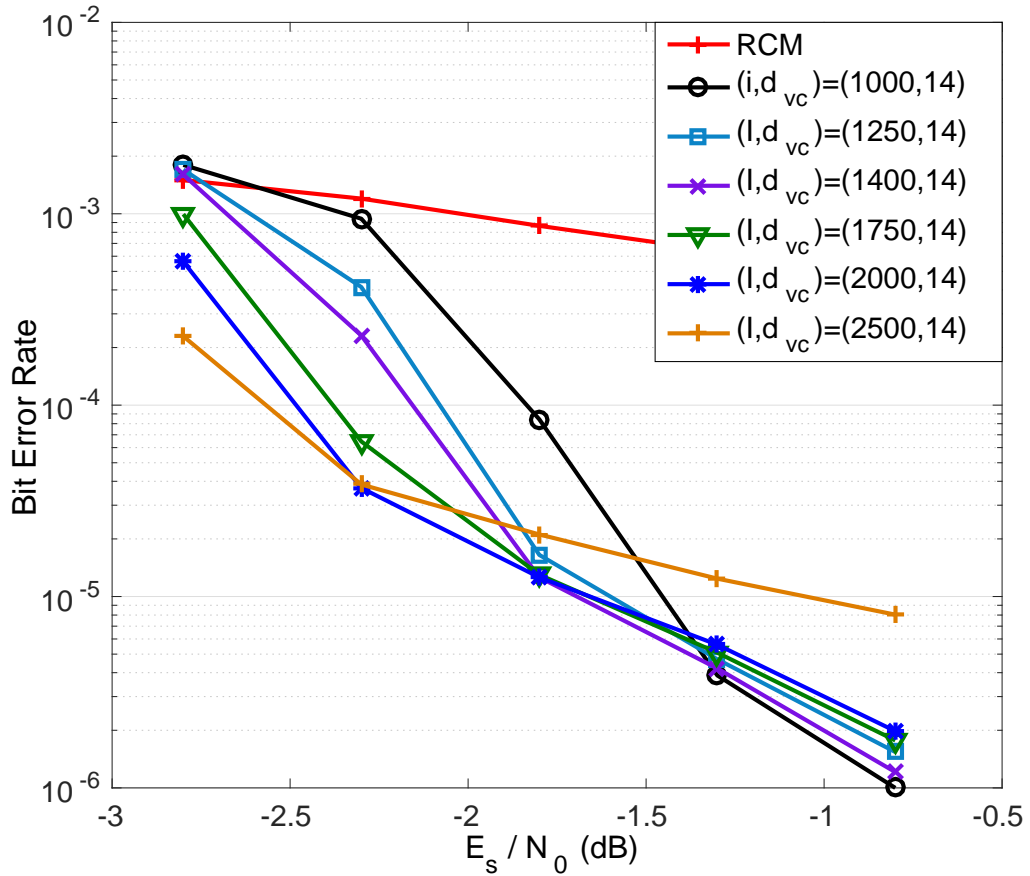


**Figure 4.7:** System performance for the pure RCM system and two pairs of hybrid schemes when  $p_1 = 0.005$ . In all the hybrid systems  $d_{vc} = 14$  and the weight set is the same as in the pure RCM system, as defined in the text. Different number of coded bits,  $I$ , are considered as indicated in the figure.

(defined before) for the RCM sub-block as the pure RCM system. In this case, the gain obtained by using hybrid systems is comparable to that in the case of  $p_1 = 0.01$ . It is interesting to see that when  $I$  increases from 0 to 1,000, the error floor is reduced greatly, which also happened in Figure 4.4. However, when  $I$  continues to increase, the error floor does not change as much as in Figure 4.4 until  $I = 2,500$ . On the other hand, the convergence threshold still improves consistently with the increase in  $I$ . If  $BER < 10^{-4}$  is taken as a criterion, the best scheme would be the one having  $I = 2,500$  bits within the 10,000 generated symbols. In Figure 4.7,  $(I, d_{vc}) = (2000, 14)$  can be

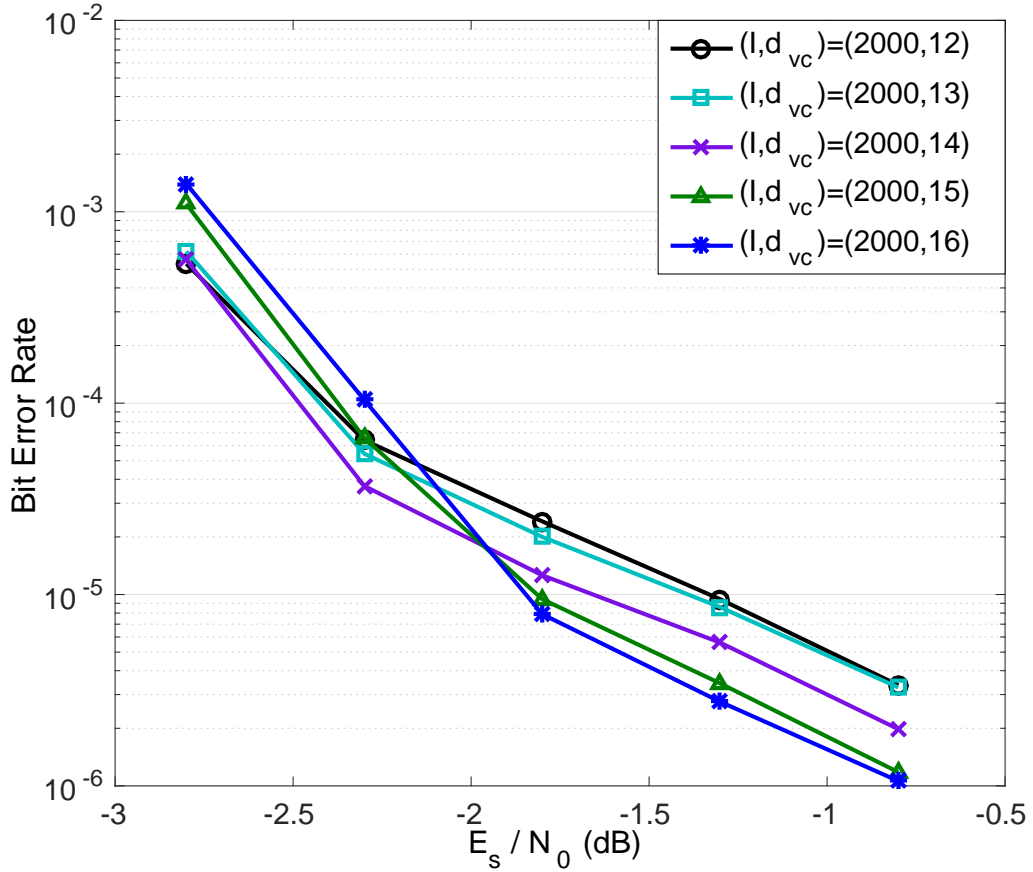


**Figure 4.8:** System performance for five hybrid schemes when  $p_1 = 0.01$ . In all the hybrid schemes  $I = 2,500$ . Different value of  $d_{vc}$  are considered as indicated in the figure.

considered as the best scheme if  $BER < 10^{-4}$  or  $BER < 10^{-5}$  are taken as criterion. We also fix  $I$  and change  $d_{vc}$  in Figure 4.8. Compared to Figure 4.5, the increase in  $d_{vc}$  leads to much smaller changes in the error floors and convergence thresholds.

For  $p_1 = 0.005$ , we also simulated two groups of hybrid schemes, shown in Figure 4.9. The schemes have the same value of  $I$  as the schemes in Figure 4.6, but with larger degrees. Comparing the schemes within each group, it is obvious that the increase of  $d_{vc}$  improves error floors to a larger degree compared to the case in which  $p_1 = 0.01$  (shown in Figure 4.6), while the convergence threshold does not degrade as much. By comparing Figure 4.6 with Figure 4.9, we can find that different design parameter sets

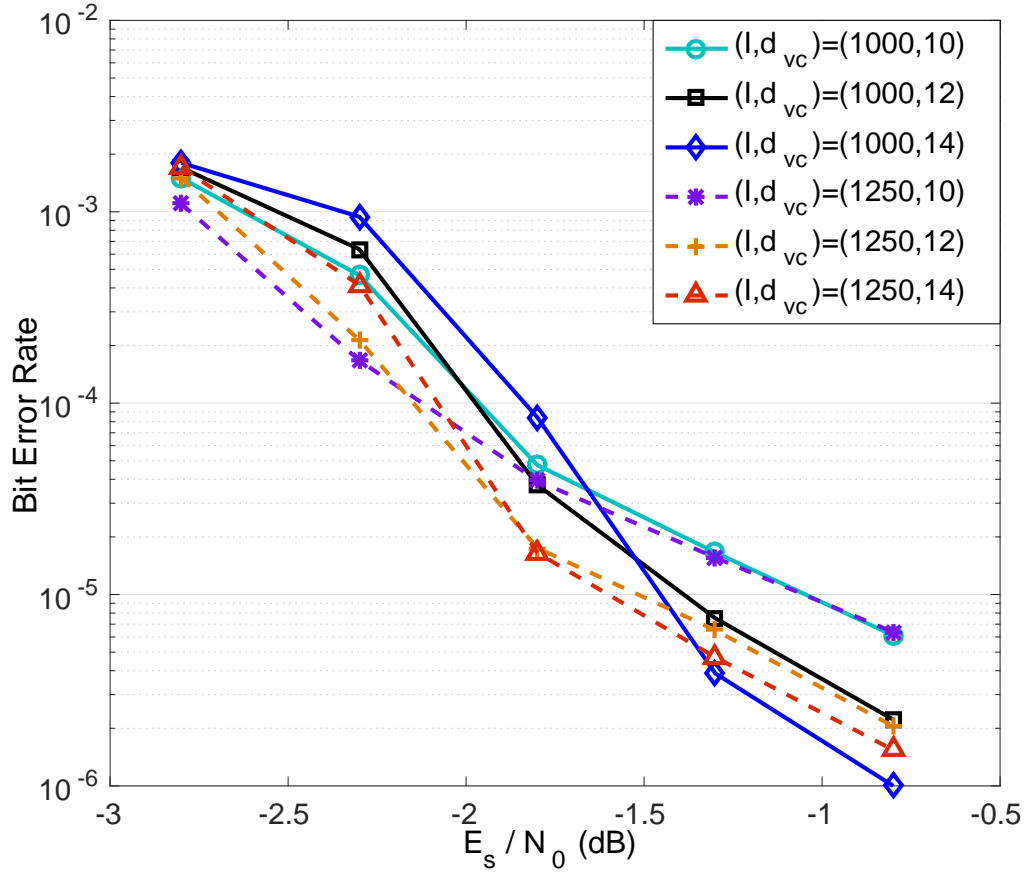


**Figure 4.9:** System performance for the pure RCM system and two groups of hybrid schemes when  $p_1 = 0.005$ . The first group has 1,000 coded bits within 10,000 generated symbols and the values of  $d_{vc}$  are 10, 12 and 14 respectively. The second group has 1,250 coded bits within 10,000 generated symbols and the values of  $d_{vc}$  are also 10, 12 and 14.

may result in similar performance.

The theoretical limit for the proposed schemes can be obtained as

$$\frac{E_s}{N_0} (dB) = 10 \log_{10} [2^{R_c H} - 1]. \quad (4.2)$$

When  $p_1 = 0.1$ , the gaps to the theoretical limit for existing joint source-channel coding schemes [102, 103, 105, 106, 110] are usually less than 2 dB for  $BER < 10^{-4}$  or  $BER < 10^{-5}$ , while, as shown in Table 4.1, for the proposed hybrid scheme the gap

**Table 4.1:** Theoretical limit and gap to the limit for  $BER < 10^{-4}$ . A throughput of 10 source bits per channel use is considered. Three nonuniform binary memoryless sources with  $p_1 = 0.1, p_1 = 0.01, p_1 = 0.005$  are considered.

$p_1$	Theoretical limit in terms of $E_s/N_0(dB)$	Gap (dB)
0.1	14	2.2
0.01	-1.2	2
0.005	-4.3	2

is around 2 dB. However, the proposed system can get a much higher throughput<sup>2</sup>. For  $p_1 = 0.01$ , the proposed scheme, with a gap of about 2 dB to the theoretical limit, performs better than the aforementioned existing systems. For  $p_1 = 0.005$ , the proposed scheme maintains a gap of about 2 dB to the theoretical limit, while keeping the same high throughput. The implication of this is that unlike other joint source-channel schemes, which are sensitive to the sparsity of the source and where the gap to capacity increases with the increase in source sparsity, the proposed hybrid schemes are robust to changes in the degree of source non-uniformity. In addition, the high throughput provided by the hybrid schemes provides a great advantage in high speed communication systems.

#### 4.5 Conclusion

In this chapter, we have designed hybrid coding schemes for i.i.d. uniform and non-uniform sources. The hybrid scheme can be optimized as a function of  $I$ , the number of coded bits within a fixed number of generated symbols (which determines the ratio between real-valued symbols and binary bits),  $d_{vc}$ , the degree of the source bits only considering the LDGM sub-block, and the weight set, which determines the performance of the RCM sub-block. For i.i.d. uniform sources, we have mitigated the error floor existing in the RCM scheme by introducing an LDGM code. After we optimize the RCM sub-block in the context of the hybrid scheme, the resulting

---

<sup>2</sup> Notice that the throughput of our scheme is 10, while most existing schemes have a throughput of 1/3 or 1/2.

performance is just 2.3 dB away from the theoretical limit for a high throughput of 7.4 source bits per channel use.

For non-uniform sources, we have considered different degrees of non-uniformity ( $p_1 = 0.1, 0.01, 0.005$ ). Generally, non-systematic codes outperform systematic codes for non-uniform sources, as they are able to produce channel symbols with distribution that better matches the channel. Therefore, we have adopted a non-systematic approach to design the hybrid coding scheme for non-uniform sources. After optimizing the weight set for non-uniform sources, we have studied the impact of design factors  $I$  and  $d_{vc}$  on the error floor and the convergence threshold. Simulation results have shown that the hybrid coding scheme is able to maintain a gap of around 2 dB to the theoretical limit when the degree of source non-uniformity increases. This result is better than with existing schemes, where the gap to the theoretical limit typically increases with the degree of non-uniformity.

## Chapter 5

### SIMPLIFIED DECODING ALGORITHM

#### 5.1 Introduction

The decoding algorithm introduced in Chapter 3 has high computational complexity, as explained in Section 3.3.2. The decoding process is implemented through message passing on the bipartite graph of the hybrid system, and the bottle-neck in terms of time complexity is in the decoding stage of the multi-level RP symbols. For each RP symbol, its density function is calculated from the channel observation and the density function of the linear combination of its associated bits. Although a deconvolution technique is introduced to reduce the computational complexity, the complexity is still high.

In this chapter, we propose a simplified decoding method that approximates the distribution of the linear combinations of the input bits as Gaussian. As will be shown, this reduces the decoding complexity in almost one order of magnitude. As we will illustrate in the sequel, the resulting performance is, in most cases, comparable to that of the original method, especially for non-uniform memoryless sources. Only when the throughput is high can we observe a small performance degradation.

The remainder of the chapter is organized as follows. Section 5.2 describes the proposed simplified algorithm. Section 5.3 analyzes the complexity of the original decoding method and of the simplified method, providing a comparison in terms of the number of additions and multiplications. Section 5.4 presents simulation results on the optimization of the hybrid scheme utilizing the simplified method, and compares the BER performance of the simplified and original decoding techniques. Finally, Section 5.5 concludes the chapter.

## 5.2 Proposed Simplified Decoding Algorithm

Since the initialization step is the same as in the original method, we focus on the computation at the RP symbol nodes, the LDGM coded bit nodes, and the source bit nodes.

### 5.2.1 Computation at the RP Symbol Nodes

Most of the complexity in the decoding process comes from the computation at this stage. Computations in each RP symbol node involve the calculation of an outgoing message by combining all the other incoming messages, as shown in Figure 5.1. Specifically, in order to compute the outgoing message on edge  $i$ , the pmf of the RP symbol from channel observation  $r_s$  and the pmf of  $x_i = \sum_{j=1, j \neq i}^{d_a} w_j b_j$ , where  $w_j$  is the weight associated with the  $j$ th neighboring input bit  $b_j$ , have to be calculated. The complexity of obtaining the pmf of the RP symbols is low as the pmf is only computed once based on the channel observation. However, getting the pmfs of all  $x_i$ 's is expensive. Even with the application of the deconvolution technique, which was introduced in [88], and we discussed in Section 3.3.2, the complexity is still high and the implementation takes a significant amount of the time.

We consider two ways to simplify the decoding procedure using a Gaussian approximation, which are equivalent. In the first method, the linear combination of all the neighboring source bits, except the  $i$ th neighboring bit, denoted as  $x_i = \sum_{j=1, j \neq i}^{d_a} w_j \cdot b_j$ ,  $x_i \sim N(m_i, \sigma_i^2)$ , is assumed to be Gaussian. Since all the  $b_j$ 's are independent variables, the mean of  $x_i$ ,  $m_i$ , and the variance of  $x_i$ ,  $\sigma_i^2$ , can be computed as

$$m_i = \sum_{\substack{j=1 \\ j \neq i}}^{d_a} w_j \cdot E\{b_j\} \quad (5.1)$$

$$\sigma_i^2 = \sum_{\substack{j=1 \\ j \neq i}}^{d_a} w_j^2 \cdot Var\{b_j\}. \quad (5.2)$$

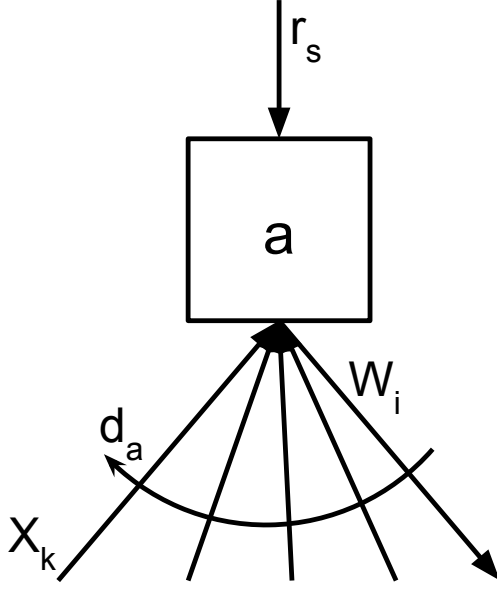


**Figure 5.1:** Simplified computation at RP symbol nodes

Therefore, the equation at an RP symbol node can then be written as

$$r_s = \Gamma \cdot w_i \cdot b_i + \Gamma \cdot \sum_{\substack{j=1 \\ j \neq i}}^{d_a} w_j \cdot b_j + n = w_i' \cdot b_i + \Gamma x_i + n = w_i' \cdot b_i + n_i', \quad (5.3)$$

where  $\Gamma$  is normalization factor, and  $n_i'$  is the equivalent noise and follows the Gaussian distribution  $N(m_{n_i}, \sigma_{n_i}^2)$ , with  $m_{n_i} = \Gamma m_i$  and  $\sigma_{n_i}^2 = \sigma_n^2 + \Gamma^2 \sigma_i^2$ . Therefore, the LLR message to the  $i$ th link can be calculated as

$$\log \frac{P(r_s | b_i = 0)}{P(r_s | b_i = 1)} = \log \frac{P(n_i' = r_s)}{P(n_i' = r_s - w_i')} \quad (5.4)$$

$$= \frac{w_i'^2 - 2 \cdot w_i' \cdot (r_s - m_{n_i})}{2 \cdot \sigma_{n_i}^2}. \quad (5.5)$$

In this way, instead of computing the pmf of  $x_i$  by convolution and deconvolution, we only need to compute the approximated mean and variance of  $x_i$ .

Another equivalent manner of making the approximation is to consider each  $b_j$  as an analog symbol following a Gaussian distribution  $N \sim (m_{b_i}, \sigma_{b_i}^2)$ , and to apply the analog message passing as described in [115]. Notice that the RP symbol comes from a Gaussian channel, and thus it is truly a Gaussian random variable  $a \sim N(r_s, \sigma_n^2)$ .

As it is well known, if  $x_1 + x_2 + x_3 = 0$  and  $x_2, x_3$  are Gaussian random variables, we can write

$$g(x_1) = (g_2 \star g_3)(-x_1) \quad (5.6)$$

$$m_{x_1} = -(m_{x_2} + m_{x_3}) \quad (5.7)$$

$$\sigma_{x_1}^2 = \sigma_{x_2}^2 + \sigma_{x_3}^2. \quad (5.8)$$

In our case, the equation at the RP symbol node is

$$w'_1 \cdot b_1 + w'_2 \cdot b_2 + \dots + w'_{d_a} \cdot b_{d_a} + X = 0, \quad (5.9)$$

where  $X = -a$ . Since each variable is assumed to be Gaussian, the message at each link can be described by just the mean and the variance, instead of using the whole densities or LLR messages. Thus, we can simply calculate the outgoing mean and variance based on all the incoming means and variances

$$m_{i,out} = \frac{-1}{w'_i} \cdot (m_{sum} - w'_i \cdot m_{i,in}) \quad (5.10)$$

$$\sigma_{i,out}^2 = \frac{1}{w'^2_i} \cdot (\sigma_{sum}^2 - w_i'^2 \cdot \sigma_{i,in}^2). \quad (5.11)$$

where,

$$m_{sum} = \sum_{i=1}^{d_a} w'_i \cdot m_{i,in} - r_s \quad (5.12)$$

$$\sigma_{sum}^2 = \sum_{i=1}^{d_a} w_i'^2 \cdot \sigma_{i,in}^2 + \sigma_n^2 \quad (5.13)$$

If the source bit node processes the messages in a LLR fashion, the outgoing mean and variance can be converted into an LLR message and passed to the source bit nodes. Otherwise, the obtained mean and variance can be passed to the corresponding neighboring source bit nodes directly.

### 5.2.2 Computation at the LDGM Coded Bit Nodes

The computations at this stage do not change with respect to the original method: from all incoming LLR messages  $v_j, j = 1, \dots, d_c$ , the goal is to calculate the  $i$ th outgoing LLR message  $u_i$ . A coded bit node also receives an observation from the channel, from which the initial message, denoted as  $v_0$ , can be computed and is incorporated in the message update in each iteration. This initial message can be calculated as

$$v_0 = \log \frac{P(r_s | c = 0)}{P(r_s | c = 1)}. \quad (5.14)$$

Thus, the  $i$ th outgoing message can be updated as

$$u_i = 2 \cdot \operatorname{atanh} \left( \prod_{\substack{j=0 \\ j \neq i}}^{d_c} \tanh \left( \frac{v_j}{2} \right) \right). \quad (5.15)$$

### 5.2.3 Computation at the Source Bit Nodes

If the source bit node processes the messages in an LLR fashion (i.e., all the incoming and outgoing messages are LLR messages), the calculation of the messages passed to the RP symbol nodes and coded bit nodes can be expressed as

$$v_i = \sum_{\substack{j=0 \\ j \neq i}}^{d_{va} + d_{vc}} u_j. \quad (5.16)$$

If the messages coming from the RP symbol nodes are means and variances, the LLR messages proceeding from the LDGM coded bit nodes should be converted to

mean and variance messages. Then, the analog messages to the  $i$ th RP symbol node can be calculated as [115]

$$m_{i,out} = \frac{\sum_{\substack{j=0 \\ j \neq i}}^{d_{va}+d_{vc}} \frac{m_{j,in}}{\sigma_{j,in}^2}}{\sum_{\substack{j=0 \\ j \neq i}}^{d_{va}+d_{vc}} \frac{1}{\sigma_{j,in}^2}} \quad (5.17)$$

$$\frac{1}{\sigma_{i,out}^2} = \sum_{\substack{j=0 \\ j \neq i}}^{d_{va}+d_{vc}} \frac{1}{\sigma_{j,in}^2}. \quad (5.18)$$

The second step is to calculate the LLR messages exchanged to the LDGM coded bits. The calculation method is identical to that of LDGM codes, except that messages coming from RP symbol nodes have to be converted to LLR messages.

#### 5.2.4 Decision

LLR messages are used for the decision of the source bits regardless of the incoming message format. If there are mean and variance messages, they have to be converted to LLR messages first. After each iteration, the value of each bit can be determined by calculating

$$d = \sum_{j=0}^{d_{va}+d_{vc}} u_j. \quad (5.19)$$

If  $d$  is greater than 0, the decision for this bit is 0. Otherwise, it is 1. In our simulations, the decoding process is terminated when every source bit node makes the same decision for five iterations in a row or the number of iterations has reached 200.

### 5.3 Computational Complexity Analysis

The computational complexity is measured in terms of number of additions, denoted as  $A$ , and number of multiplications, denoted as  $M$ . To facilitate the analysis, we denote the degree of the RP node as  $D$ , and the length of the pmf vector obtained by convolving  $D$  pmf messages as  $L_D$ . For simplicity, we ignore insignificant computations, such as the computation to obtain the pmf of the RP symbol based on the channel

observation. Also, the operations of subtraction and division are counted as addition and multiplication.

### 5.3.1 Complexity of the Original Method

#### 5.3.1.1 Convolution

As discussed in Section 3.3.2, the pmf of the linear combination is obtained by convolving all the incoming pmfs of  $w_i b_i$ . Suppose the linear combination of the first  $i$  neighboring bits is

$$z_i = g_i + \sum_{j=1}^{i-1} w_j b_j = x_i + z_{i-1} \quad (5.20)$$

where  $g_i = w_i b_i$ , the  $i$ th neighboring weighted bit. The pmf of  $z_i$  can be obtained by the convolution of the pmfs of  $g_i$  and  $z_{i-1}$ . The convolution process can be expressed as

$$P_{z_i}[n] = \sum_{k=-\infty}^{\infty} P_{g_i}[k] P_{z_{i-1}}[n - k] = p_0 P_{z_{i-1}}[n] + p_1 P_{z_{i-1}}[n - w_i]. \quad (5.21)$$

where  $P_{z_i}[n]$  is the density of  $z_i$  at  $n$ ,  $P_{g_i}[k]$  is the density of  $g_i$  at  $k$ , and  $p_0$  and  $p_1$  are the probabilities of  $b_i$  being 0 and 1. The pmf of  $g_i$  is given by

$$P_{g_i}[k] = \begin{cases} p_0, & k = 0 \\ p_1, & k = w_i \\ 0, & otherwise \end{cases}$$

The pmf of  $z_{i-1}$ ,  $\mathbf{P}_{z_{i-1}}$  of length  $L_{i-1}$ , is obtained by the convolution of the previous  $i - 1$  incoming pmfs. Thus, the length of the pmf vector of  $z_i$ ,  $\mathbf{P}_{z_i}$ , is  $L_i = L_{i-1} + |w_i|$ . (5.21) takes 1 addition and 2 multiplications to compute the density at one index for  $z_i$ . Therefore, the number of operations required to obtain the pmf of  $z_i$  is approximately  $L_i$  additions and  $2L_i$  multiplications. Since  $L_i$  depends on the absolute values of  $w_i$ 's, larger values of weights results in longer pmf vectors, which leads to more operations in the computation. In Table 5.1, the complexity for the convolution at each stage is shown. More specifically, the number of additions and multiplications required to obtain the pmf for each  $z_i, i = 0, \dots, D$ , starting with  $z_1 = x_1$ , is shown. In each row,

**Table 5.1:** Complexity Analysis of the Convolution

$z_i$	length of $\mathbf{P}_{g_i}$	length of $\mathbf{P}_{z_{i-1}}$	length of $\mathbf{P}_{z_i}$ ( $L_i$ )	(A, M)
$z_2$	$ w_2  + 1$	$ w_1  + 1$	$L_2 = \sum_{i=1}^2  w_i  + 1$	$L_2, 2L_2$
$z_3$	$ w_3  + 1$	$L_2$	$L_3 = \sum_{i=1}^3  w_i  + 1$	$L_3, 2L_3$
$z_4$	$ w_4  + 1$	$L_3$	$L_4 = \sum_{i=1}^4  w_i  + 1$	$L_4, 2L_4$
$\vdots$	$\vdots$	$\vdots$	$\vdots$	$\vdots$
$z_D$	$ w_D  + 1$	$L_{D-1}$	$L_D = \sum_{i=1}^D  w_i  + 1$	$L_D, 2L_D$

the number of operations required for convolving the  $i$ th incoming pmf of  $g_i$ ,  $\mathbf{P}_{g_i}$ , with the pmf of  $z_{i-1}$ ,  $\mathbf{P}_{z_{i-1}}$  is provided. By combining the number of additions at each stage, the total number of additions, denoted as  $A_c$ , can be computed as

$$\begin{aligned}
 A_c &= L_2 + L_3 + L_4 + \cdots + L_D \\
 &= \sum_{i=1}^2 |w_i| + \sum_{i=1}^3 |w_i| + \sum_{i=1}^4 |w_i| + \cdots + \sum_{i=1}^D |w_i| + D - 1 \\
 &= (D - 1)|w_1| + (D - 1)|w_2| + (D - 2)|w_3| + (D - 3)|w_4| + \cdots \\
 &\quad + 2|w_{D-1}| + |w_D| + D - 1,
 \end{aligned} \tag{5.22}$$

Define another variable  $B_c$  as

$$B_c = |w_1| + 2|w_2| + 3|w_3| + \cdots + D|w_D|. \tag{5.23}$$

Then,

$$\begin{aligned}
 A_c + B_c &= D|w_1| + (D + 1)|w_2| + (D + 1)|w_3| + \cdots + (D + 1)|w_D| + D - 1 \\
 &= (D + 1) \sum_{i=1}^D |w_i| - |w_1| + D - 1 = (D + 1)L_D - |w_1| - 2,
 \end{aligned} \tag{5.24}$$

As explained in Section 2.2, weight sets are balanced and consist of pairs of weights. For instance,  $\{\pm 1, \pm 2, \pm 4, \pm 4\}$  and  $\{\pm 1, \pm 1, \pm 1, \pm 1, \pm 2, \pm 2, \pm 2, \pm 2\}$  used in Chapter 4 have four pairs of weights and eight pairs of weights respectively. Therefore, it is

safe to assume the weights paired as  $\{(w_1, w_D), (w_2, w_{D-1}), \dots, (w_{D/2}, w_{D/2+1})\}$ . Thus,  $B_c$  can be expressed by substituting the absolute value of the weight for the absolute value of the other weight in the pair

$$\begin{aligned} B_c &= |w_D| + 2|w_{D-1}| + 3|w_{D-1}| + \dots + (D-1)|w_2| + D|w_1| \\ &= A_c + |w_1| - (D-1). \end{aligned} \quad (5.25)$$

Therefore, the total numbers of additions and multiplications in the convolution are

$$A_c = \frac{(D+1)(L_D+1)}{2} - |w_1| - 2, \quad (5.26)$$

$$M_c = 2A_c = (D+1)(L_D+1) - 2|w_1| - 4. \quad (5.27)$$

### 5.3.1.2 Deconvolution

The technique of deconvolution is used to obtain the pmf of  $x_i = \sum_{\substack{j=1 \\ j \neq i}}^D w_j b_j$  efficiently [88]. The technique is implemented by removing the pmf of  $x_i$  from the pmf of  $z_D$ , which is obtained by convolving all incoming pmf of  $x_i$ 's. The density of  $z_D$  at  $k$  can be expressed as

$$P(z_D = k) = P(b_i = 0)P(x_i = k) + P(b_i = 1)P(x_i = k - w_i), \quad (5.28)$$

where  $k \in [-\frac{L_D-1}{2}, \frac{L_D-1}{2}]$ . Therefore,

$$P(x_i = k) = \frac{P(z_D = k) - P(b_i = 1)P(x_i = k - w_i)}{P(b_i = 0)}, \quad (5.29)$$

which takes 1 addition and 2 multiplications. There is another formula to update the densities in the opposite direction [88]

$$P(x_i = k) = \frac{P(z_D = k + w_i) - P(b_i = 0)P(x_i = k + w_i)}{P(b_i = 1)}. \quad (5.30)$$

Notice that (5.29) is applied when  $w_i$  is a positive number, while (5.30) is used when  $w_i$  is negative, but the number of computations in (5.29) and (5.30) is the same. To obtain the complete pmf of  $x_i$ ,  $L_D$  additions and  $2L_D$  multiplications are needed. Since

there are  $D$  deconvolution operations, one for each link, the total number of additions, denoted as  $A_d$ , and the total number of multiplications, denoted as  $M_d$ , are

$$A_d = DL_D, M_d = 2DL_D. \quad (5.31)$$

### 5.3.1.3 Computation of Outgoing Messages

(3.9) and (3.10) are used to update each outgoing message. Thus, updating  $P(b_i = 0)$  takes  $L_D - 1$  additions and  $L_D$  multiplications, which is also the complexity required to update  $P(b_i = 1)$ . As there are  $D$  outgoing messages to be updated, the total required number of additions and multiplications are  $2D(L_D - 1)$  and  $2DL_D$ .

In summary, the computational complexity for each RP symbol node in each iteration using the original method is shown in Table 5.2.

**Table 5.2:** Computational Complexity of the Original Method

Operation	Addition	Multiplication
Convolution	$\frac{(D+1)(L_D+1)}{2} -  w_1  - 2$	$(D+1)(L_D+1) - 2 w_1  - 4$
Deconvolution	$DL_D$	$2DL_D$
Message Update	$2D(L_D - 1)$	$2DL_D$
Total	$\frac{6DL_D + (L_D - 3)(D + 1)}{2} -  w_1 $	$5DL_D + D + L_D - 3 - 2 w_1 $

### 5.3.2 Complexity of the Simplified Method

In the simplified method, the first step is to compute

$$P = \sum_{j=1}^D w_j E\{b_j\}, Q = \sum_{j=1}^D w_j^2 Var\{b_j\}, \quad (5.32)$$

so that  $m_i$  and  $\sigma_i^2$  in (5.1) and (5.2) can be obtained efficiently by subtracting the  $i$ th component from  $P$  and  $Q$ . One addition and two multiplications are needed to obtain each  $E\{b_j\}$ , while three additions and four multiplications are needed to obtain each  $Var\{b_j\}$ . The summations for  $P$  and  $Q$  both take  $D - 1$  additions and  $D$  multiplications

( $w_j^2$  can be precomputed so that its complexity is not counted). Thus, the total numbers of operations to obtain  $P$  and  $Q$  are  $6D - 2$  additions and  $8D$  multiplications.

The second step is to update the outgoing messages for each link. For each link, the subtraction involved in getting  $m_i$  and  $\sigma_i^2$  takes one addition and one multiplication each. Obtaining the outgoing LLR message by (5.5) takes two additions and two multiplications. Thus, the complexity of updating outgoing messages on one link is four additions and four multiplications, so that the second step takes a total of  $4D$  additions and  $4D$  multiplications. The complexity is provided in Table 5.3

**Table 5.3:** Complexity of the Simplified Method

Operation		Addition	Multiplication
Step 1	$E\{b_j\}$ 's	$D$	$2D$
	$Var\{b_j\}$ 's	$3D$	$4D$
	$P$	$D - 1$	$D$
	$Q$	$D - 1$	$D$
Step 2	$m_i$ 's	$D$	$D$
	$\sigma_i^2$ 's	$D$	$D$
	D messages	$2D$	$2D$
Total		$10D - 2$	$12D$

### 5.3.3 Complexity Comparison

In order to compare the complexity of the original method and the simplified method, we study the following cases

- $W_1 = \{\pm 1, \pm 2, \pm 4, \pm 4\}$
- $W_2 = \{\pm 2, \pm 3, \pm 4, \pm 8\}$
- $W_3 = \{\pm 1, \pm 1, \pm 1, \pm 1, \pm 2, \pm 2, \pm 2, \pm 2\}$ ,

which are the weight sets used in Chapter 4 for the uniform and non-uniform sources. The number of operations for each weight set is shown in Table 5.4. For simplicity, the term  $|w_1|$  is removed from the results in Table 5.2, as it does not affect the complexity

in practice. The numbers inside parentheses are the numbers of additions and multiplications. As mentioned previously,  $D$  is the degree of the RP symbol node and  $L_D$

**Table 5.4:** Complexity Comparison

	$W_1$	$W_2$	$W_3$
$D$	8	8	16
$L_D$	23	35	25
Original Method (Appr.)	(642, 948)	(984, 1440)	(1220, 2038)
Simplified Method (Appr.)	(78, 96)	(78, 96)	(158, 192)

is the length of the pmf vector of the linear combination  $\sum_{j=1}^D w_j b_j$ . The complexity of the original method depends both on  $D$  and  $L_D$ , which can be seen from the results in Table 5.2. Therefore, an increase in either variable could result in an increase of the total complexity. This can be observed by comparing  $W_1$  and  $W_2$ , where  $L_D$  increases when larger values of weights are considered, and by comparing  $W_1$  and  $W_3$ , where  $D$  increases while the value of  $L_D$  is very similar. However, the number of operations for the simplified method only depends on the value of  $D$ , as it only approximates the mean and variance of the linear combination and the computations do not rely on the true pmf. In all three cases, the required number of operations for the original method is approximately 10 times larger than the required number for the simplified technique. Therefore, the proposed simplified method effectively reduces the complexity by around one order of magnitude.

## 5.4 Simulation Results

### 5.4.1 Optimization of the Hybrid Scheme with Simplified Decoding

Our first objective is to study the impact of the design parameters over the system performance when the simplified decoding method is used. For this part, we focus on the cases in which the code rates are  $R_c = 0.5$  and  $R_c = 1$ . The length of the input binary stream is fixed to 10,000. Therefore, the total number of symbols at the output of the encoder will be 20,000 (for throughput  $T = 1$ ) and 10,000 (for  $T = 2$ ).

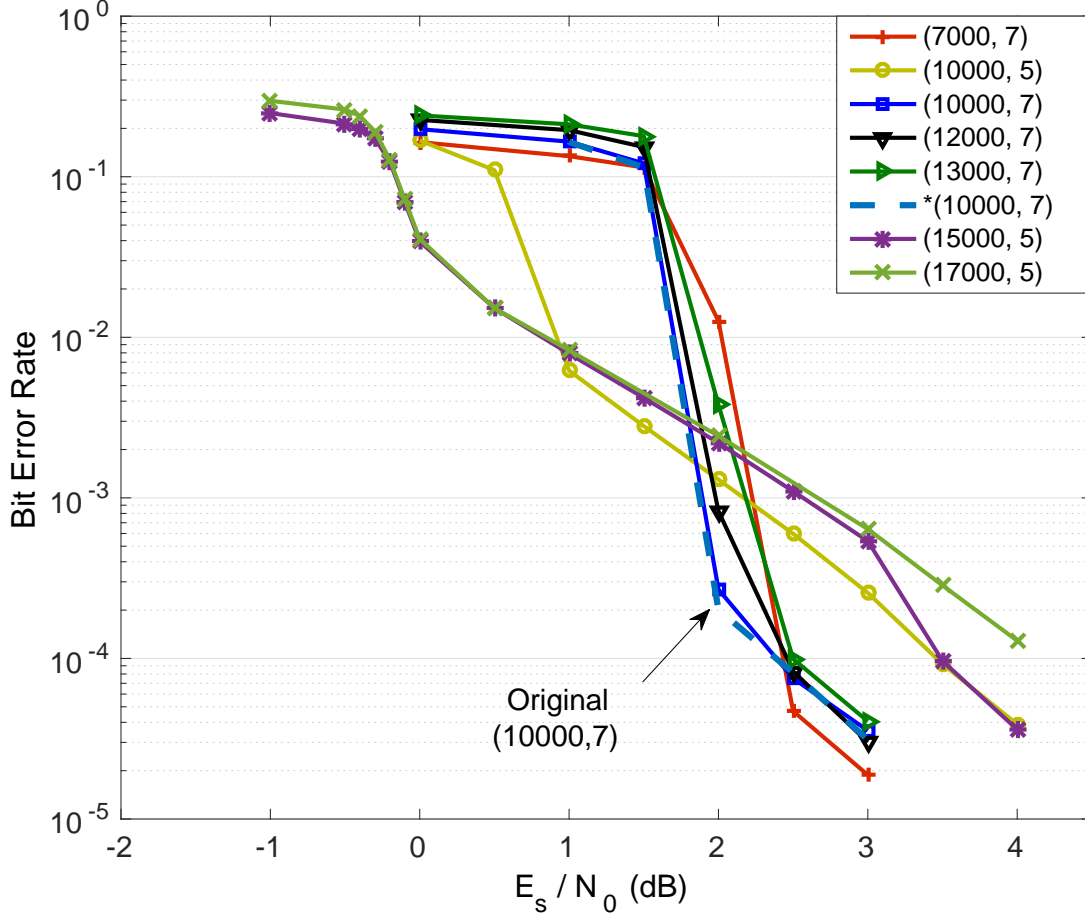


**Figure 5.2:** System performance for the simplified decoding method in the case of uniform sources when  $T = 1$ . The labels represent parameters  $(I, d_{vc})$ . The dashed line curve corresponds to the system performance using the original decoding method.

Since QAM signaling is utilized, the channel will be used 10,000 and 5,000 times respectively, and the throughput will be  $T = 1$  and  $T = 2$ , respectively. We consider i.i.d. uniform sources and i.i.d. non-uniform sources with  $p_1 = 0.1$ . In order to evaluate the system performance, we use the gap to the Shannon Limit when  $BER < 10^{-4}$  as criterion. The theoretical limit can be obtained as:

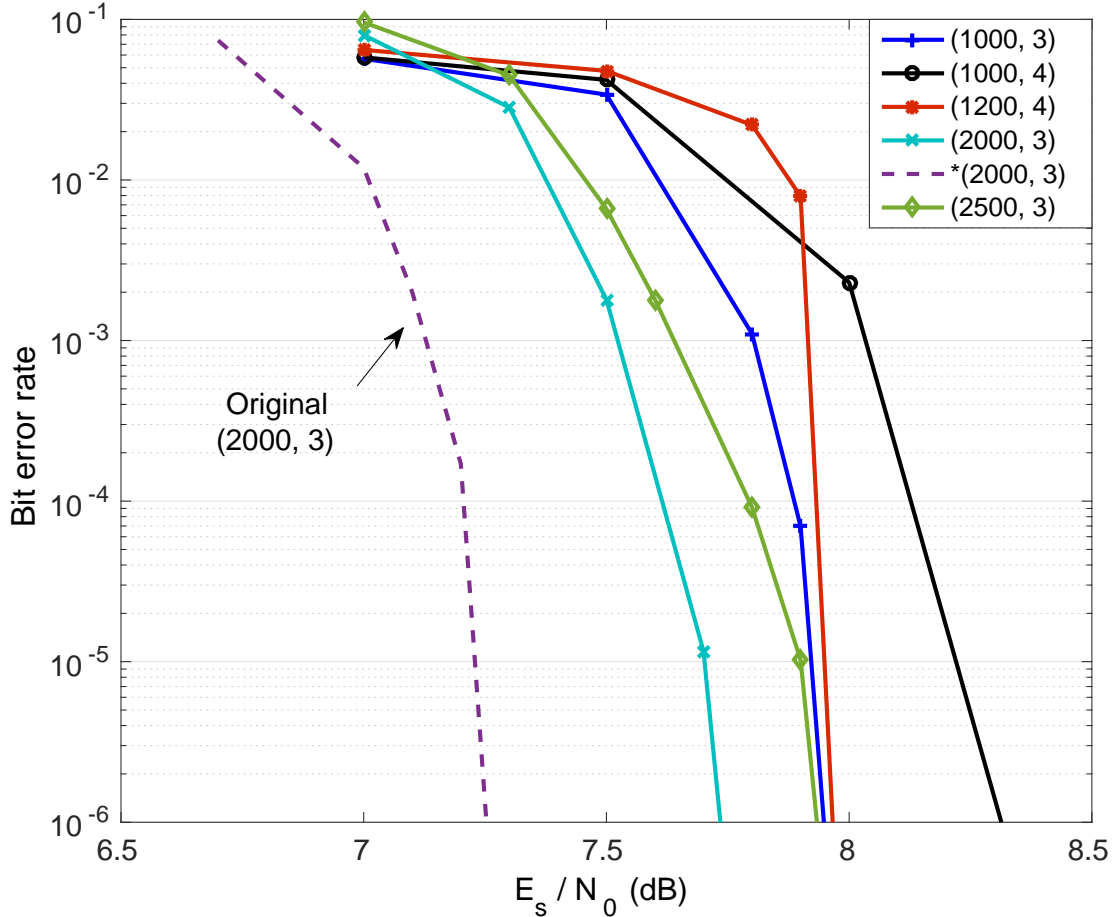
$$\frac{E_s}{N_0} (dB) = 10 \log_{10}(2^{R_c H} - 1). \quad (5.33)$$

For the optimization, we also adopt a non-systematic approach. We use the weight set  $W = \{\pm 2, \pm 3, \pm 7, \pm 10\}$  for the implementation of the RCM system. We fixed the analog part and evaluated the system by optimizing the LDGM part using the same strategy as in Chapter 4. We have implemented many systems based on different proportion of digital bits,  $I$ , and different degrees for the LDGM sub-block,  $d_{vc}$ . As discussed before, the value of  $I$  should be able to maintain a balance between the functionality of the analog sub-block and the digital sub-block, while  $d_{vc}$  mainly concerns with the functionality of the digital sub-block.

For the case of uniform sources, the simulation results for  $T = 1$  using the simplified decoder are shown in Figure 5.2. As observed in Chapter 4.4 for the original decoder, within certain range higher degree,  $d_{vc}$ , leads to lower error floors and worse convergence threshold. For comparison purposes, we simulated the system with  $(I, d_{vc}) = (10000, 7)$  using the original decoding method. Notice that both decoding methods, original and simplified, result in almost identical performance, just 2.5 dB away from the Shannon limit for  $BER \sim 10^{-4}$ . However, the simplified method is almost 10 times faster than the original method.

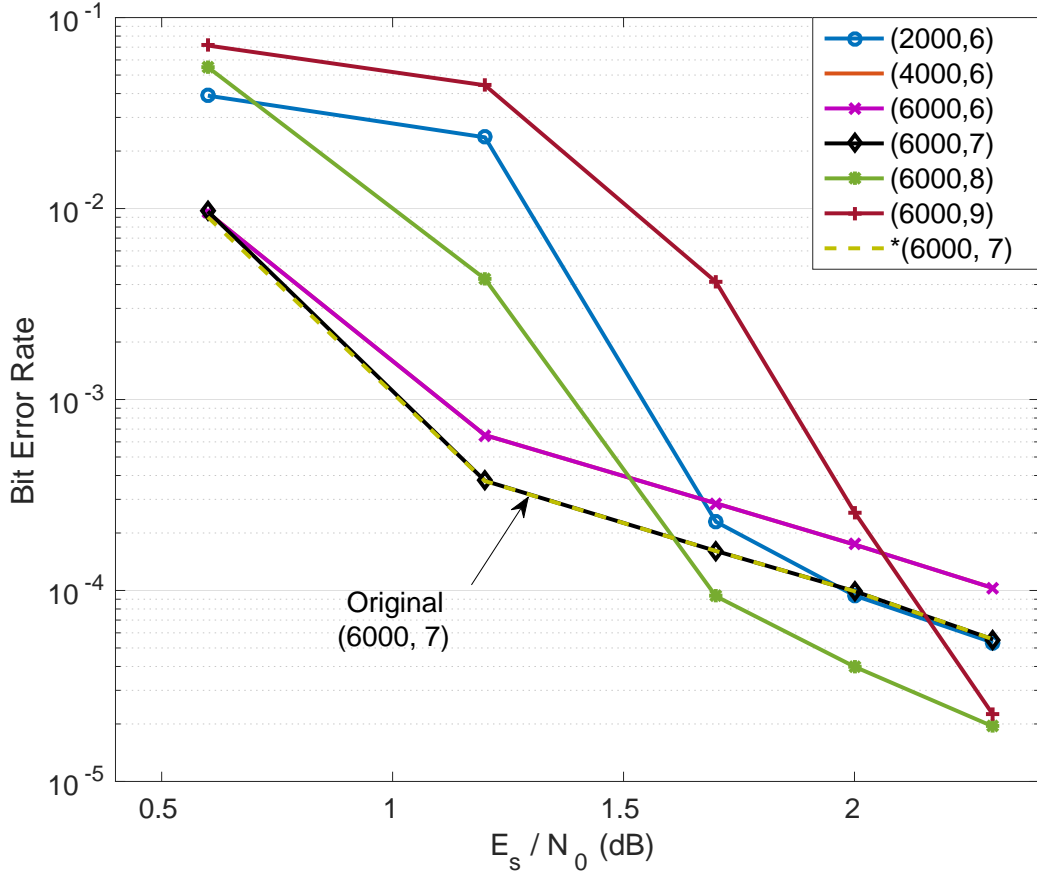
Figure 5.3 shows the performance of simplified decoding for i.i.d. uniform sources when the throughput is  $T = 2$  and different number of bits,  $I$ , within the 10,000 generated symbols are used. When compared to Figure 5.2, here we do not have any error floors and the performance is characterized just by the convergence threshold. The convergence threshold improves when  $I$  increases from 1,000 to 2,000. However, further increases of  $I$  lead to performance degradation. This behavior is similar to the one shown in Section 4.4 with the original decoding method. In order to compare the simplified method to the original decoding method, we simulated the best system  $(I, d_{vc}) = (2000, 3)$  with the original decoding method (dashed line in the figure). Notice that the degradation using the simplified method is just 0.5 dB, but the simplified method still produces a very reasonable performance, only 3 dB away from the theoretical limit for  $BER \sim 10^{-4}$ .

Figure 5.4 shows the system performance for the case of non-uniform sources



**Figure 5.3:** System performance for the simplified decoding method in the case of uniform sources when  $T = 2$ . The labels represent parameters  $(I, d_{vc})$ . The dashed line curve corresponds to the system performance using the original decoding method.

with  $p_1 = 0.1$  when the transmission rate is  $T = 2$ , and the same weight set as in the uniform case is used. Compared to Figure 5.3, in the case of non-uniform sources a more powerful LDGM code is necessary to achieve good performance, and the influence of parameters  $I$  and  $d_{vc}$  on the system performance (error floors and convergence thresholds) is greater. We chose the system with the best convergence threshold,  $(I, d_{vc}) = (6000, 7)$ , and simulated it with the original decoding method. For  $BER = 4 \times 10^{-4}$ , the performance is 1.6 dB away from the theoretical limit. Different from the case of uniform sources with throughput  $T = 2$ , presented in Figure 5.3, Figure



**Figure 5.4:** System performance for the simplified decoding method in the case of non-uniform sources with  $p_0 = 0.1$  when  $T = 2$ . The labels represent parameters  $(I, d_{vc})$ . The dashed line curve corresponds to the system performance using the original decoding method.

5.4 shows that for the considered non-uniform source, the use of the simplified method leads to no performance degradation. That is, in the case of non-uniform sources the simplified decoding method can be successfully applied at rates higher than in the case of uniform sources.

#### 5.4.2 Performance Comparison with the Original Decoding Method

As demonstrated in Section 5.3, on average, the simplified method is 10 times faster than the original decoding method. This complexity reduction should be at

the cost of decoding accuracy, as the precise information of the pmf is replaced by an approximation. The simulation results in Section 5.4.1 have presented some comparison between the original method and the simplified method. A preliminary observation is that for the same design parameters, the simplified method can achieve almost the same performance as the original method when the rate is low, while a small degradation occurs with a higher rate. However, when the non-uniformity increases, identical performance is achieved at higher rates.

In order to further study the problem, we compare the BER performance of the original method and of the simplified method in different settings. More specifically, we study the case of i.i.d. uniform sources and i.i.d. non-uniform sources where  $p_1 = 0.1, 0.01, 0.005$ . For each  $p_1$ , BER performance with the two decoding algorithms is compared for different throughputs. We fix the RCM sub-block by using the optimized weight set for uniform and non-uniform sources in Chapter 4. For each throughput, the hybrid scheme with the original decoding algorithm is optimized over the parameter set  $(I, d_{vc})$  first. Then, the simplified algorithm is implemented to assess the performance loss. In all the simulations, the total number of generated symbols is fixed to 10,000, i.e.,  $M + I = 10,000$  where  $M$  is the number of RP symbols, while the block length is varied to obtain different throughputs.

#### 5.4.2.1 Uniform Sources

For i.i.d uniform sources, we use the weight set  $\{\pm 2, \pm 3, \pm 4, \pm 8\}$  from Section 4.3 for the RCM sub-block. From Section 5.4.1, we know that when the entropy of the source is high, i.e., low degree of non-uniformity, the simplified method can not afford to use high rates without serious performance degradation. Therefore, instead of using a throughput of 7.4 source bits per channel use as in Section 4.3, we use lower code rates, which are still comparable to the rates used in digital coding schemes. In this case,  $T = 1$  and  $T = 2$  are considered. Figure 5.5 shows the performance of the two decoding methods. The blue dashed lines show the performance of the optimized hybrid scheme with the original decoding method, while the black solid lines show the performance

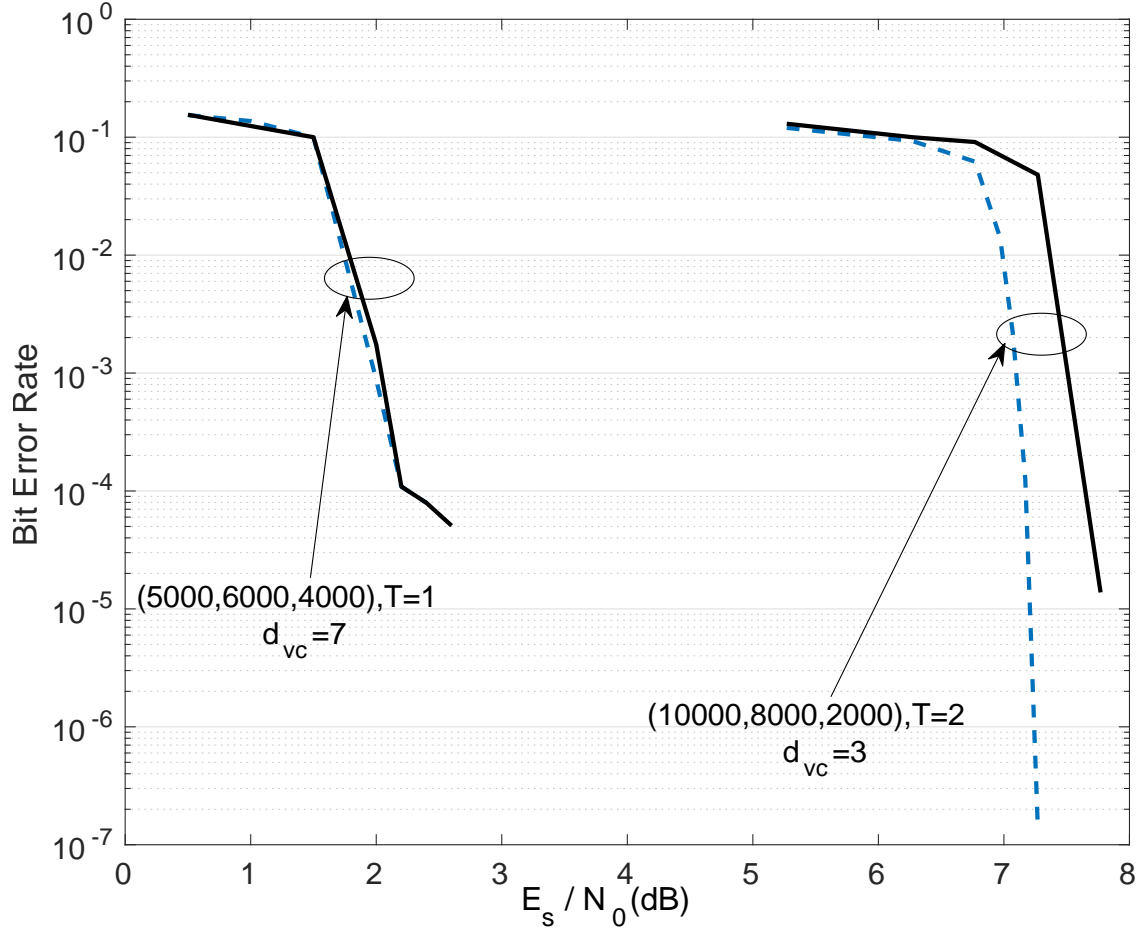


**Figure 5.5:** Performance comparison of the simplified decoding method and the original decoding method for i.i.d. uniform sources. The labels represent parameters  $\{(K, M, I)\}$ , throughput  $T$ , and  $d_{vc}$ . The blue dashed line indicates the performance of the original method, while the black solid line indicates the performance of the simplified method with the same design.

of the hybrid scheme with the same design but using the simplified decoding method. Notice the similarities to the results in Figure 5.2 and Figure 5.3, where for  $T = 1$ , the scheme with the simplified method achieves almost the same performance as the original algorithm, while for  $T = 2$ , there is a performance degradation of 0.5 dB if we use  $BER < 10^{-4}$  as the reference point. Moreover, we can observe that the scheme with lower throughput has a larger ratio of coded bits. The reason behind this is that a smaller number of RP symbols is required to achieve a certain level of errors, while

leaving room for more digital bits to get more decoding precision. For instance, 10,000 source bits require 8,000 RP symbols to eliminate “general” errors to a certain level, so that the digital bits are able to reduce the number of residual errors, as shown in the right group. When the block length decreases to 5,000, that number of RP symbols would be an overkill, i.e., the performance would not improve much by using the same number of RP symbols. Instead, the proportion of RP symbols should be reduced so that more digital coded bits can be introduced to obtain more precise decoding. The performance of the original and the simplified decoding methods is shown in Table 5.5.

**Table 5.5:** Gap to the theoretical limit for hybrid schemes using the original and the simplified decoding methods when  $p_1 = 0.5$ . The theoretical limit is in terms of  $E_s/N_0$ . The gap is measured at  $BER < 10^{-4}$ . All results are in dB.

Throughput	$[E_s/N_0]_{lim}$	Gap (original)	Gap (simplified)	Degradation
1	0	2.1	2.1	0
2	4.77	2.4	2.9	0.5

#### 5.4.2.2 Non-uniform Sources

For  $p_1 = 0.1$ , we use the weight set  $\{\pm 1, \pm 1, \pm 1, \pm 1, \pm 2, \pm 2, \pm 2, \pm 2\}$  from Section 4.3 for the RCM sub-block. We simulate hybrid schemes with throughputs  $T = 2$ ,  $T = 4$ , and  $T = 5$ , as shown from left to right in Figure 5.6. As observed previously, when  $p_1$  decreases from 0.5 to 0.1, the degradation shown in Figure 5.5 with  $T = 2$  disappears in Figure 5.6. The reason is that when the degree of non-uniformity increases, the amount of information transmitted through the channel is reduced when the throughput is maintained. Therefore, the hybrid scheme can afford the loss of information due to the use of the simplified method again, and obtain the same performance as the original method. A conclusion is that when the degree of non-uniformity increases, i.e.,  $p_1$  decreases, we are able to use the simplified decoding method with higher throughput and obtain results that are comparable to those obtained using the original decoding method. When the throughput is further increased, the degradation

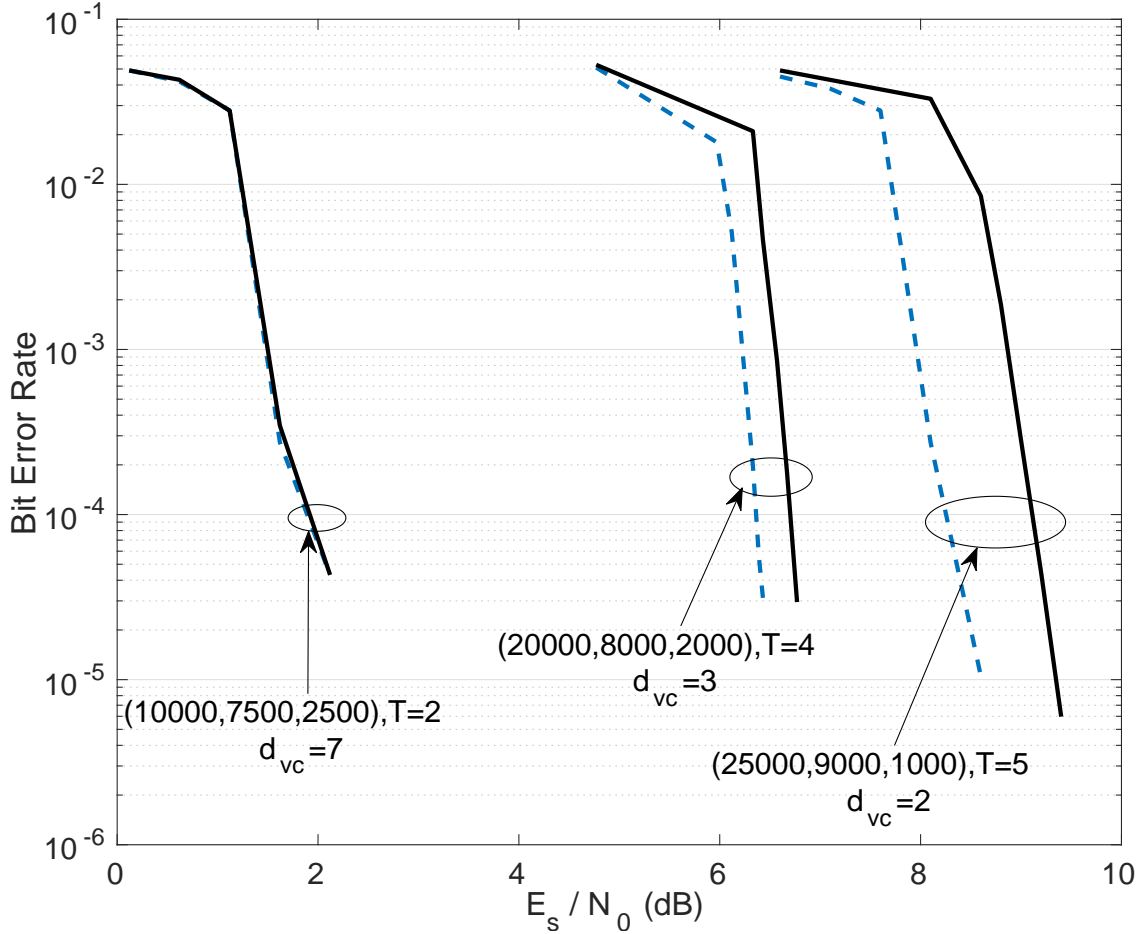


**Figure 5.6:** Performance comparison of the simplified decoding method and the original decoding method for i.i.d. non-uniform sources with  $p_1 = 0.1$ . The labels represent parameters  $\{(K, M, I)\}$ , throughput  $T$ , and  $d_{vc}$ . The blue dashed line indicates the performance of the original method, while the black solid line indicates the performance of the simplified method with the same design.

resulting from the simplified decoding method starts to increase again. For  $T = 4$ , there is a degradation of 0.3 dB when  $BER < 10^{-4}$ , while for  $T = 5$ , the degradation increases to 0.7 dB, as shown in Table 5.6. We also observe that the portion of RP symbols decreases as the throughput decreases.

For i.i.d. non-uniform sources with  $p_1 = 0.01$ , we maintain the weight set for the RCM sub-block. As explained previously, with the increase of the non-uniformity of the source, a higher throughput can be maintained. Therefore, we simulated hybrid

**Table 5.6:** Gap to the theoretical limit for hybrid schemes using the original and simplified decoding methods when  $p_1 = 0.1$ . The theoretical limit is in terms of  $E_s/N_0$ . The gap is measured at  $BER < 10^{-4}$ . All the results are in dB.

Throughput	$[E_s/N_0]_{lim}$	Gap (original)	Gap (simplified)	Degradation
2	-0.38	2.3	2.3	0
4	4.27	1.9	2.2	0.3
5	6.1	2.1	2.8	0.7

schemes with the two decoding methods and high throughputs of  $T = 4$ ,  $T = 6$ , and  $T = 8$ , as shown from left to right in Figure 5.7. The simplified method obtains the same performance as the original technique in all three cases. There is only a small gap in terms of convergence threshold. Notice that the throughputs used here are close to the one used in Section 4.4. The performance of the original and simplified decoding methods for  $p_1 = 0.01$  is shown in Table 5.7.

**Table 5.7:** Gap to the theoretical limit for hybrid schemes using the original and simplified decoding methods when  $p_1 = 0.01$ . The theoretical limit is in terms of  $E_s/N_0$ . The gap is measured at  $BER < 10^{-4}$ . All results are in dB.

Throughput	$[E_s/N_0]_{lim}$	Gap (original)	Gap (simplified)	Degradation
4	-6	2.2	2.2	0
6	-3.98	1.8	1.8	0
8	-2.48	2	2	0

For i.i.d. non-uniform sources with  $p_1 = 0.005$ , we further increase the throughput. Figure 5.8 shows the performance of two decoding methods with  $T = 6$ ,  $T = 8$ , and  $T = 9$ . For  $T = 6$ , the performance of the two decoding methods are very similar, while for  $T = 8$  and  $T = 9$  there is gap in terms of convergence threshold. but not in the error floor region. The performance of the original and simplified decoding methods for  $p_1 = 0.005$  is shown in Table 5.8.

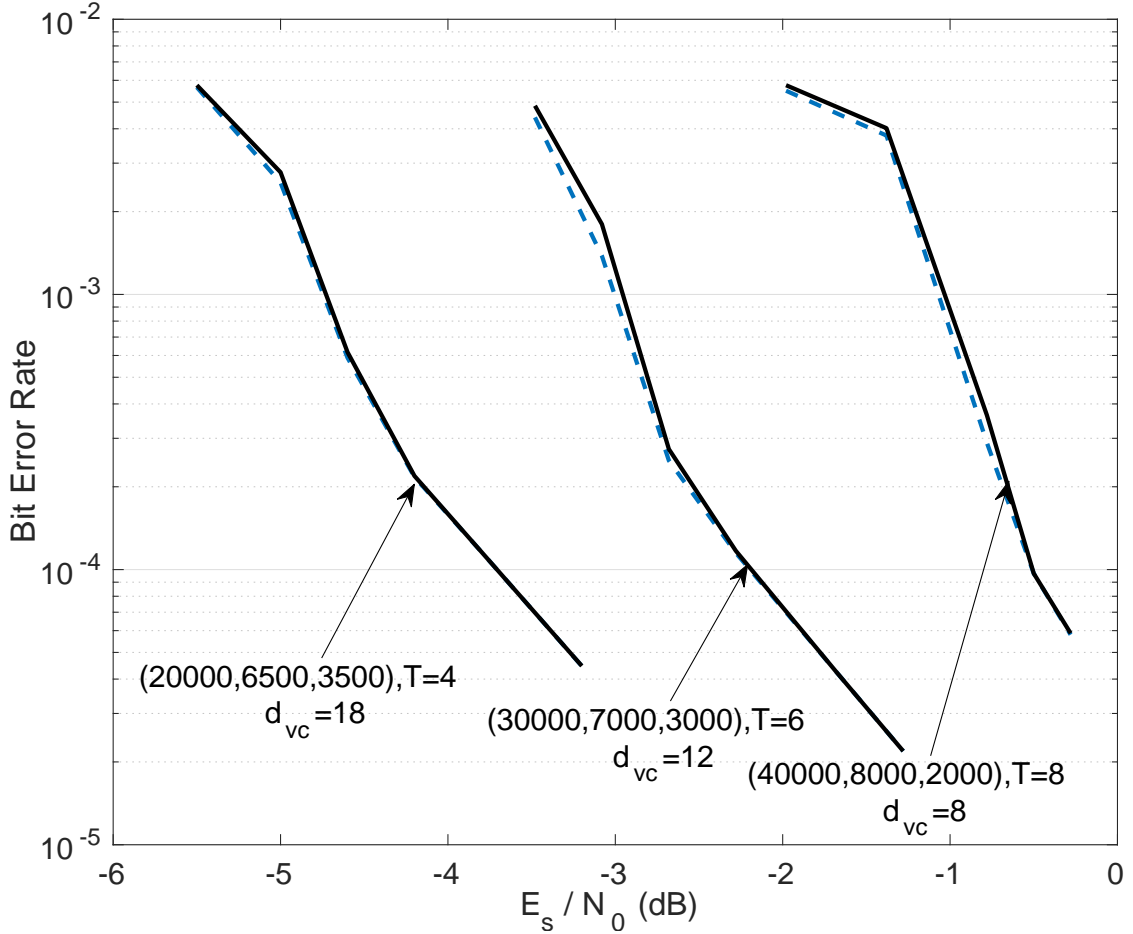


**Figure 5.7:** Performance comparison of the simplified decoding method and the original decoding method for i.i.d. non-uniform sources with  $p_1 = 0.01$ . The labels represent parameters  $\{(K, M, I)\}$ , throughput  $T$ , and  $d_{vc}$ . The blue dashed line indicates the performance of the original method, while the black solid line indicates the performance of the simplified method with the same design.

### 5.4.2.3 Observations

There are some observations from Figure 5.5, Figure 5.6, Figure 5.7, and Figure 5.8 that are worth mentioning. The most important one is that the performance of the simplified decoding method starts to degrade when the throughput increases. However, this degradation is offset when the value of  $p_1$  decreases. The second observation is that when the throughput increases, the proportion of RP symbols also increases, as

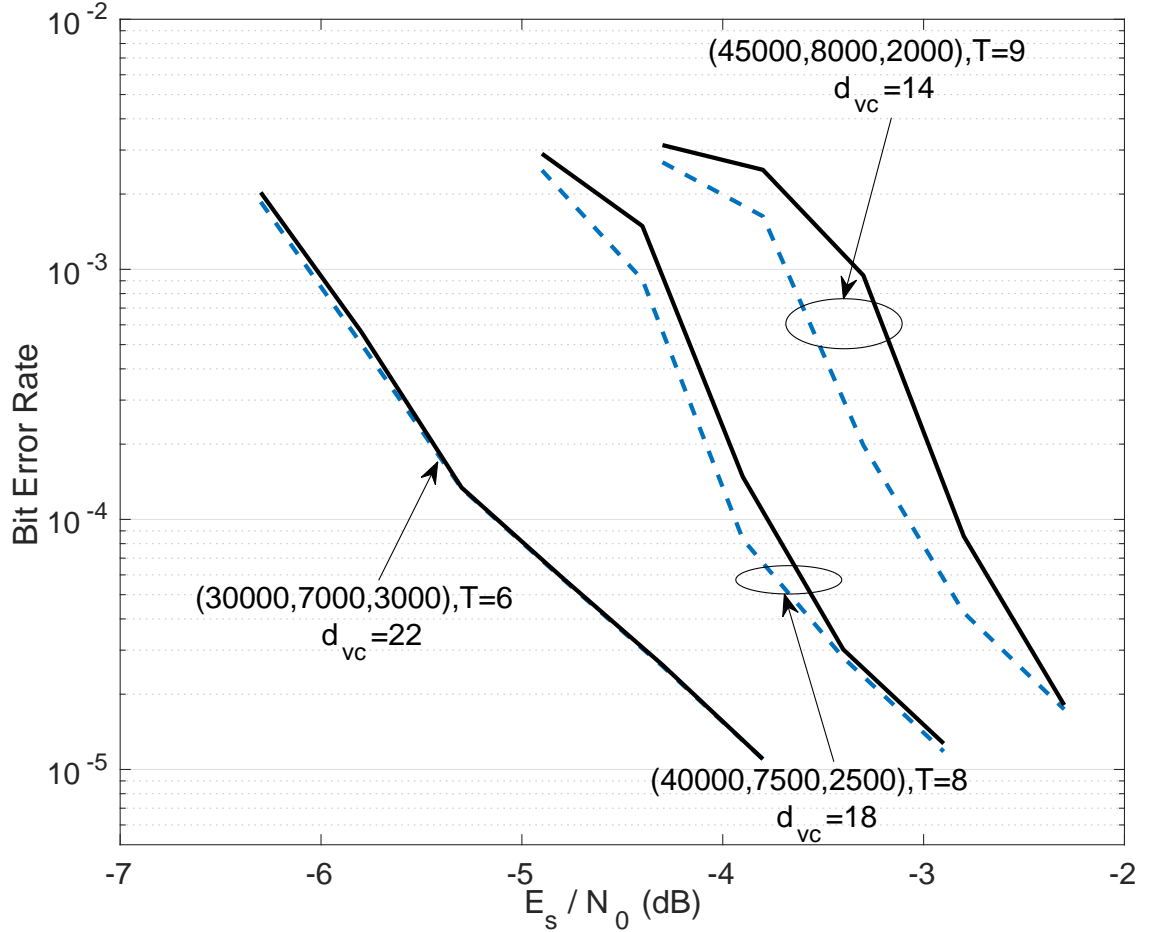


**Figure 5.8:** Performance comparison of the simplified decoding method and the original decoding method for i.i.d. non-uniform sources with  $p_1 = 0.005$ . The labels represent parameters  $\{(K, M, I)\}$ , throughput  $T$ , and  $d_{vc}$ . The blue dashed line indicates the performance of the original method, while the black solid line indicates the performance of the simplified method with the same design.

is shown in all four figures. As explained previously, this is because an RP symbol is more capable of carrying more information (i.e., higher entropy) than a binary bit. Since the number of generated symbols is fixed, when the amount of information to be sent increases, the proportion of RP symbols has to be increased to keep up with the rate, which comes at the cost of more residual errors. However, since the source block is longer, even with a larger number of residual errors, the same BER level can still be achieved. The third observation is that  $d_{vc}$  does decrease when the throughput

**Table 5.8:** Gap to the theoretical limit for hybrid schemes using the original and simplified decoding methods when  $p_1 = 0.005$ . The theoretical limit is in terms of  $E_s/N_0$ . The gap is measured at  $BER < 10^{-4}$ . All results are in dB.

Throughput	$[E_s/N_0]_{lim}$	Gap (original)	Gap (simplified)	Degradation
6	-6.8	1.8	1.8	0
8	-5.4	1.6	1.7	0.1
9	-4.8	1.9	2.1	0.2

increases, which is also shown in all four figures. Notice that the throughput is increased by increasing the source block length, which leads to a larger number of source bits and smaller number of coded bits. If the same  $d_{vc}$  is used, cycles would be generated, which would degrade the system performance. At the same time,  $d_{vc}$  should still be large enough to maintain the power of the LDGM code to correct residual errors. The fourth observation is obtained by comparing the hybrid schemes with the same throughput but different values of  $p_1$ . For instance,  $\{20000, 8000, 2000\}$  in Figure 5.6 and  $\{20000, 6500, 3500\}$  in Figure 5.7, or  $\{40000, 8000, 2000\}$  in Figure 5.7 and  $\{40000, 7500, 2500\}$  in Figure 5.8. It can be seen that the proportion of the RP symbols decreases when  $p_1$  decreases. The reason is the same as for the second observation: as  $p_1$  decreases, the amount of information contained in the block with the same length has been reduced. Therefore, we do not need the same number of RP symbols to carry the information. Thus, some of the RP symbols can be replaced by coded bits to gain some precision in the decoding process. These observations suggest a relationship between the amount of information that needs to be carried through the channel and the capability of correcting the errors to a certain level, providing guidance for the design.

## 5.5 Conclusion

In this chapter, we have proposed a simplified method for the decoding process of the hybrid scheme. The method is to simplify the computations at the RP symbol

nodes by Gaussian approximations of the density function of the linear combination. Thus, the linear combination can be treated as noise, and the operations of convolution and deconvolution can be replaced by simple calculations over the mean and variance of the approximated distributions. We have analyzed the complexity of the original and simplified decoding methods in terms of the required number of additions and multiplications. The analysis has shown that the simplified method can reduce the computational complexity by one order of magnitude on average. We have studied the impact of the design parameters by optimizing the hybrid scheme with simplified decoding. In order to evaluate the performance loss with the simplified method, we have compared the performance of the two decoding methods for sources with  $p_1 = 0.5, 0.1, 0.01, 0.005$ . For each of them, hybrid schemes with different throughputs have been studied by comparing the performance of the optimized hybrid scheme using the original decoding method to the performance for the simplified decoding method. The results have shown that, in most cases, the performance of the simplified method is comparable to that of the original method.

## Chapter 6

### MULTIPLE ACCESS CHANNEL

#### 6.1 Introduction

It is well known (see [118] and [119]) that two jointly ergodic sources  $(\mathbf{U}^1, \mathbf{U}^2)$ , defined over countably infinite alphabets, can be compressed at rates  $(R'_1, R'_2)$  provided that

$$R'_1 \geq H(\mathbf{U}^1 | \mathbf{U}^2) \tag{6.1}$$

$$R'_2 \geq H(\mathbf{U}^2 | \mathbf{U}^1) \tag{6.2}$$

$$R'_1 + R'_2 \geq H(\mathbf{U}^1, \mathbf{U}^2). \tag{6.3}$$

Each source is compressed independently and a joint decoder is applied to recover the original sequences. The Slepian-Wolf result can be seen as a problem of channel coding with side information [120], [121]. Therefore, powerful channel codes can be utilized to exploit prior knowledge at decoder side, such as turbo [90], Low-Density Parity Check (LDPC) [91, 92], [93], and concatenated LDGM [99, 100] codes.

The transmission of correlated sources over a multiple access channel with transmitted energy constraint presents more challenges than the case of just source compression. Although it is optimal to separate the source and channel coding when the energy constraint is defined at the receiver (see for instance [123]), when the energy constraint is at the transmitter the separation principle is not optimal [33]. Interestingly, the theoretical limit in this case is not known. Designing the codewords of the different sources to take advantage of the correlation among sources is necessary to optimize performance [33], but the optimal way to do this is not known.

We consider the scenario where two correlated binary sources are transmitted over a MAC channel. The basic idea is to maintain the correlation between sources in the corresponding codewords, and to exploit the preserved correlation at the decoder site. With the proposed hybrid scheme, the correlation can be exploited by iteratively exchanging information between the decoders of both senders, as done in [43] when digital codes are used. The idea is to use the same RCM structure for both senders so that the low-density nature of the encoder maintains much of the correlation in the resulting codewords.

However, because of the existence of multi-level RP symbols proceeding from the RCM sub-block, the decoding process becomes more cumbersome than for digital coding schemes. On the one hand, symbol reinforcement, which is the basis for good digital schemes (see [43]), becomes more ambiguous for RP symbols, which leads to degradation in the system performance. On the other hand, the complexity to decode superimposed multi level RP symbols is very high. Therefore, we will present a novel effective decoding structure to tackle these problems. The resulting performance is very close to the theoretical limit assuming separation between source and channel coding, even for high information rates.

The remainder of this chapter is organized as follows. Section 6.2 introduces the multiple access channel model used in this chapter and presents the theoretical limit assuming separation between source and channel coding. Section 6.2 provides an overview of the hybrid coding scheme, while Section 6.3.1 explains how the encoder is applied to MAC. Section 6.3.2 provides an overview of the decoding procedure, which is explained in detail in Section 6.4. Section 6.5 presents the simulation results, and Section 6.6 concludes the chapter.

## 6.2 Multiple Access Channel

Figure 6.1 shows the system model for the two user MAC. Each source is encoded independently with a hybrid encoder of rate  $R_{c_i}$ , producing sequences  $\mathbf{X}^1$  and  $\mathbf{X}^2$ , which are transmitted over the AWGN MAC. The average energy used by sender  $i$  is

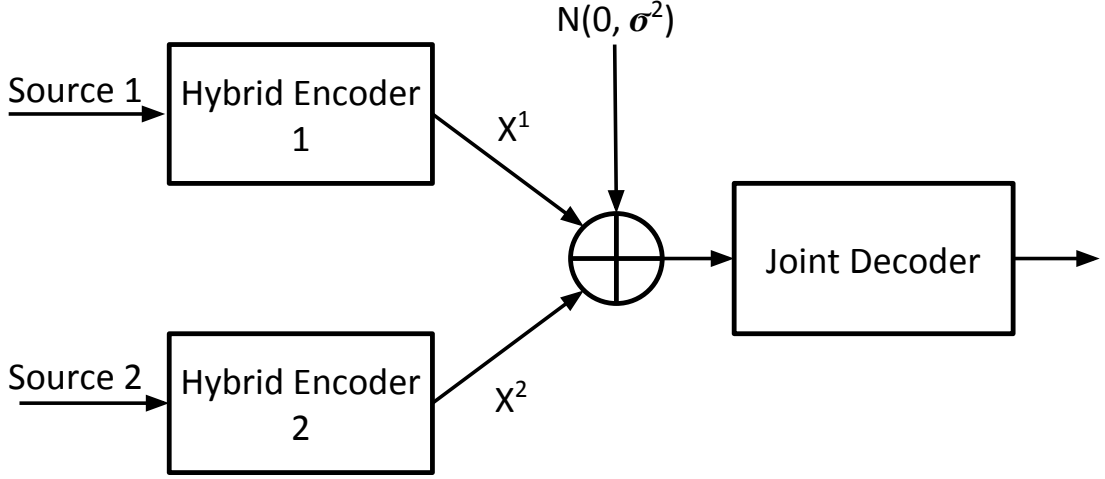


**Figure 6.1:** System diagram for a multiple access channel.

denoted as  $E_{s_i}$ . Thus, the average energy per channel use is  $E_s = E_{s_1} + E_{s_2}$ . To define a reference point to compare the performance of the proposed hybrid coding scheme, we consider the theoretical limit assuming separation between source and channel coding. The separation approach requires compression of the correlated sources to the Slepian-Wolf limit first, and then utilizing a capacity achieving code. The theoretical limit of the two user MAC with QAM modulation (assuming separation) can be defined as:

$$R_1 < \log_2\left(1 + \frac{E_{s1}}{N_0}\right), \quad (6.4)$$

$$R_2 < \log_2\left(1 + \frac{E_{s2}}{N_0}\right), \quad (6.5)$$

$$R = R_1 + R_2 < \log_2\left(1 + \frac{E_s}{N_0}\right), \quad (6.6)$$

where  $R_i$  is the number of information bits transmitted per channel use for sender  $i$  and  $E_s = E_{s_1} + E_{s_2}$ . Therefore, the energy spent to transmit one source bit is  $E_{so} = E_s/(4R_c)$ . We will consider symmetric systems where  $R_c = R_{c1} = R_{c2}$  and  $E_{s1} = E_{s2}$ . Therefore, the information rate,  $R$ , is defined as  $R = 2H(\mathbf{U}^1, \mathbf{U}^2)R_c$ ,

where  $H(\mathbf{U}^1, \mathbf{U}^2)$  is the joint entropy of the two sources. Thus, the theoretical limit in terms of  $E_{so}/N_0$  can be computed as

$$\frac{E_{so}}{N_0} (dB) = 10 \log_{10} \left( \frac{2^R - 1}{4R_c} \right). \quad (6.7)$$

### 6.3 Proposed Joint Source Channel Coding Structure

#### 6.3.1 Proposed Hybrid Encoder

As discussed previously, we consider the scenario where two correlated binary sources are transmitted over a multiple access channel. As shown in Figure 6.2, each source is encoded independently using a hybrid encoder. The structure of each encoder is a hybrid encoder. Therefore,  $X^1$  and  $X^2$  contain both RP symbols and digital bits, which are superimposed in the MAC.

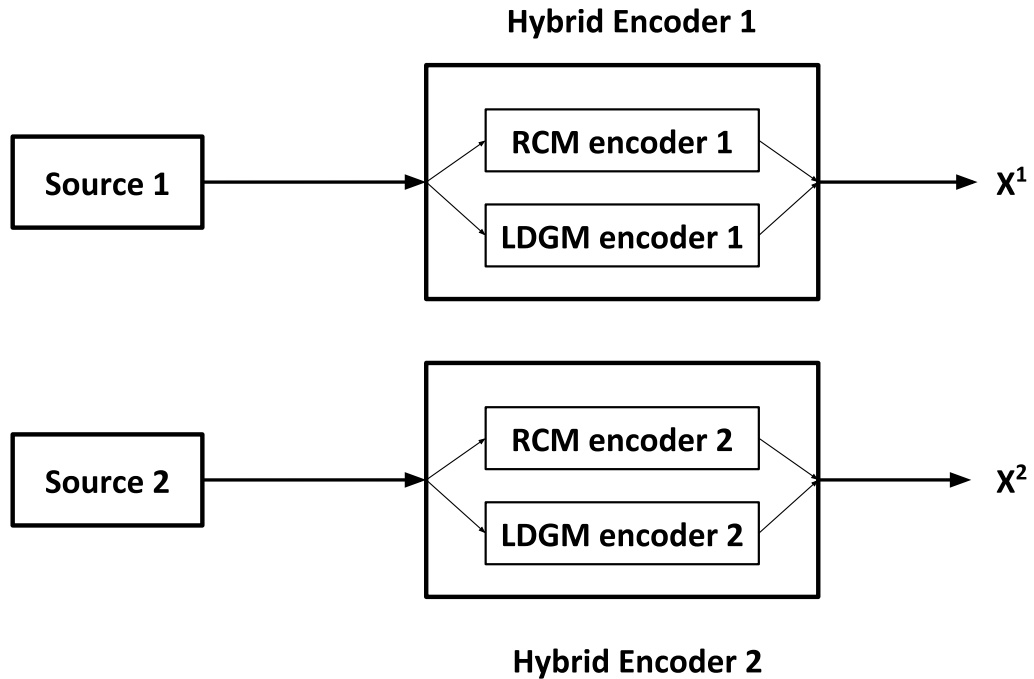


**Figure 6.2:** Encoder structure of the proposed hybrid coding scheme for the MAC.

To obtain good performance, correlation between sources should be preserved as much as possible in the generated codewords, so that it can be exploited at the decoder

site. To achieve this, source bits are also transmitted over the MAC, which is different from the case of point-to-point communications considered in Chapter 4, where only RP symbols and coded bits are transmitted through the channel. Because the sources are highly correlated at the bit level, there is mutual reinforcement between senders in most of the positions of the source bits, with few positions that have interference. These mutual reinforced positions help correct positions with interference in the iterative decoding process. In addition, the same RCM encoder structure is used for both hybrid encoders to maintain the correlation in the generated RP symbols, i.e., the generator matrices for both RCM systems are the same,  $G_r^1 = G_r^2$ . However, for the positions with interference, it is difficult to assign the bit to the right sender by just looking at the received symbols. If the assignment is wrong, this will reinforce the error in the other decoder and degrade the performance. These errors are specific for the MAC case, and occur in addition to the errors in the original hybrid coding scheme. To resolve this ambiguity, each sender uses a different LDGM code. This leads to a loss in the degree of correlation that can be exploited in the decoder for the coded bits.

### 6.3.2 Synthetic Joint Decoder

At the receiver, a joint decoder should be used to jointly decode the two sources. Figure 6.3 shows the standard structure of a joint decoder from [43] applied to the proposed hybrid scheme. Notice that two hybrid decoders connect to each other through the source bit nodes and the channel observation links. The structure of each decoder is the same as in Figure 3.1. Belief propagation starts from one decoder and messages are exchanged between the two decoders through the source bit nodes and the channel observation links in each iteration. However, the ambiguity mentioned before appears when updating the messages proceeding from the multi-level RP symbols. To see this, recall that the channel observation  $r_s$  is expressed as

$$r_s = \Gamma a^1 + \Gamma a^2 + n, \quad (6.8)$$

where  $a^1$  and  $a^2$  are RP symbols before modulation,  $\Gamma$  is a normalization factor and  $n \sim N(0, \sigma^2)$ . Assuming a noiseless MAC channel and highly correlated binary sources,

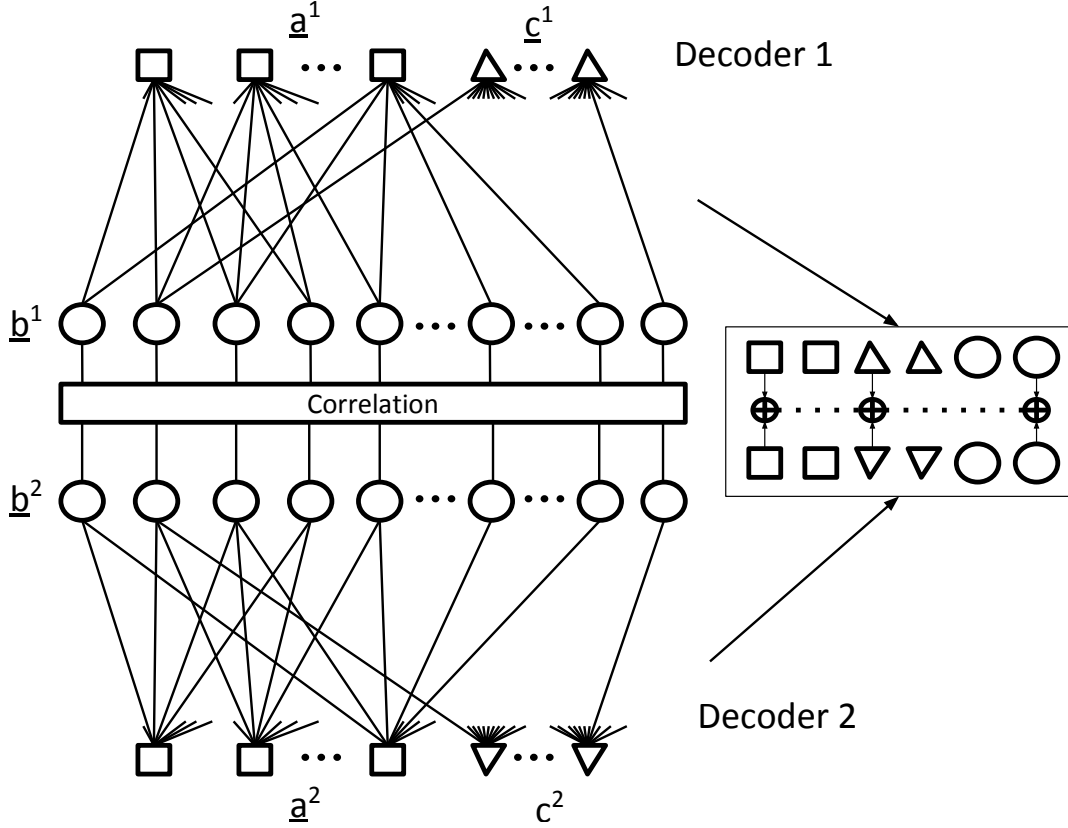


**Figure 6.3:** Standard joint decoder for MAC applied to the hybrid scheme.

the received symbols for the source bits can only have three possible values: most of them are  $2\sqrt{E_s/2}$  and  $-2\sqrt{E_s/2}$  with few 0's. The values of  $2\sqrt{E_s/2}$  and  $-2\sqrt{E_s/2}$  correspond to positions where mutual reinforcement occurs. Therefore, the transmitted bits pairs can be decoded easily. With multi-level RP symbols, this interpretation becomes more complicated, as the received symbols at each position can be produced by different combinations of  $a^1$  and  $a^2$ . More specifically, in each iteration, the density function of each RP node has to be calculated based on the density function of the other RP node in the pair. Defining the set of possible RP symbol values as  $\mathbb{S}$ , we have

$$P(r_s|a^p = k) = \sum_{m \in \mathbb{S}} P(r_s|a^p = k, a^q = m), k, m \in \mathbb{S}, \quad (6.9)$$

where  $p, q = 1, 2$ . For instance, assuming a noiseless channel, if  $\mathbb{S} = [-6, 6]$  and both senders send a 4 (the normalization factor is not considered), the observation

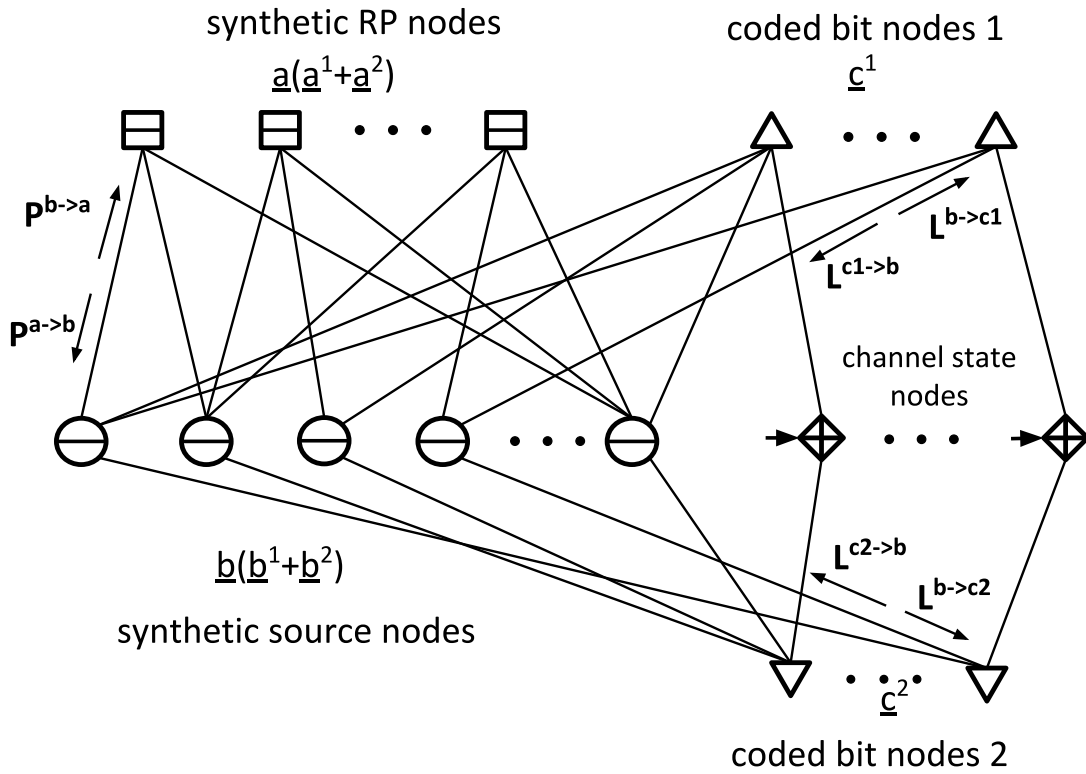


**Figure 6.4:** Structure of the proposed synthetic decoder for the MAC.

for the superimposed RP symbol  $(a^1 + a^2)$  would be 8. Instead of a unique solution as in the case of binary bits, the pairs  $(2, 6), (3, 5), (4, 4), (5, 3), (6, 2)$  are all equally likely. The larger the set  $\mathbb{S}$  is, the more candidate pairs will exist. Therefore, there is uncertainty even at the positions with mutual reinforcement. This ambiguity can produce estimation errors in the RP nodes, and further introduce errors to the source bit nodes, degrading the performance of the RCM sub-block in both decoders so that the LDGM codes are not able to correct the large number of errors.

To address this issue, we propose a decoder composed of the Cartesian product of the source bit nodes (synthetic source bit nodes), the Cartesian product of the RP nodes (synthetic RP nodes), and the coded bit nodes for each LDGM code, as shown in Figure 6.4. The basic idea of using synthetic nodes is to integrate the nodes

corresponding to the two decoders into one “super” node, merging corresponding links. Notice that the RCM generator matrices for the two senders are the same, and thus every two RP symbol nodes at the same position (one from decoder 1 and one from decoder 2) have the same links and weight order. Therefore, every two RP symbol nodes in Figure 6.3 can be integrated into one synthetic RP symbol node, as shown in Figure 6.4. Analogously, for the source bit nodes we integrate the source bit nodes from the two decoders into one synthetic source bit node. Then, we use this structure to compute the messages within the RCM sub-block. Notice that the links between synthetic RP nodes and synthetic source bit nodes transfer joint messages, as described in the sequel. When computing the messages within the LDGM sub-block, the source bit nodes from the two senders are treated individually, as the LDGM encoders for the two senders are different, and the coded bit nodes for each sender remain as individual nodes connected to the corresponding individual component of the synthetic source bit nodes. Thus, only the RCM sub-block propagates the joint messages, which as we will see in the sequel are the density functions of the synthetic source bit nodes, i.e., the sum of the two source bits, and the LDGM sub-block aims at distinguishing between senders by using different LDGM codes for each source. By utilizing synthetic nodes, the performance can be improved significantly, and the computational complexity can also be reduced.

#### 6.4 Algorithm for Synthetic Decoding

As shown in Figure 6.4, there are two forms of messages propagated in the graph: joint messages propagated in the RCM sub-block, and individual messages propagated between coded bit nodes and its neighboring individual source node components in the LDGM sub-block. Table 6.1 presents all the notations used in the synthetic decoding algorithm.

**Table 6.1:** Definitions for the synthetic decoding algorithm

$b$	Synthetic source bit nodes representing the sum of the source bits $b^s = b^1 + b^2$ .
$a$	Synthetic RP nodes representing the sum of the RP symbols $a^s = a^1 + a^2$ .
$r_b$	Channel observation for the superimposed source bits.
$r_s$	Channel observation for the superimposed RP symbols.
$r_c$	Channel observation for the superimposed coded bits.
$\mathbf{P}_0^b$	Channel message for the synthetic source bit node.
$\mathbf{P}_0^a$	Channel message for the synthetic RP node.
$L_0^{c^{(1,2)}}$	Channel message for the coded bit nodes.
$P^{a \rightarrow b}$	pmf message from a synthetic RP node to a neighboring synthetic source bit node.
$P^{b \rightarrow a}$	pmf message from a synthetic source bit node to a neighboring synthetic RP node.
$P^{RP}(\cdot)$	pmf of a synthetic source bit node considering information within the RCM sub-block.
$P^{L1}(\cdot)$	pmf of a source bit node in decoder 1 considering information within LDGM 1.
$P^{L2}(\cdot)$	pmf of a source bit node in decoder 2 considering information within LDGM 2.
$L^{b \rightarrow c^q}$	LLR message from an individual source bit node to a neighboring coded bit node of LDGM $q$ ( $q = 1, 2$ ).
$L^{c^q \rightarrow b}$	LLR message from a coded bit node to a neighboring individual source bit node of LDGM $q$ ( $q = 1, 2$ ).

#### 6.4.1 Computation at the Synthetic RP node

As explained before, the RP symbol nodes corresponding to the same position have the same number of links, and the weights associated with the links are arranged in the same manner. Each node in the pair also connects to the source bit nodes in the same position in their respective graphs, as shown in Figure 6.3. Therefore, as explained before, every pair of RP symbol nodes can be integrated into a synthetic node, so that information can be jointly considered. Figure 6.5 shows the structure of a synthetic RP symbol node. To calculate the messages exchanged from the synthetic

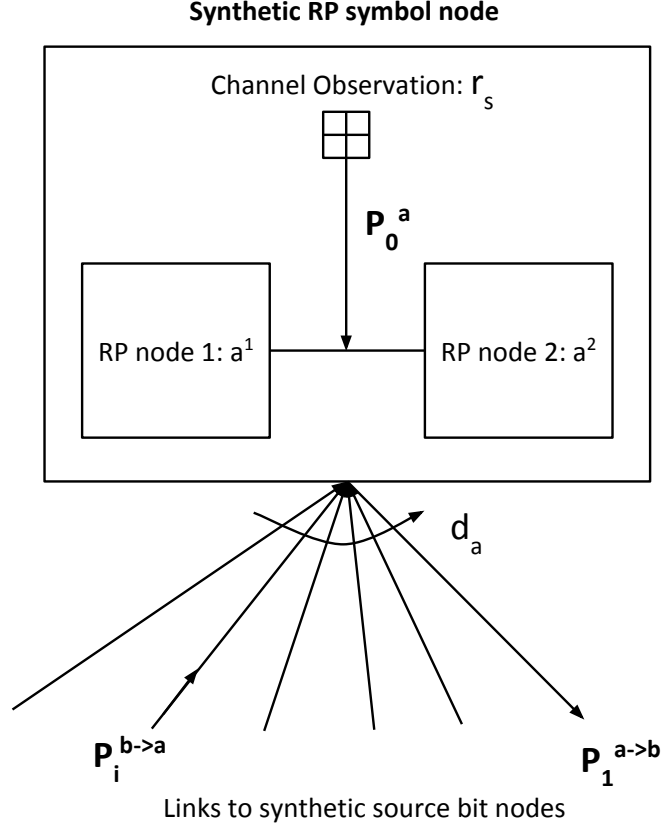


**Figure 6.5:** Structure of a synthetic RP node for the MAC.

RP node to its neighboring synthetic source bit nodes,  $\mathbf{P}^{a \rightarrow b}$ , we have to consider the message proceeding from the channel observation  $r_s$ ,  $\mathbf{P}_0^a$ , and the messages proceeding from  $d_a$  neighboring synthetic source bit nodes,  $\mathbf{P}^{b \rightarrow a}$ .

To obtain the message proceeding from the channel observation  $r_s$ , which will not change with the iteration number, we consider the equation

$$r_s = \Gamma a^s + n = \Gamma(a^1 + a^2) + n = \Gamma \sum_{i=1}^{d_a} w_i b_i^s + n, \quad (6.10)$$

where  $\Gamma$  is a normalization factor. Based on (6.10), we calculate the pmf vector  $\mathbf{P}_0^a$  for  $a^s$ , which consists of the density at each possible value of  $a^s$  computed from the distribution  $N(r_s, \sigma^2)$ . Notice that  $\mathbf{P}_0^a$  is normalized so that the sum of the densities

in the vector is 1. Specifically,  $P_0^a(k)$  is defined as

$$P_0^a(k) = P(r_s | a_s = k), k \in [-2l, 2l], \quad (6.11)$$

Notice that if  $a^q \in [-l, l], q = 1, 2$ , then  $a^s \in [-2l, 2l]$ . Thus, the vector  $\mathbf{P}_0^a$  can be built as

$$\mathbf{P}_0^a = [P_0^a(-2l), \dots, P_0^a(2l)] \quad (6.12)$$

To calculate the joint messages exchanged from the synthetic RP node to its neighboring synthetic source bit nodes,  $\mathbf{P}^{a \rightarrow b}$ , we start by considering the relationship between  $a^s$  and  $b_i^s$ , as shown in (6.10). Notice that  $b_i^s = b_i^1 + b_i^2 \in [0, 1, 2]$ , the summation of two source bits in the same position, characterizes the joint message to be passed. Without loss of generality, to calculate the message to the first neighboring synthetic source bit node

$$\mathbf{P}_1^{a \rightarrow b} = [P_1^{a \rightarrow b}(0), P_1^{a \rightarrow b}(1), P_1^{a \rightarrow b}(2)], \quad (6.13)$$

where  $P_1^{a \rightarrow b}(k)$  is the probability that  $b_1^1 + b_1^2 = b_1^s = k$ , we consider

$$a^s = w_1 b_1^s + \sum_{i=2}^{d_a} w_i b_i^s. \quad (6.14)$$

Therefore, we can obtain

$$P_1^{a \rightarrow b}(0) = \sum_{k \in [-2l, 2l]} P(a^s = k) P\left(\sum_{i=2}^{d_a} w_i b_i^s = k\right), \quad (6.15)$$

$$P_1^{a \rightarrow b}(1) = \sum_{k \in [-2l, 2l]} P(a^s = k) P\left(\sum_{i=2}^{d_a} w_i b_i^s = k - w_1\right), \quad (6.16)$$

$$P_1^{a \rightarrow b}(2) = \sum_{k \in [-2l, 2l]} P(a^s = k) P\left(\sum_{i=2}^{d_a} w_i b_i^s = k - 2w_1\right), \quad (6.17)$$

where  $P(a^s = k) \propto P_0^a(k)$  is obtained from channel message vector  $\mathbf{P}_0^a$  in (6.12), and  $P(\sum_{i=2}^{d_a} w_i b_i^s = k)$  can be obtained by convolving the incoming pmf messages  $\mathbf{P}^{b \rightarrow a}$ . In

order to reduce the computational complexity, the pmf of  $\sum_{i=1}^{d_a} w_i b_i^s$  is computed first by convolving the pmfs of messages  $w_i b_i^s$ , which can be obtained from  $\mathbf{P}_i^{b \rightarrow a}$ , the pmfs of messages  $b_i^s$ , and the value of  $w_i$ . When computing the pmf of  $\sum_{i=2}^{d_a} w_i b_i^s$ , we just deconvolve the pmf of  $w_1 b_1^s$  from the pmf of the whole linear combination. The zig-zag deconvolution technique in [88] is extended here to get the values in (6.15), (6.16) and (6.17). See appendix for more details.

#### 6.4.2 Computation at the LDGM Coded Bit Node

The computation at the LDGM coded bit node is the same as in a regular LDGM code [116]. However, since the coded bit node for source 1,  $c^1$ , is connected to the coded bit node for source 2,  $c^2$ , through a channel state node, i.e.,  $r_c = c^1 + c^2 + n$ , the channel message is different at each iteration. The channel message for  $c^1$ , defined as  $L_0^{c^1}$ , can be computed as

$$\begin{aligned} L_0^{c^1} &= \log \frac{P(r_c | c^1 = 0)}{P(r_c | c^1 = 1)} \\ &= \log \frac{P(r_c | c^1 = 0, c^2 = 0)P(c^2 = 0) + P(r_c | c^1 = 0, c^2 = 1)P(c^2 = 1)}{P(r_c | c^1 = 1, c^2 = 0)P(c^2 = 0) + P(r_c | c^1 = 1, c^2 = 1)P(c^2 = 1)}, \end{aligned} \quad (6.18)$$

Notice that  $P(c^2 = k)$  is calculated by using the messages calculated proceeding from the synthetic source bit nodes connected to  $c^2$  (see Section 6.4.3.2). The channel message for  $c^2$ ,  $L_0^{c^2}$ , can be computed in the same way.

After obtaining  $L_0^{c^q}$ ,  $q = 1, 2$ , for sender  $q$  in each iteration, the messages to the source bit nodes,  $L_i^{c^q \rightarrow b}$ ,  $q = 1, 2$ , are calculated as in regular LDGM codes, using the channel message calculated in (6.18), and the messages proceeding from the synthetic source bit nodes (see Section 6.4.3).

#### 6.4.3 Computation at the Synthetic Source Bit Node

The messages from the synthetic RP symbol nodes,  $\mathbf{P}^{a \rightarrow b}$ , and the individual messages from LDGM coded bit nodes,  $L^{c^1 \rightarrow b}$  and  $L^{c^2 \rightarrow b}$ , are the inputs to the synthetic source bit node, as shown in Figure 6.6. The synthetic source bit node as a whole receives the joint messages,  $\mathbf{P}^{a \rightarrow b}$ , while each individual source bit node receives the

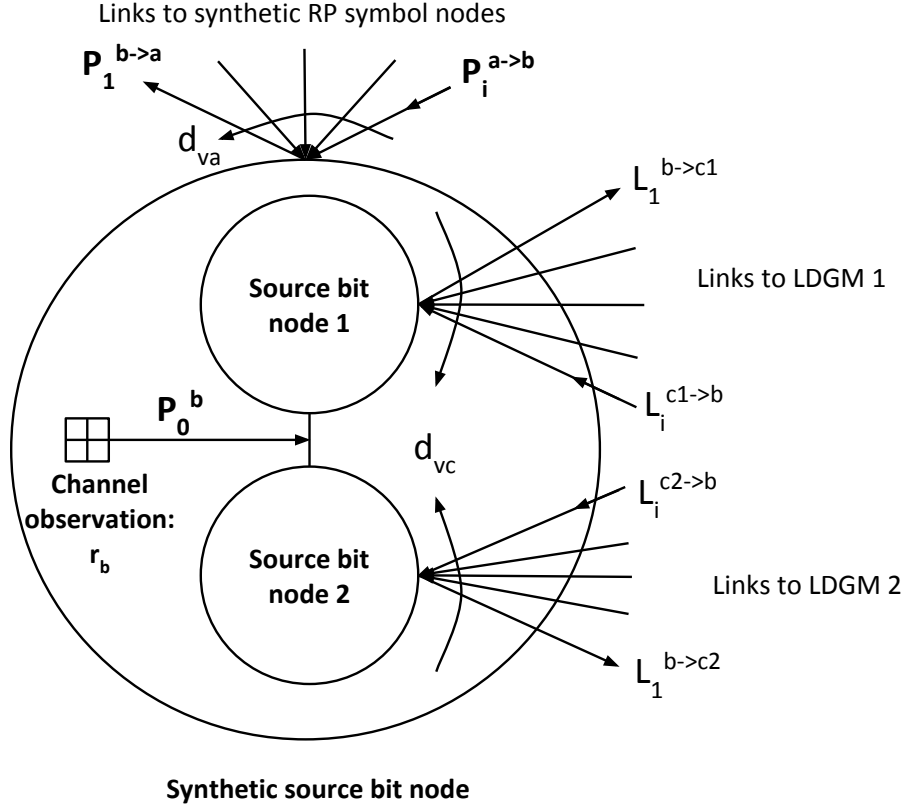


**Figure 6.6:** Structure of a synthetic source bit node.

individual messages from its corresponding LDGM coded bit nodes, i.e., source bit node 1 receives  $L^{c1 \rightarrow b}$ , and source bit node 2 receives  $L^{c2 \rightarrow b}$ .

Message passing starts with initial messages computed from the channel observation  $r_b$ . Denote the sum of the source bits from the two senders in a given position as  $b^s = b^1 + b^2$ . From the channel observation,  $r_b = b^s + n$ , we build the vector

$$\begin{aligned} \mathbf{P}_0^b &= [P(r_b|b^s = 0), P(r_b|b^s = 1), P(r_b|b^s = 2)] \\ &= [P_0^b(0), P_0^b(1), P_0^b(2)], \end{aligned} \tag{6.19}$$

This vector corresponds to the initial message proceeding from the channel, and will be used in each iteration of the decoding algorithm. Notice that  $\mathbf{P}_0^b$  is normalized.

There are two types of messages calculated in the synthetic source bit nodes as computed below.

#### 6.4.3.1 Messages to synthetic RP nodes ( $P^{b \rightarrow a}$ )

Without loss of generality, assume the joint message to the first neighboring synthetic RP node,  $\mathbf{P}_1^{b \rightarrow a}$ , is to be computed. From incoming messages  $L^{c^1 \rightarrow b}$ , the probability of  $b^1$  being 0 or 1 based on the information proceeding from LDGM 1, denoted as  $P^{L1}(0) = 1 - P^{L1}(1)$ , can be obtained as

$$P^{L1}(0) = \frac{e^{\sum_{i=1}^{d_{vc}} L_i^{c^1 \rightarrow b}}}{1 + e^{\sum_{i=1}^{d_{vc}} L_i^{c^1 \rightarrow b}}}. \quad (6.20)$$

$$(6.21)$$

Similarly,  $P^{L2}(0)$  and  $P^{L2}(1)$  can be obtained from  $L^{c^2 \rightarrow b}$ .

The messages proceeding from the synthetic RP nodes can be combined as

$$P^{RP}(k) = \beta \prod_{i=1}^{d_{va}} P_i^{a \rightarrow b}(k), k = 0, 1, 2, \quad (6.22)$$

where  $P^{RP}(k)$  is the probability that  $b^s = b^1 + b^s = k$  using only the information proceeding from the synthetic RP nodes.

Thus, we obtain the messages to the first neighboring synthetic RP node,  $\mathbf{P}_1^{b \rightarrow a} = [P_1^{b \rightarrow a}(0), P_1^{b \rightarrow a}(1), P_1^{b \rightarrow a}(2)]$ , by considering the information proceeding from the channel, neighboring synthetic RP nodes and LDGM codes as

$$P_1^{b \rightarrow a}(0) = \beta [P^{RP}(0) / P_1^{a \rightarrow b}(0)] P^{L1}(0) P^{L2}(0) P_0^b(0) \quad (6.23)$$

$$P_1^{b \rightarrow a}(1) = \beta [P^{RP}(1) / P_1^{a \rightarrow b}(1)] (P^{L1}(0) P^{L2}(1) + P^{L1}(1) P^{L2}(0)) P_0^b(1) \quad (6.24)$$

$$P_1^{b \rightarrow a}(2) = \beta [P^{RP}(2) / P_1^{a \rightarrow b}(2)] P^{L1}(1) P^{L2}(1) P_0^b(2), \quad (6.25)$$

where  $P_0^b(\cdot)$  is the initial pmf message computed from the channel observation and  $\beta$  is the normalization factor.

### 6.4.3.2 Individual messages to coded bit nodes ( $L^{b \rightarrow c^1}, L^{b \rightarrow c^2}$ )

When updating the outgoing messages to the LDGM coded bit nodes, an observation into the internal state of the synthetic source bit node is required. Notice that the two individual source bit nodes are connected by the channel observation and there is correlation between them, which needs to be exploited properly. Assume the LLR message exchanged to the first neighboring coded bit node in LDGM 1,  $L_1^{b \rightarrow c^1}$ , is to be computed. The process starts by computing the probability of  $b^1$  at iteration  $m$  by considering all incoming messages

$$\begin{aligned} P^m(b^1 = 0) &= P^{L^1}(0)[P^{m-1}(b^2 = 0)(1-p) + P^{m-1}(b^2 = 1)p][P_0^b(0) \\ &\quad + P_0^b(1)P^{m-1}(b^2 = 1)][P^{RP}(0) + P^{RP}(1)P^{m-1}(b^2 = 1)] \end{aligned} \quad (6.26)$$

$$\begin{aligned} P^m(b^1 = 1) &= P^{L^1}(1)[P^{m-1}(b^2 = 0)p + P^{m-1}(b^2 = 1)(1-p)][P_0^b(2) \\ &\quad + P_0^b(1)P^{m-1}(b^2 = 0)][P^{RP}(2) + P^{RP}(1)P^{m-1}(b^2 = 0)], \end{aligned} \quad (6.27)$$

where  $P_0^b(\cdot)$  is the initial estimate calculated in (6.19) and  $P^{m-1}(b^2 = k)$  is the estimate of  $b^2$  from the previous iteration. Thus, the LLR message, denoted as  $L_s^1$ , can be obtained as  $L_s^1 = \log \frac{P^m(b^1=0)}{P^m(b^1=1)}$ . Therefore, the message passed to the first neighboring coded bit node in LDGM 1 is computed as

$$L_1^{b \rightarrow c^1} = L_s^1 - L_1^{c^1 \rightarrow b}. \quad (6.28)$$

Similarly,  $L_s^2$  and  $L^{b \rightarrow c^2}$  can be computed.

### 6.4.3.3 Decision

As there are joint messages and individual messages, the decision can be made utilizing either the overall joint messages or the overall LLR values. Here, the overall

joint messages are used, choosing the pair that has the highest possibility

$$P(b^1 = 0, b^2 = 0) = 0.5(1 - p) \cdot P^{RP}(0) \cdot P^{L1}(0) \cdot P^{L2}(0) \cdot P_0^b(0), \quad (6.29)$$

$$P(b^1 = 0, b^2 = 1) = 0.5p \cdot P^{RP}(1) \cdot P^{L1}(0) \cdot P^{L2}(1) \cdot P_0^b(1), \quad (6.30)$$

$$P(b^1 = 1, b^2 = 0) = 0.5p \cdot P^{RP}(1) \cdot P^{L1}(1) \cdot P^{L2}(0) \cdot P_0^b(1), \quad (6.31)$$

$$P(b^1 = 1, b^2 = 1) = 0.5(1 - p) \cdot P^{RP}(2) \cdot P^{L1}(1) \cdot P^{L2}(1) \cdot P_0^b(2). \quad (6.32)$$

#### 6.4.4 Simplified Method for MAC

Even with the synthetic decoder structure, which simplifies the decoding algorithm by jointly considering the messages, the decoding complexity is still high. In order to reduce computational complexity, we can apply the simplified method proposed in Chapter 5 to this scenario. Specifically, we approximate the distribution of the synthetic RP symbol node, i.e., the value of  $a^s$ , as a Gaussian distribution. The difference with Section 5.2.1 is that the value of the neighboring synthetic source bit nodes,  $b^s$ , may be 0, 1, and 2, while only binary values are considered in Chapter 5.

Using the same notation as in Section 5.2.1, we denote the linear combination of synthetic source bits except the  $i$ th one as

$$x_i = \sum_{\substack{j=1 \\ j \neq i}}^{d_a} w'_j b_i^s, \quad (6.33)$$

where  $w'_j = \Gamma w_j$  ( $\Gamma$  is a normalization factor), and  $b_i^s = b_i^1 + b_i^2, \in [0, 1, 2]$ . Thus the mean,  $m_i$ , and the variance,  $\sigma_i^2$ , can be properly computed. As we have

$$r_s = w'_i b_i^s + x_i + n = x'_i b_i^s + n'_i \quad (6.34)$$

where  $n'_i$  is the equivalent noise by considering  $x_i$  as noise and  $n'_i \sim N(m_i, \sigma_i^2 + \sigma_2)$ . Therefore, the pmf message to the  $i$ th neighboring synthetic source bit node,  $\mathbf{P}_1^{a \rightarrow b}$ , can be obtained as

$$P_1^{a \rightarrow b}(0) = \beta P(r_s | b_i^s = 0) \quad (6.35)$$

$$P_1^{a \rightarrow b}(1) = \beta P(r_s | b_i^s = 1) \quad (6.36)$$

$$P_1^{a \rightarrow b}(2) = \beta P(r_s | b_i^s = 2), \quad (6.37)$$

where  $\beta$  is the normalization factor, and  $P(r_s | b_i^s = k), k = 0, 1, 2$ , can be computed using the Gaussian density function. Therefore, the complicated computations at the synthetic RP symbol node are replaced by simple calculations, and the complexity is reduced.

## 6.5 Simulation Results

We consider a scenario where high correlation exists between two sources. The correlation is defined by parameter  $p$ , the probability that source bits of the two senders located at the same position differ. We will study the case where  $p = 0.01$  and  $p = 0.005$ . The performance of the system is evaluated by calculating the gap to the theoretical limit assuming separation between source and channel coding when  $BER < 10^{-4}$ .

### 6.5.1 System Optimization

For each sender, the information block length is fixed to  $K = 10,000$  and the total number of generated symbols is fixed to  $L = 20,000$ ,  $M$  of which coming from the RCM system and  $I = 20000 - M$  of them proceeding from the LDGM code. As discussed previously, the source bits are also transmitted through the channel. Therefore, the overall code rate is  $R_c = 1/3$ . As mentioned before, QAM modulation is used so that there are 15,000 symbols transmitted over the channel.

Table 6.2 shows the joint entropy  $H(\mathbf{U}^1, \mathbf{U}^2)$  of the correlated sources, the information rate  $R$ , and the theoretical limits assuming separation between source and channel coding. Notice that  $p$  is known at the decoder in all cases.

For the implementation of the RCM system, we use a weight set that leads to good performance for the case of point-to-point transmission of asymmetric sources,

**Table 6.2:** Theoretical limits for different values of  $p$  ( $R_c = 1/3$ )

$p$	$H(U^1, U^2)$	$R$	$[E_{so}/N_0]_{lim}(dB)$
0.01	1.08	0.72	-3.13
0.005	1.04	0.69	-3.31

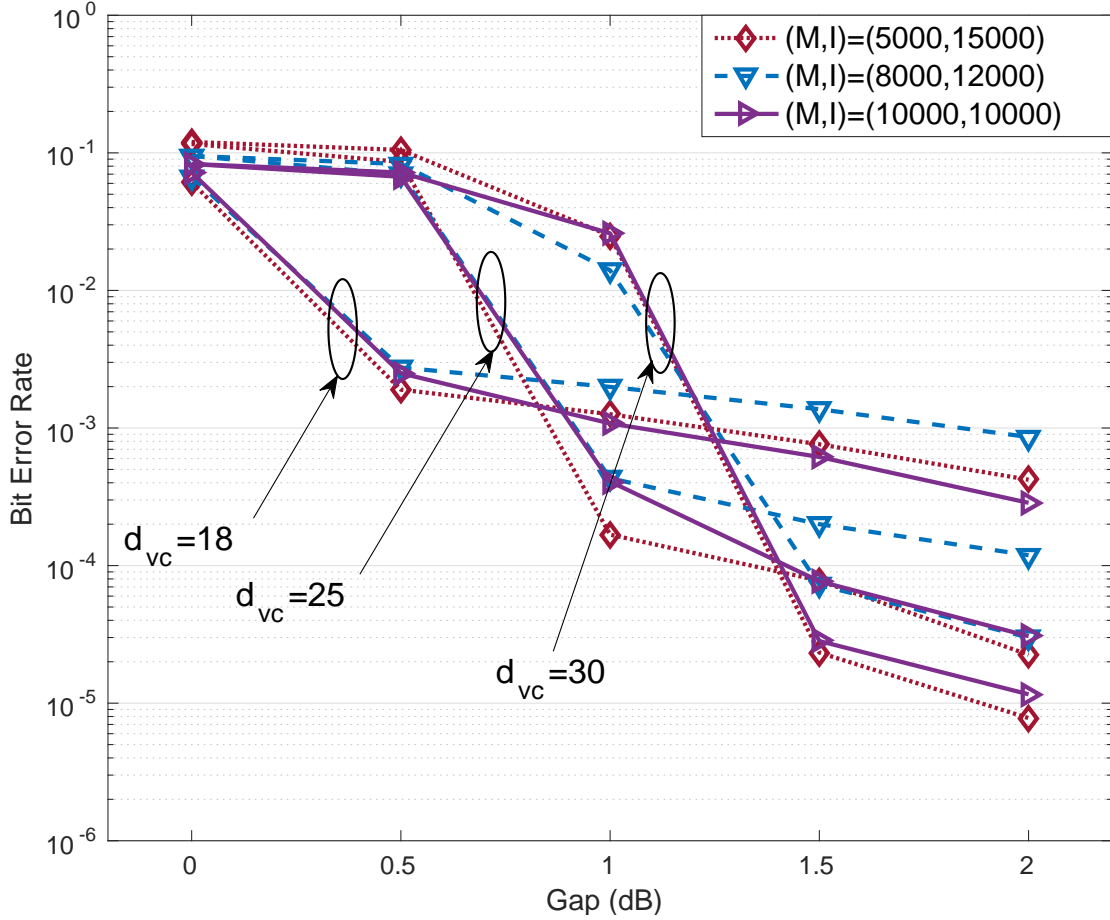
studied in [117]:  $\{\pm 1, \pm 1, \pm 1, \pm 1, \pm 2, \pm 2, \pm 2, \pm 2\}$ . The basic unit of generator matrix  $G_0$  is constructed as:

$$G_0 = \begin{bmatrix} \pi(A_1) & \pi(A_2) & \pi(A_1) & \pi(A_2) & \pi(A_1) & \pi(A_2) & \pi(A_1) & \pi(A_2), \\ \pi(A_2) & \pi(A_1) & \pi(A_2) & \pi(A_1) & \pi(A_2) & \pi(A_1) & \pi(A_2) & \pi(A_1), \\ \pi(A_1) & \pi(A_2) & \pi(A_1) & \pi(A_2) & \pi(A_1) & \pi(A_2) & \pi(A_1) & \pi(A_2), \\ \pi(A_2) & \pi(A_1) & \pi(A_2) & \pi(A_1) & \pi(A_2) & \pi(A_1) & \pi(A_2) & \pi(A_1). \end{bmatrix},$$

By varying  $M$ ,  $I$ , and  $d_{vc}$ , the degree of the source bit node (individual) when considering only the LDGM sub-block, we assess the effect of these design parameters.

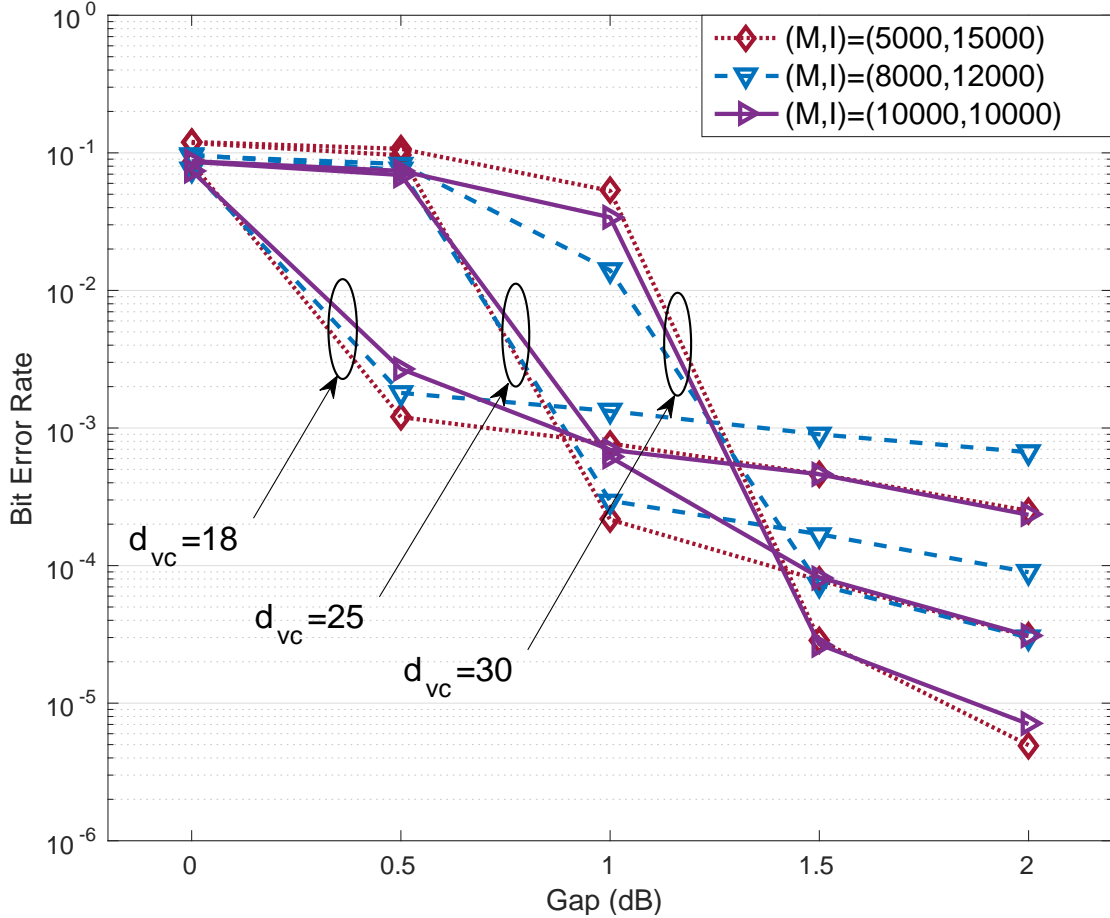
Figure 6.7 shows the system performance when  $p = 0.01$ . Three groups of hybrid systems have been simulated, with different ratios between the number of RP symbols and the number of LDGM coded bits. The number of digital bits,  $I$ , decreases from 15000 to 10000, while the number of RP symbols increases from 5000 to 10000, For a fixed value of  $d_{vc}$ , the change of the error floor is insignificant with the increase of RP symbols, but with a larger value of  $d_{vc}$ , the change of RP symbols leads to more variations in error floors (compare the cases of  $d_{vc} = 18$  and  $d_{vc} = 30$ ). The error floor also shows dangling behavior, similar to [117], where error floor dangles with the increase of  $I$ , the number of coded bits.  $d_{vc}$  has more impact on the error floors and the convergence threshold: increasing  $d_{vc}$  can significantly reduce the error floor and degrade the convergence threshold. The system  $(M, I, d_{vc}) = (5000, 15000, 25)$  can be considered as the best scheme in terms of  $BER < 10^{-4}$  and it is 1.3 dB away from the theoretical limit assuming separation.

Figure 6.8 shows the system performance when  $p = 0.005$ . The same groups of hybrid systems have been simulated. The change in the ratios between the number of



**Figure 6.7:** Simulation results for three groups of hybrid schemes when  $p = 0.01$ . For each group,  $(M, I)$  is fixed and  $d_{vc}$  varies from 18 to 30.

RP symbols and LDGM coded bits shows more impact than in the case of  $p = 0.01$ . The systems with  $(5000, 15000)$  and  $(10000, 10000)$  have similar error floors for each value of  $d_{vc}$ , while the systems with  $(8000, 12000)$  have higher error floors in each case. The explanation for this is that the decrease in  $I$  reduces the power of LDGM codes to correct residual errors while the increased portion of RP symbols is not enough to improve its performance of the joint estimation of the bit pairs, which leads to the increase of the error floor. A further increase in the number of RP symbols would improve the performance of the RCM sub-block, so that more correct joint estimations are made. This would make it easier for the LDGM to correct errors and distinguish between senders, leading to a reduction in the error floor. As in the case of  $p = 0.01$ ,

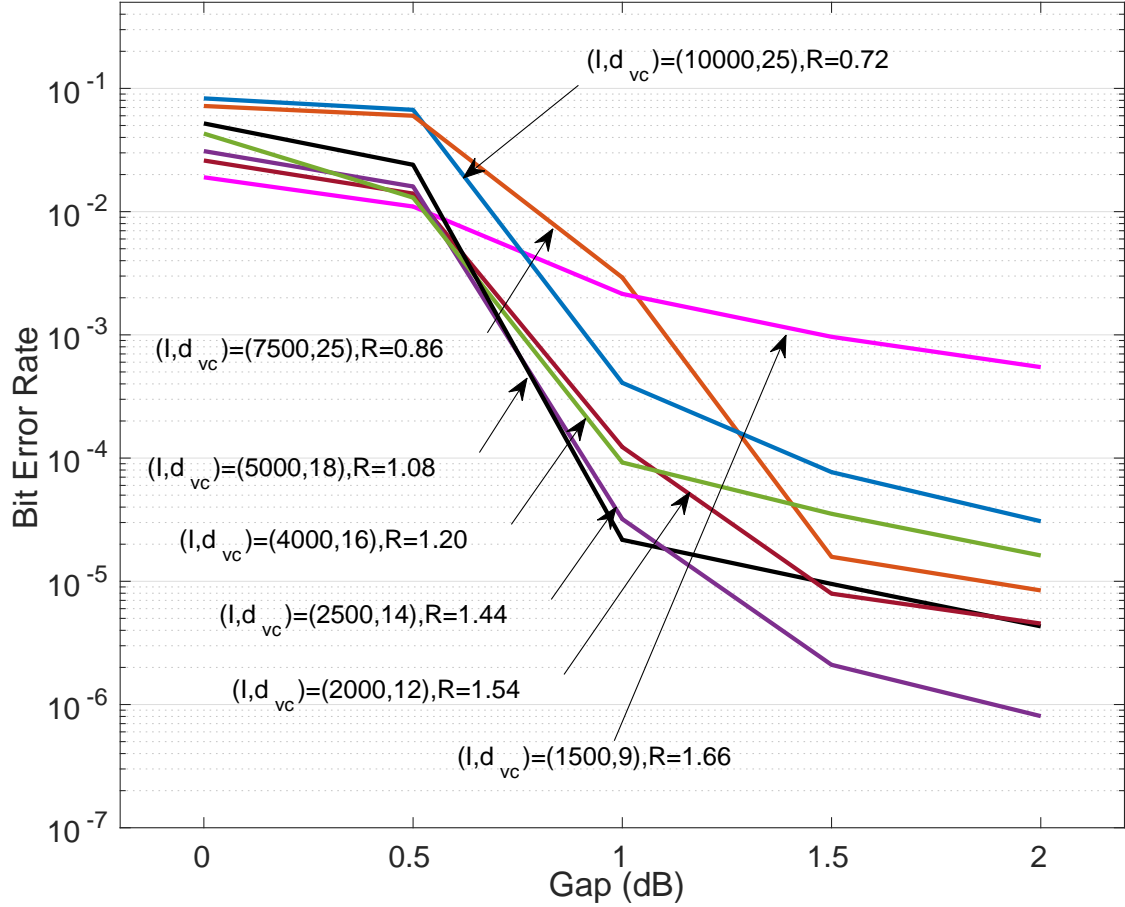


**Figure 6.8:** Simulation results for three groups of hybrid schemes when  $p = 0.005$ . For each group,  $(M, I)$  is fixed and  $d_{vc}$  varies from 18 to 30.

the best scheme maintains a gap of 1.3 dB to the theoretical limit.

### 6.5.2 High Transmission Rate System

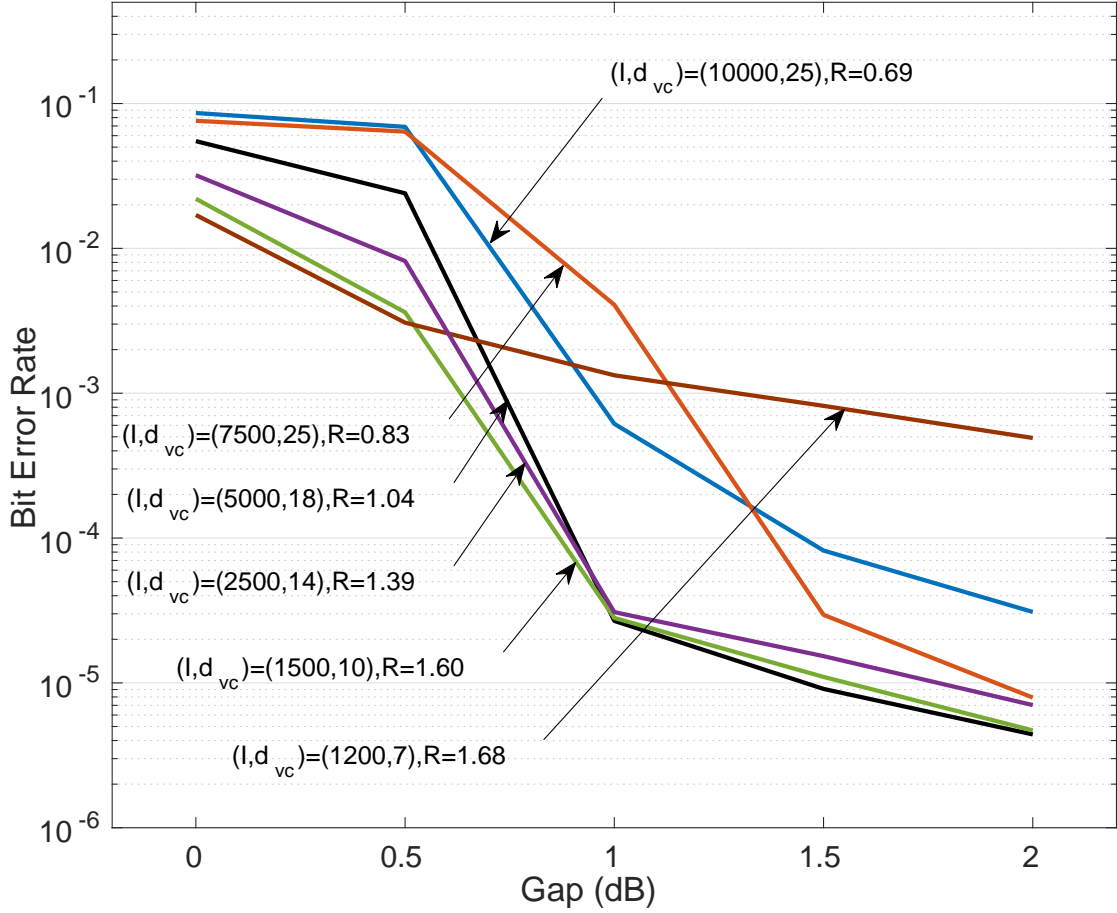
As discussed in [116] and [117], the hybrid coding scheme can be utilized to build a high transmission rate system with good BER performance. In addition, the use of multi-level real-valued symbols improves the robustness of the system in many aspects, such as its ability to maintain the gap to the theoretical limit with the increase of source non-uniformity, as shown in [117] and in Section 6.5.1. In this section, we have implemented several hybrid coding schemes with different information rates for  $p = 0.01$  and  $p = 0.005$ . The source block length is also fixed to  $K = 10,000$ , and



**Figure 6.9:** Performance of the proposed system with different information rates when  $p = 0.01$  and  $M = I$ .

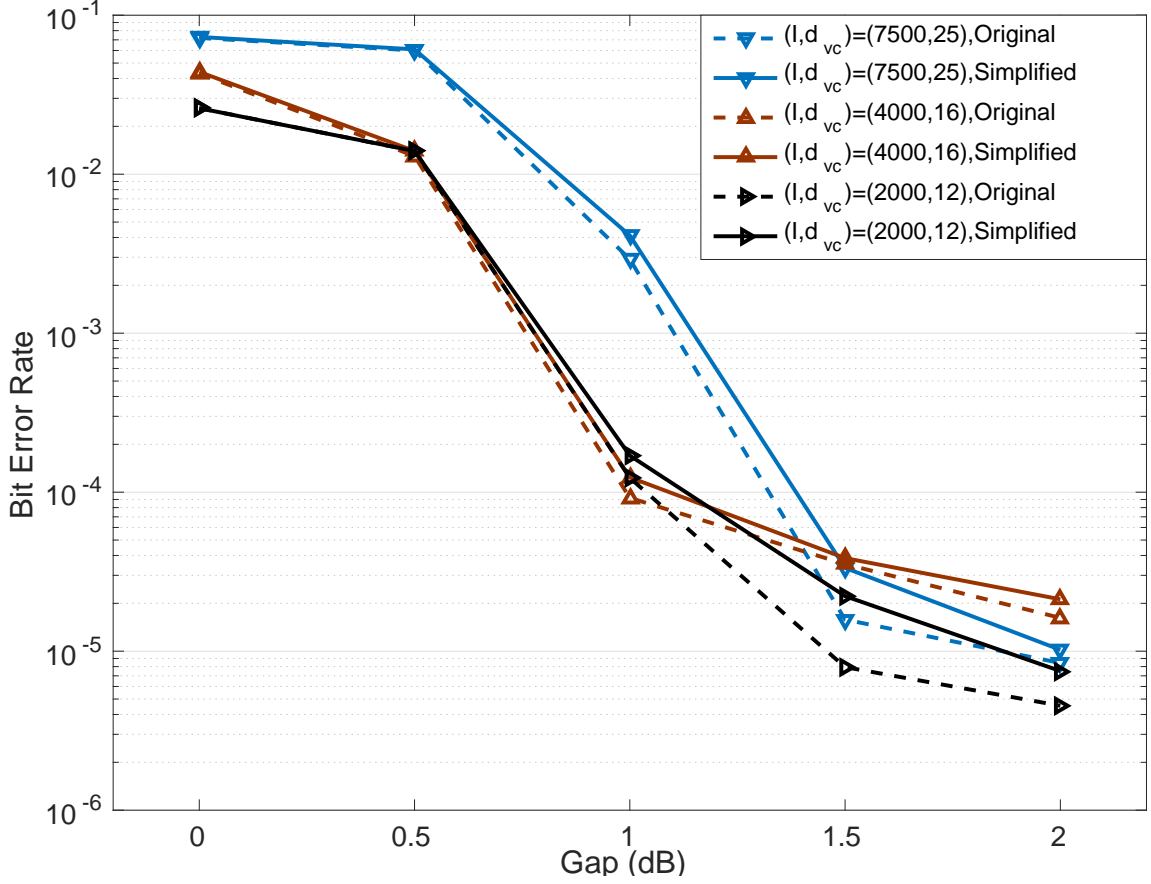
the number of generated symbols is decreased continually so that the information rate increases. As shown in Figure 6.7 and Figure 6.8, the system with the same number of RP symbols and LDGM coded bits, i.e.,  $M = I$ , shows well balanced performance, i.e., good convergence threshold and low error floor. Therefore, we keep this ratio in our simulations.

Figure 6.9 shows the performance of the hybrid coding scheme with different information rates for  $p = 0.01$ . It is clear that for a wide range of rates, the system maintains the gap to the theoretical limit with the increase of information rate. Indeed the performance in terms of convergence threshold and error floor improves when the



**Figure 6.10:** Performance of the proposed system with different information rates when  $p = 0.005$  and  $M = I$ .

information rate increases (compare the cases of  $R = 0.72$  and  $R = 1.44$ ). The explanation is that, in order to transmit the source bits over the MAC using the hybrid coding scheme, only a certain number of generated symbols (including RP symbols and coded bits) is necessary. If more RP symbols are used, more ambiguity is introduced, and the effect of RP symbols overcomes the gain obtained by using more symbols. When the number is further decreased, i.e., higher information rate, the performance starts to degrade. Figure 6.10 shows the performance of the hybrid coding scheme with different information rates for  $p = 0.005$ . The same trend observed in Figure 6.9 can be seen here. By comparing schemes with similar information rates in Figure 6.9 and Figure



**Figure 6.11:** Performance comparison between the original decoding method and the simplified decoding method when  $p = 0.01$  and  $M = I$ .

6.10, we can find that the schemes in Figure 6.10 are able to maintain the gap to the theoretical limit when the non-uniformity of the source increases.

### 6.5.3 System with Simplified Decoding Method

To evaluate the performance of the simplified method over MAC, we choose schemes from Figure 6.9 and Figure 6.10, with transmission rates ranging from low to high, and implement them with the simplified decoding method.

Figure 6.11 compares the performance of the original method (dashed lines) and of the simplified decoding method (solid lines) when  $p = 0.01$ . Notice that the performance of the simplified algorithm is close to that of the original method, even when the transmission rate increases. For all the three schemes, the degradation observed

for the simplified decoding method is smaller than 0.2 dB. Table 6.3 shows, for each transmission rate, the gap to the theoretical limit assuming separation for the original decoding method and for the simplified decoding method when  $p = 0.01$ .

**Table 6.3:** Gap to the theoretical limit assuming separation for hybrid schemes using the original and the simplified decoding methods over MAC when  $p_1 = 0.01$ . The theoretical limit is in terms of  $E_{so}/N_0$ . The gap is measured at  $BER < 10^{-4}$ . All results are in dB.

Transmission rate	$[E_s/N_0]_{lim}$	Gap (orgi.)	Gap (simp.)	Degradation
0.86	-2.9	1.3	1.4	0.1
1.20	-2.3	1	1.1	0.1
1.54	-1.7	1.05	1.2	0.15

Figure 6.12 compares the performance of the original decoding method (dashed lines) and of the simplified decoding method (solid lines) when  $p = 0.005$ . For low rates, for instance, (7500, 7500) and (2500, 2500), the two decoding methods achieve almost identical performance. When the transmission rate is further increased, degradation starts to appear, as in Section 5.4. Table 6.4 shows, for each transmission rate, the gap to the theoretical limit assuming separation for the original decoding method and for the simplified decoding method when  $p = 0.005$ .

**Table 6.4:** Gap to the theoretical limit assuming separation for hybrid schemes using the original and the simplified decoding methods over MAC when  $p_1 = 0.005$ . The theoretical limit is in terms of  $E_{so}/N_0$ . The gap is measured at  $BER < 10^{-4}$ . All results are in dB.

Transmission rate	$[E_s/N_0]_{lim}$	Gap (orgi.)	Gap (simp.)	Degradation
0.83	-3.1	1.4	1.4	0
1.39	-2.1	1	1	0
1.60	-1.8	0.9	1.4	0.5

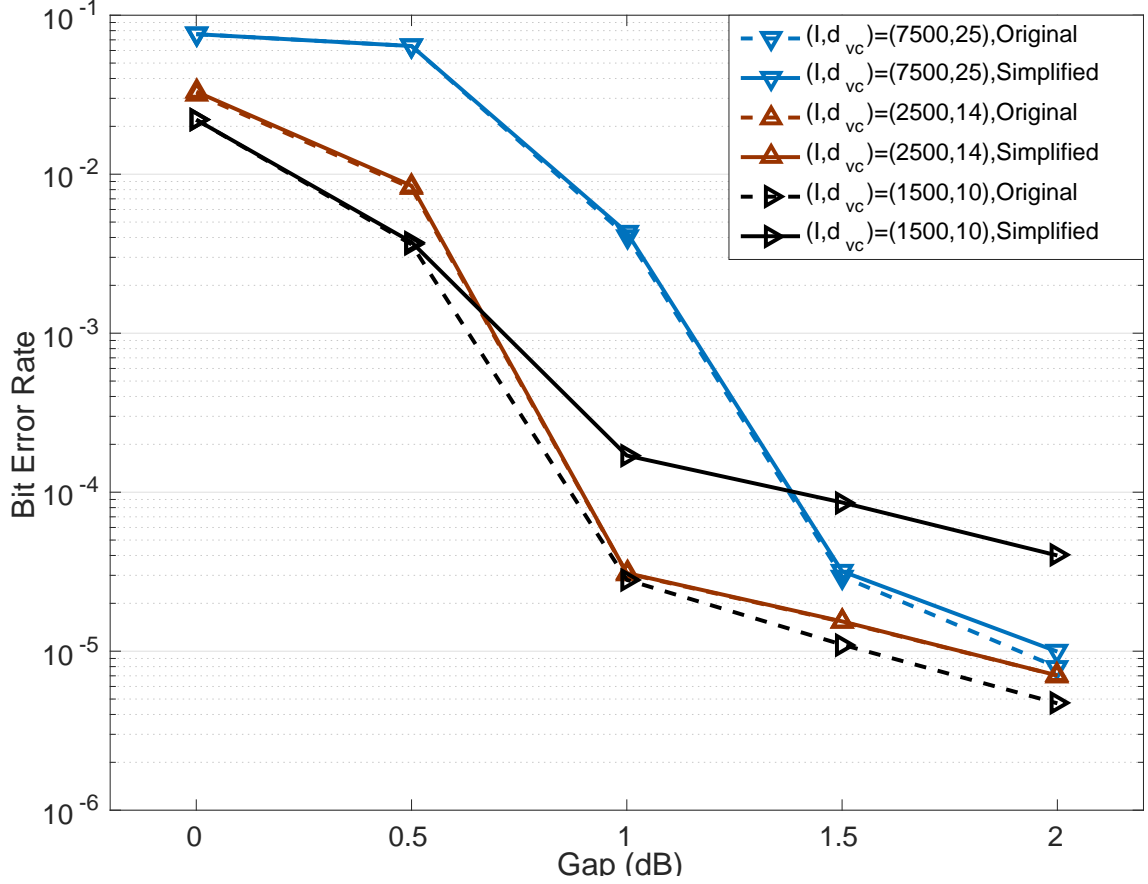


**Figure 6.12:** Performance comparison between the original method and the simplified method when  $p = 0.005$  and  $M = I$ .

## 6.6 Conclusion

We have introduced a hybrid analog-digital joint source-channel coding scheme for the transmission of correlated sources over multiple access channels. Each source is encoded independently using a properly designed encoder structure that can preserve the correlation in the generated codeword. The proposed synthetic decoder structure and the synthetic decoding algorithm allow the exploitation of the correlation and alleviate the ambiguity introduced by multi-level real-valued symbols. The performance of the hybrid coding scheme is very close to the theoretical limits assuming separation, while achieving high information rate. Thus, the proposed hybrid coding scheme has great potential for the design of high speed communication systems. Its robustness to the

transmission rate and the non-uniformity of the source is a great advantage to many traditional digital coding techniques. We have also discussed the extension of the simplified decoding method for the synthetic decoding algorithm, showing that its performance is similar to that of the original decoding method.

## Chapter 7

### CONCLUSION AND FUTURE WORK

In this dissertation, we have explored hybrid analog-digital coding schemes for digital sources in various scenarios. The objective is to design a robust coding scheme with good BER performance by properly integrating analog and digital coding systems. In our work, the hybrid coding scheme is constructed by parallel concatenation of an RCM system and an LDGM code. The binary source bits are mapped into multi-level RP symbols through random projections, and to coded binary bits through random XOR operations. Therefore, the symbols generated in the hybrid scheme are a mixture of real-valued symbols and binary bits, which are transmitted over noisy channels with two independent QAM constellation with the same average energy constraint. Real-valued symbols are mapped to modulation constellation points directly based on their values, while coded bits use an independent 4-QAM scheme. At the receiver, belief propagation is applied to a bipartite graph to decode the digital source iteratively. As shown in the dissertation, RCM has several advantages over traditional techniques, such as smooth rate adaptation, wide dynamic range, and robustness to the channel and the sparsity of the source. By introducing an LDGM code, the error floor problem can be taken care of, and the result coding scheme has excellent performance.

#### 7.1 Summary of Contributions

##### 7.1.1 Point to Point AWGN Channels

The first problem studied in this dissertation was the design of robust coding schemes for point to point AWGN channels. We started by tackling the error floor problem in high SNR with uniform sources. Regular LDGM codes are integrated with the RCM scheme optimized as a stand-alone system. As shown in Section 4.3, the

error floor can be reduced by optimizing the digital part of the system. We have shown that the requirement for the RCM sub-system within a hybrid scheme is different from a stand-alone RCM system. By optimizing the RCM sub-system, the performance is further improved and is only 2.3 dB away from the theoretical limit.

In the case of nonuniform sources, we have designed hybrid coding schemes to exploit the redundancy. More specifically, we have optimized the RCM scheme, using larger weight sets so that more source bits are involved in generating the RP symbols. In this way, the sparsity in the source can be exploited properly in the decoding process to distinguish between RP symbols. In addition, more powerful LDGM codes are employed, i.e., with lower rate and higher degrees. We have shown that hybrid coding schemes are capable of maintaining a gap to the theoretical limit of around 2 dB, independently of the degree of source non-uniformity, outperforming many traditional digital coding techniques, where the gap to the theoretical limit increases with the degree of source non-uniformity. The robustness of the hybrid coding scheme and its capability for high transmission rate make it a promising technique for high speed communication systems.

### 7.1.2 Simplified Decoding Method

The existence of real-valued RP symbols increases the decoding complexity. Although the computational complexity is not impractical after the introduction of proper techniques to compute the pmfs, it is still high compared to many coding techniques. We have proposed a simplified decoding algorithm based on a Gaussian approximation, so that many operations can be reduced to simple formulas. We have analyzed the computational complexity of the original and simplified decoding algorithm, showing that the simplified algorithm reduces the complexity by around one order of magnitude. The BER performance of the simplified decoding algorithm is identical to the original one in many cases, and only experiences minor degradation in some cases. This makes it possible to implement a fast version of the hybrid scheme without performance degradation.

### 7.1.3 Transmission of Correlated Sources over Multiple Access Channels

The transmission of correlated sources over MAC presents many challenges. In our proposed joint source-channel coding approach, each source is independently encoded with a hybrid encoder. We have used the same RCM encoder structure for both sources to maintain the correlation in the generated codewords, while different LDGM code structures are used to distinguish between senders. We have designed a synthetic decoder structure by integrating nodes and merging links for the two RCM decoders in the joint decoder, while keeping nodes from LDGM decoders as individual nodes. This synthetic decoder alleviates the ambiguity problem introduced by multi-level real-valued RP symbols through jointly considering the messages exchanged between RP nodes and source bit nodes. We have optimized the scheme and have shown that the performance is close to the theoretical limit assuming separation. We have also shown that the hybrid scheme is capable of high transmission rates over MAC, which is a great advantage over existing coding schemes. The adaptation of the simplified method to the synthetic algorithm can also reduce the complexity in many cases, making the proposed scheme a promising candidate for multi-user communication systems.

## 7.2 Future Work

The work developed in this dissertation can provide multiple research directions, as described below.

### 7.2.1 Density Evolution

The discretized density evolution (DDE) method proposed in [124] provides an excellent tool to analyze and optimize the performance of LDPC codes in a theoretical manner. Moreover, density evolution can predict the code performance in a much shorter time. However, a main problem in optimizing the hybrid coding scheme is the lack of theoretical analysis, which is complicated by the existence of multi-level RP symbols. It is a great challenge to develop an innovative way to apply the density evolution framework for the analysis of the hybrid coding schemes.

### 7.2.2 Matrix Design

There are several constraints on the choice of the weight set and on the design of the RCM generator matrix. These constraints are forced based on energy efficiency and on the goal of maximizing the distance between codewords. However, these constraints also affect the randomness of the generator matrix. In [125], weights are randomly selected from a predefined distribution, and positions of non-zero entries in each row are randomly chosen. This opens the door to the possibility of a more flexible choice of the weight set and of matrix design. Research on the relationship between the design and the performance of the hybrid coding scheme can be challenging and interesting.

### 7.2.3 Rate Adaptation

The focus of this dissertation is on the BER performance of the hybrid coding scheme in a specific SNR range. As mentioned in the dissertation, the RCM scheme has excellent performance for rate adaptation [88], while LDGM codes are also promising candidates for rate adaptation [95]. It would be interesting to study the rate adaptation problem with the hybrid coding scheme in general scenarios.

### 7.2.4 Multi-User Communication

Multi-user communication systems are acquiring an increased importance. Our study of the application on the hybrid coding scheme to multiple access channels can be a starting point for the research on hybrid coding schemes in more complicated multi-user contexts, such as MIMO channels. It is certain that this type of scenarios will require some adaptation for the hybrid coding scheme to be efficiently deployed.

### 7.2.5 General Coding Designs

The hybrid coding scheme studied in this dissertation is constructed by the parallel concatenation of an RCM scheme and an LDGM code, but this is a very particular case. Other design schemes, (e.g., serial concatenation rather than parallel), are also possible, and the component analog and digital sub-blocks can be generalized in order to improve performance.

## BIBLIOGRAPHY

- [1] C.E. Shannon, "A Mathematical Theory of Communication," *Bell Syst. Tech. J.*, vol 27, pp. 379-423, July 1948.
- [2] S. Vembu, S. Verd6, and Y. Steinberg, "The Source-Channel Separation Theorem Revisited," *IEEE Trans. Inform. Theory*, vol IT-41, no. 1, pp. 44-54, January 1995.
- [3] M. Khansari and M. Vetterli, "Time-varying Channels with Side Information and Separation Principle," *Technical Report UCB/ERL M94/103*, Electronics Research Lab, University of California at Berkeley, December 1994.
- [4] A.J. Viterbi and J.K. Omura, "Principles of Digital Communications and Coding," *McGraw-Hill*, New York, 1979.
- [5] V. A. Vaishampayan and N. Farvardin, "Joint Design of Block Source Codes and Modulation Signal Sets," *IEEE Trans. Inform. Theory*, vol. 38, pp. 1230-1248, July 1992.
- [6] N. Farvardin and V. Vaishampayan, "Optimal Quantizer Design for Noisy Channels: an Approach to Combined Source-Channel Coding," *IEEE Trans. Inform. Theory*, vol. 33, pp. 827-838, November 1987.
- [7] J.J Spilker, Jr., "Digital Communications by Satellite," Englewood Cliffs, NJ: Prentice Hall 1977.
- [8] E. Ayanoglu and R.M. Gray, "The Design of Joint Source and Channel Trellis Waveform Coders," *IEEE Trans. Inform. Theory*, vol. 33, pp. 855-865, November 1987.
- [9] N. Farvardin, V. Vaishampayan, "On the Performance and Complexity of Channel-Optimized Vector Quantization," *IEEE Trans. on Info. Theory*, vol. 37, no. 1, pp. 155-160, January 1991.
- [10] A. Goldsmith, "Joint Source/Channel Coding for Wireless Channels," *Proc. IEEE 45th Vehicular Technology Conference*, vol. 2, pp. 614-618, 1995.
- [11] I. E. Aguerri, D. Gunduz, "Joint Source-Channel Coding with Time-Varying Channel and Side-Information," *IEEE Trans. on Info. Theory*, vol. 62, no. 2, February 2016.

- [12] H. Jafarkhani, P. Ligdas, N. Farvardin, "Adaptive Rate Allocation in a Joint Source-Channel Coding Framework for Wireless Channels," *Proc. IEEE VTC*, vol. 1, pp. 492-496, April 1996.
- [13] B. He, C.N. Manikopoulos, "Performance Analysis of ARQ Protocol with Delayed Detection for Joint Source and Channel Coding," *Proceedings of the 35th Annual Conference on Information Sciences and Systems*, March 2001.
- [14] Bin He, C.N. Manikopoulos, "Performance of an ARQ protocol based on Joint Source and Channel Coding on Nonindependent Channel," *Vehicular Technology Conference 2001. VTC 2001 Fall. IEEE VTS 54th*, vol. 4, pp. 2502-2505 vol.4, 2001, ISSN 1090-3038.
- [15] F. H. Liu, P. Ho, V. Cuperman, "Joint Source and Channel Coding using a Non-linear Receiver over Rayleigh Fading Channel," *Proc. of the IEEE Comm. Theory Mini Conf. in conj. with GLOBECOM'93*, pp. 16, 1993.
- [16] J. J. Xiao, Z. Q. Luo, N. Jindal, "Linear Joint Source-Channel Coding for Gaussian Sources through Fading Channels," *IEEE Global communications conference*, pp. 1-5, San Francisco, CA 2006.
- [17] P. G. Poddar, S. S. Dayanand, "A Simplified Joint Source and Channel Coding System for Data Transmission over Fading Channel," *Wireless Personal Communication*, vol. 94, no. 3, pp. 1341-1358, June 2017.
- [18] J. Garcia-Frias and J. D. Villasenor, "Combining Hidden Markov Source Models and Parallel Concatenated Codes," *IEEE Communications Letters*, pp. 111-113, July 1997.
- [19] J. Garcia-Frias and John D. Villasenor, "Joint Source Channel Coding and Estimation of Hidden Markov Structures," *Proc. ISIT'98*, pp. 201, August 1998.
- [20] J. Garcia-Frias and J. D. Villasenor, "Simplified Methods for Combining Hidden Markov Models and Turbo Codes," *VTC99*, September 1999, Amsterdam, The Netherlands.
- [21] J. Garcia-Frias and J. D. Villasenor, "Joint Source Channel Coding and Estimation of Hidden Markov Structures," *ISIT98*, August 1998, Boston, Massachusetts.
- [22] J. Garcia-Frias and J. D. Villasenor, "Turbo Decoding of Hidden Markov Sources with Unknown Parameters," *DCC98*, March 1998, Snowbird, Utah.
- [23] J. Garca-Fras and J. D. Villasenor, "Markov Structures in Turbo Decoding," *ITW98*, February 1998, San Diego, California.
- [24] J. Garca-Fras and J. D. Villasenor, "Joint Source-Channel Decoding of Turbo Codes," *International Symposium on Turbo Codes and Related Topics*, September 1997, Brest, France.

- [25] A. Albanese, J. Blmer, J. Edmonds, M. Luby, M. Sudhan, "Priority Encoding Transmission," *IEEE Trans. Inf. Theory*, vol. 42, no. 6, pp. 1737-1744, November 1996.
- [26] K. Fazel and J.J. Lhuillier, "Application of Unequal Error Protection Codes on Combined Source-Channel Coding of Images," *Proceedings of the International Conference on Communications*, pp. 320.5.1-320.5.6, 1990.
- [27] A. Vosoughi, P. Cosman, L. B. Milstein, "Joint Source-Channel Coding and Unequal Error Protection for video plus depth," *IEEE Signal Process. Lett.*, vol. 22, no. 8, pp. 31-34, August 2014.
- [28] M. Stoufs, A. Munteanu, P. Schelkens, J. Cornelis, "Optimal Joint Source-Channel Coding using Unequal Error Protection for the Scalable Extension of H.264/MPEG-4 AVC," *Proc. IEEE Int. Conf. Image Process.*, vol. 6, pp. 517-520, 2007.
- [29] S. Z. Azami, P. Duhamel, O. Rioul, "Joint Source-Channel Coding: Panorama of methods," *Proc. CNES Workshop Data Compression*, pp. 1232-1254, 1996.
- [30] G. Feideropoulou, M. Trocan, J. E. Fowler, B. Pesquet-Popescu, J.-C. Belfiore, "Joint Source-Channel with Partially Coded Index Assignment for Robust Scalable Video," *IEEE Signal Process. Lett.*, vol. 13, no. 4, pp. 201-204, April 2006.
- [31] W. Xiaohan, X. Wu, "Index Assignment Optimization for Joint Source-Channel MAP Decoding," *IEEE Trans. on Commun.*, vol. 58, no. 3, pp. 901-910, 2010.
- [32] H. Oztoprak, S. Villette, A. Kondo, "Index Assignment-Based Channel Coding," *IET Commun.*, vol. 6, no. 2, pp. 172-178, 2012.
- [33] T.M. Cover, A. El Gamal, and M. Salehi, "Multiple Access Channels with Arbitrarily Correlated Sources." *IEEE Trans. Inform. Theory*, vol. 26, no. 6, pp. 648 - 657, November 1980.
- [34] J. Garcia-Frias, "Joint Source-Channel Decoding of Correlated Sources over Noisy Channels," *Proc. DCC'01*, Snowbird, Utah, March 2001, .
- [35] Y. Zhao and J. Garcia-Frias, "Turbo Codes for the Multiple Access Channel with Correlated Senders," *Proc. Internet Quality Service Conf., IT-COM*, September 2003.
- [36] W. Zhong, Y. Zhao, and J. Garcia-Frias, "Turbo-like Codes for Distributed Joint Source-Channel Coding of Correlated Senders in Multiple Access Channels," *Proc. Asilomar'03*, November 2003.
- [37] J. Garca-Fras and Y. Zhao, "Near Shannon/Slepian-Wolf Performance for Unknown Correlated Sources over AWGN Channels," *IEEE Transactions on Communications*, pp. 555-559, April 2005.

- [38] W. Zhong and J. Garca-Fras, "LDGM Codes for Channel Coding and Joint Source Channel Coding of Correlated Sources," *EURASIP Journal on Applied Signal Processing*, pp. 942-953, May 2005.
- [39] W. Zhong and J. Garcia-Frias, "Transmission of Correlated Senders over Multiple-Access Channels using LDGM Codes," *Proc. Allerton'04*, September, 2004.
- [40] W. Zhong, H. Chai, and J. Garcia-Frias, "LDGM Codes for Transmission of Correlated Senders over MAC," *Proc. Allerton'05*, September 2005.
- [41] Y. Zhao, W. Zhong, and J. Garcia-Frias, "Transmission of Correlated Senders over a Rayleigh Fading Multiple Access Channel," *Signal Processing*, vol. 86, pp. 3150-3159, November 2006.
- [42] W. Zhong, J. Garcia-Frias, "Parallel LDGM Codes for the Transmission of Highly Correlated Senders over Rayleigh Fading Multiple Access Channels," *Proc. CISS'06*, March 2006.
- [43] J. Garcia-Frias, Y. Zhao and W. Zhong, "Turbo-Like Codes for Transmission of Correlated Sources over Noisy Channels," *IEEE SIGNAL PROCESSING MAGAZINE [58]*, September 2007.
- [44] M. Sartipi, F. Fekri, "Source and Channel Coding in Wireless Sensor Networks using LDPC Codes," *Proc. 2004 IEEE SECON*, pp. 309-316, 2004.
- [45] Q. Xu, V. Stankovic, Z. Xiong, "Distributed Joint Source-Channel Coding of Video using Raptor Codes," *IEEE J. Sel. Areas Commun.*, vol. 25, no. 4, pp. 851-861, 2007.
- [46] E. J. Cands, J. Romberg, T. Tao, "Robust Uncertainty Principles: Exact Signal Reconstruction from Highly Incomplete Frequency Information," *IEEE Trans. on Info. Theory*, vol. 52, pp. 489-509, February 2006.
- [47] D. L. Donoho, "Compressed Sensing," *IEEE Trans. Inf. Theory*, vol. 52, no. 4, pp. 1289-1306, Apr. 2006.
- [48] E. J. Candes, T. Tao, "Near-Optimal Signal Recovery from Random Projections: Universal Encoding Strategies?," *IEEE Trans. Inf. Theory*, vol. 52, no. 12, pp. 5406-5425, Dec. 2006.
- [49] E. J. Cands, "Compressive Sampling," *Proc. 2006 Intl. Congress of Mathematicians*, pp. 1433-1452, 2006.
- [50] R. Gribonval, M. Nielsen, "Highly Sparse Representations from Dictionaries are Unique and Independent of the Sparseness Measure," *Tech. Rep.*, October 2003.

- [51] J. A. Tropp, "Just Relax: Convex Programming Methods for Identifying Sparse Signals in Noise," *IEEE Trans. Inf. Theory*, vol. 52, no. 3, pp. 1030-1051, March 2006.
- [52] Y. C. Pati, R. Rezaifar, P. S. Krishnaprasad, "Orthogonal Matching Pursuit: Recursive Function Approximation with Applications to Wavelet Decomposition," *Proc. 27th Annu. Asilomar Conf. Signals Syst. Comput.*, vol. 1, pp. 40-44, November 1993.
- [53] R. DeVore, V. N. Temlyakov, "Some Remarks on Greedy Algorithms," *Adv. Comput. Math.*, vol. 5, pp. 173-187, 1996.
- [54] J. Tropp, A. Gilbert, "Signal Recovery from Random Measurements via Orthogonal Matching Pursuit," *IEEE Trans. Inf. Theory*, vol. 53, no. 12, pp. 4655-4666, 2007.
- [55] T. Blumensath, M. E. Davies, "Iterative Hard Thresholding for Compressed Sensing," *Applied and Computational Harmonic Analysis*, vol. 27, no. 3, pp. 265-274, 2009.
- [56] W. Dai, O. Milenkovic, "Subspace Pursuit for Compressive Sensing Signal Reconstruction," *IEEE Trans. Inf. Theory*, vol. 55, no. 5, pp. 2230-2249, 2009.
- [57] M. E. Tipping, "Sparse Bayesian Learning and the Relevance Vector Machine," *Journal of Machine Learning Research*, vol. 1, pp. 211-244, September 2001.
- [58] S. Ji, Y. Xue, L. Carin, "Bayesian Compressive Sensing," *IEEE Trans. Signal Processing*, vol. 56, no. 6, pp. 2346-2356, June 2008.
- [59] I. Esnaola and J. Garcia-Frias, "Linear Analog Coding of General Multivariate Gaussian Sources," *Allerton Conference on Communication, Control, and Computing*, September 2009.
- [60] I. Esnaola and J. Garcia-Frias, "Distributed Analog Linear Coding of Correlated Gaussian Sources over Multiple Access Channels," *ISWCS'09*, September 2009.
- [61] I. Esnaola and J. Garcia-Frias, "Analysis and Optimization of Distributed Linear Coding of Gaussian Sources," *CISS'09*, March 2009.
- [62] I. Esnaola and J. Garcia-Frias, "MMSE Estimation of Distributely Coded Correlated Gaussian Sources Using Random Projections," *Globecom'08*, December 2008.
- [63] J. Garcia-Frias and I. Esnaola, "Distributed Compression of Correlated Real Sequences Using Random Projections," *ITW'08*, May 2008.
- [64] I. Esnaola and J. Garcia-Frias, "Distributed Compression of Correlated Signals Using Random Projections," *DCC'08*, March 2008.

- [65] I. Esnaola and J. Garcia-Frias, "Linear Analog Coding of General Multivariate Gaussian Sources," *ITW'09*, October 2009.
- [66] J. Garcia-Frias and I. Esnaola, "Exploiting Prior Knowledge in The Recovery of Signals from Noisy Random Projections," *DCC'07*, March 2007.
- [67] I. Esnaola and J. Garcia-Frias, "Exploiting Prior Knowledge in The Recovery of Non-Sparse Signals from Noisy Random Projections," *CISS'07*, March 2007.
- [68] M. Duarte, M. Wakin, D. Baron, R. Baraniuk, "Universal Distributed Sensing via Random Projections," *Proc. 2006 IEEE IPSN*, pp. 177-185, 2006.
- [69] W. Bajwa, J. Haupt, A. Sayeed, R. Nowak, "Joint Source-Channel Communication for Distributed Estimation in Sensor Networks," *IEEE Trans. Inf. Theory*, vol. 53, no. 10, pp. 3629-3653, 2007.
- [70] S. Feizi, M. Medard, M. Effros, "Compressive Sensing over Networks," *Proc. 2010 Allerton Conference on Communication Control and Computing*, pp. 1129-1136, 2010.
- [71] S. Feizi, M. Medard, "A Power Efficient Sensing/Communication Scheme: Joint Source-Channel-Network Coding by Using Compressive Sensing," *Proc. 2011 Allerton Conference on Communication Control and Computing*, pp. 1048-1054, 2011.
- [72] F. Chen, F. Lim, O. Abari, A. Chandrakasan, V. Stojanovic, "Energy-Aware Design of Compressed Sensing Systems for Wireless Sensors under Performance and Reliability Constraints," *IEEE Trans. Circuits Syst. I Reg. Papers*, vol. 60, no. 3, pp. 650-661, 2013.
- [73] T. F. Zhao, X. Z. Ke and P. L. Yang, "Position and Velocity Aided Routing Protocol in Mobile Ad Hoc Networks," *International Journal of Digital Content Technology and its Applications (JDCTA)*, 2010.
- [74] P. L. Yang, X. Z. Ke, T. F. Zhao, "Study of Ultraviolet Mobile Ad Hoc Network," *In Symposium on Photonics and Optoelectronics (SOPO09)*, 2009.
- [75] T. F. Zhao, X. Z. Ke, P. L. Yang, "Local-map-based Candidate Node-encircling Pre-configuration Cycles Construction in Survivable Mesh Networks," *2009 First International Conference on Future Information Networks*, pp. 249-252, 2009.
- [76] K. Wu and X. Guo, "Compressive Sensing of Digital Sparse Signals," *Proc. IEEE WCNC*, pp. 1488-1492, March 2011.
- [77] U. Nakarmi and N. Rahnavard, "BCS: Compressive Sensing for Binary Sparse Signals," *Proc. MILCOM*, pp. 15, 2012.

- [78] M. Shirvanimoghaddam, Y. Li, B. Vucetic, J. Yuan, and P. Zhang, "Binary Compressive Sensing via Analog Fountain Coding," *IEEE Trans. Signal Process.*, vol. 63, no. 24, pp. 6540-6552, December 2015.
- [79] M. Shirvanimoghaddam, Y. Li, and B. Vucetic, "Near-Capacity Adaptive Analog Fountain Codes for Wireless Channels," *IEEE Commun. Lett.*, vol. 17, no. 12, pp. 2241-2244, December 2013.
- [80] S. Sarvotham, D. Baron, R. Baraniuk, "Sudocodes-Fast Measurement and Reconstruction of Sparse Signals," *Proc. 2006 IEEE ISIT*, pp. 2804-2808, 2006.
- [81] F. Wu, J. Fu, Z. Lin, B. Zeng, "Analysis on Rate-Distortion Performance of Compressive Sensing for Binary Sparse Source," *Proc. 2009 IEEE DCC*, pp. 113-122, 2009.
- [82] X. L. Liu, C. Luo, F. Wu, "Formulating Binary Compressive Sensing Decoding with Asymmetrical Property," *Proc. 2011 IEEE DCC*, pp. 213-222, 2011.
- [83] D. Baron, S. Sarvotham, R. Baraniuk, "Bayesian Compressive Sensing via Belief Propagation," *IEEE Trans. Signal Process.*, vol. 58, no. 1, pp. 269-280, 2010.
- [84] S. Nanda, K. Balachandran, and S. Kumar, "Adaptation Techniques in Wireless Packet Data Services," *Communications Magazine, IEEE*, 38(1):54-64, January 2000.
- [85] Q. Xia and M. Hamdi, "Smart Sender: A Practical Rate Adaption Algorithm for Multirate IEEE 802.11 WLANs," *Wireless Communications, IEEE Transactions on*, 7(5):1764-1775, May 2008.
- [86] J. Li and K. Narayanan, "Rate-Compatible Low Density Parity Check Codes for Capacity-Approaching ARQ Scheme in Packet Data Communications," *Proc. International Conference on Communications, Interner and Information Technology(CIIT)*, US Virgin Islands, pp. 201-206, November 2002.
- [87] H. Cui, C. Luo, K. Tan, F. Wu, and C. W. Chen, "Seamless Rate Adaptation for Wireless Networking," *Proc. of the 14th ACM MSWiM '11*, 2011.
- [88] H. Cui, C. Luo, J. Wu, C. W. Chen and F. Wu, "Compressive Coded Modulation for Seamless Rate Adaptation," *IEEE Trans. on Wireless Communications*, pp. 4892-4904, October 2013.
- [89] B. Sklar, "Digital Communications: Fundamentals and Applications," *Prentice-Hall, Inc.*, Upper Saddle River, NJ, USA, 1988.
- [90] C. Berrou, A. Glavieux, and P. Thitimajshima, "Near Shannon Limit Error-Correcting Coding and Decoding: Turbo Codes," *Proc. ICC'93*, May 1993.

- [91] R.G. Gallager, "Low-Density Parity-Check Codes," *IEEE Trans. Inform. Theory*, vol. 8, no. 1, pp. 21 - 28, January 1962.
- [92] R. G. Gallager, "Low-Density Parity-Check Codes," *M.I.T Press*, 1963.
- [93] D. J. C. MacKay and R. M. Neal, Near Shannon Limit Performance of Low Density Parity Check Codes," *Electronic Letters*, vol. 33, no. 6, pp. 457-458, March 1997.
- [94] D. J. C. MacKay, "Good Error-Correcting Codes Based on Very Sparse Matrices," *IEEE Trans. on Information Theory*, vol. 45, no. 2, pp. 399-431, March 1999.
- [95] H. Lou and J. Garcia-Frias, "Rate-Compatible Low-Density Generator Matrix Codes," *IEEE Transaction on Communications*, vol. 56, no. 3, March 2008.
- [96] S. Wicker and S. Kim, "Fundamentals of Codes, Graphs and Iterative Decoding," *Kluwer International Series in Engineering and Computer Science*, 2003.
- [97] J. Garcia-Frias, W. Zhong, and Y. Zhao, "Iterative Decoding Schemes for Source and Channel Coding of Correlated Sources," *Proc. Asilomar'02*, November 2002.
- [98] J. Garcia-Frias and W. Zhong, "Approaching Near Shannon Performance by Iterative Decoding of Linear Codes with Low-Density Generator Matrix," *IEEE Communications Letters*, vol. 7, no. 6, pp. 266-268, June 2003.
- [99] W. Zhong and J. Garcia-Frias, "LDGM Codes for Channel Coding and Joint Source-Channel Coding of Correlated Sources," *EURASIR Journal on Applied Signal Processing*, 2005:6, 942-953.
- [100] W. Zhong, H. Chai, and J. Garcia-Frias, "Approaching the Shannon Limit Through Parallel Concatenation of Regular LDGM codes," *Proc. ISIT'05*, September 2005.
- [101] J. Hagenauer, "Source-Controlled Channel Decoding," *IEEE Trans. on Communications*, pp. 2449-2457, September 1995.
- [102] G.-C. Zhu and F. Alajaji, "Design of Turbo Codes for Non-Equiprobable Memoryless Sources," *Proc. Allerton'01*, October 2001.
- [103] G.-C. Zhu and F. Alajaji, "Turbo Codes for Non-Uniform Memoryless Sources over Noisy Channels," *IEEE Communications Letters*, pp. 64-66, February 2002.
- [104] S. Shamai, and S. Verdu, "The Empirical Distribution of Good Codes," *IEEE Trans. Inform. Theory*, vol. 43, pp. 836-846, May 1997.
- [105] G.-C. Zhu, F. Alajaji, J. Bajcsy, and P. Mitran, "Non-Systematic Turbo Codes for Non-Uniform I.I.D. Sources over AWGN Channels," *Proc. CISS'02*, March 2002.

- [106] G.-C. Zhu, F. Alajaji, J. Bajcsy, and P. Mitran, "Transmission of Nonuniform Memoryless Sources via Nonsystematic Turbo Codes," *IEEE Trans. on Communications*, pp. 1344-1354, August 2004.
- [107] G. I. Shamir and J. J. Boutros, "Non-Systematic Low-Density Parity-Check Codes for Nonuniform Sources," *Proc. ISIT'05*, September 2005.
- [108] G. I. Shamir, L. Wang, and J. J. Boutros, "High Rate Non-Systematic LDPC Codes for Nonuniform Sources," *Proc. of Intern. Symp. on Turbo Codes*, Munich, Germany, April 3-7, 2006.
- [109] F. Cabarcas, R. D. Souza, and J. Garcia-Frias, "Source-Controlled Turbo Coding of Non-Uniform Memoryless Sources Based on Unequal Energy Allocation," *ISIT04*, June 2004, Chicago, Illinois.
- [110] F. Cabarcas, R. D. Souza, and J. Garcia-Frias, "Turbo Coding of Strongly Nonuniform Memoryless Sources with Unequal Energy Allocation and PAM Signaling," *IEEE Trans. on Signal Processing*, pp. 1942-1946, May 2006.
- [111] I. Ochoa, P. M. Crespo, and M. Hernaez, "LDPC Codes for Non-Uniform Memoryless Sources and Unequal Energy Allocation," *IEEE Communications Letters*, pp. 794-796, September 2010.
- [112] K. H. Lee and D. P. Peterson, "Optimal Linear Coding for Vector Channels," *IEEE Trans. on Communications*, pp. 1283-1290, December 1976.
- [113] F. R. Kschischang, B. J. Frey, and H.-A. Loeliger, "Factor Graphs and the Sum-Product Algorithm," *IEEE Trans. on Information Theory*, pp. 498-519, February 2001.
- [114] J. Pearl, "Probabilistic Reasoning in Intelligent Systems: Networks of Plausible Inference," *Morgan Kaufmann*, 1988.
- [115] F. N. Hu, "Analog Codes for Analysis of Iterative Decoding and Impulse Noise Correction," *Doctoral Dissertation, Jacobs University*, pp. 36 - 39, August 2008.
- [116] L. Li and J. Garcia-Frias, "Hybrid Analog-Digital Coding Scheme Based on Parallel Concatenation of Linear Random Projections and LDGM Codes," *Proc. CISS'14*, March 2014.
- [117] L. Li and J. Garcia-Frias, "Hybrid Analog-Digital Coding for Nonuniform Memoryless Sources," *Proc. CISS'15*, March 2015.
- [118] D. Slepian and J.K.Wolf, "Noiseless Coding of Correlated Information Sources." *IEEE Trans. Inform. Theory*, vol. 19, no. 4, pp. 471-480, July 1973.

- [119] T.M. Cover, "A Proof of the Data Compression Theorem of Slepian and Wolf for Ergodic Sources." *IEEE Trans. Inform. Theory*, vol. 21, no. 2, pp. 226-228, March 1975.
- [120] A.D. Wyner, "Recent Results in Shannon Theory." *IEEE Trans. Inform. Theory*, vol. 20, no. 1, pp. 2 - 10, January 1974.
- [121] S. Shamai (Shitz) and S. Verdú, "Capacity of Channels with Uncoded Side Information." *Eur. Trans. Telecommunication*, vol. 6, no. 5, pp. 587 - 600, September - October 1995.
- [122] J. Barros and S.D. Servetto, "Network Information Flow with Correlated Sources." *IEEE Trans. Inform. Theory*, vol. 52, no. 1, pp. 112 - 128, January 2003.
- [123] M. Gastpar, "Gaussian Multiple-Access Channels Under Received-Power Constraints." *Proc. ITW'04*, October 2004.
- [124] S. Y. Chung, G. D. Forney, T. J. Richardson, and R. Urbanke. "On the design of low-density parity-check codes within 0.0045 db of the shannon limit," *IEEE Communication Letters*, 5:58-60, February 2001.
- [125] M. Shirvanimoghaddam, Y. Li, and B. Vucetic, "Near-capacity adaptive analog fountain codes for wireless channels," *IEEE Communications Letters*, vol. 17, no. 12, pp. 2241-2244, December 2013.

## Appendix

### DECONVOLUTION TECHNIQUE FOR MAC

In this part, we explain the extension of the deconvolution technique [88] to the case of MAC. Denote  $\sum_{i=1}^{d_a} w_i b_i^s$  as  $q$  (notice that  $q$  is different from  $a^s$ , as the information of  $a^s$  comes from the channel while the information of  $q$  is obtained only from incoming messages) and  $\sum_{i=2}^{d_a} w_i b_i^s$  as  $r$ . Thus,

$$q = w_1 b_1^s + r \quad (\text{A.1})$$

Because  $b_1^s$  has three possible values: 0, 1 and 2, the following can be obtained:

$$\begin{aligned} P(q = k) &= P(r = k)P(b_1^s = 0) + P(r = k - w_1)P(b_1^s = 1) \\ &+ P(r = k - 2w_1)P(b_1^s = 2), k \in [-2l, 2l], \end{aligned} \quad (\text{A.2})$$

when  $P(b_1^s = 0) > P(b_1^s = 2)$ ,

$$\begin{aligned} P(r = k) &= \frac{P(q = k) - P(r = k - w_1)P(b_1^s = 1) - P(r = k - 2w_1)P(b_1^s = 2)}{P(b_1^s = 0)}, \\ &k \in [-2l, 2l], \end{aligned} \quad (\text{A.3})$$

where  $P(r = k) = 0$  when  $k < -2l$  or  $k > 2l$ . If  $w_1 < 0$ ,  $r$ 's pmf vector is updated from the right to left. Otherwise, the vector is updated from the left to the right.

On the other hand, if  $P(b_1^s = 2) \geq P(b_1^s = 0)$ , the following can derived from (A.2):

$$\begin{aligned} P(r = k) &= \frac{P(q = k + 2w_1) - P(r = k + 2w_1)P(b_1^s = 0) - p(r = k + w_1)P(b_1^s = 1)}{P(b_1^s = 2)}, \\ &k \in [-2l, 2l]. \end{aligned} \quad (\text{A.4})$$

In this case, the update direction for the pmf of  $r$  also depends on if  $w_1$  is positive or negative. The reason to have both Equation (A.2) and (A.4) to implement the deconvolution is computational accuracy, which is also the reason for using two equations for deconvolution in different cases in [88]. When  $P(b_1^s = 0)$  or  $P(b_1^s = 2)$  is very small, the division is not accurate and the other way should be used. The method can be implemented recursively and iteratively regardless of the updating direction.

Therefore, by using deconvolution, the pmf of  $\sum_{i=2}^{d_a} w_i b_i^s$  can be obtained with much lower complexity and (6.15), (6.16) and (6.17) can be finally used to obtain the outgoing pmf to  $b_1^s$  as well as other neighboring synthetic source bit nodes.